July 1992 UILU-ENG-92-2221

Decision and Control Laboratory

ON THE EFFICIENT AND ACCURATE APPLICATION OF PARTIAL DIFFERENTIAL EQUATION SOLVERS OF MAXWELL'S EQUATIONS IN THE TIME DOMAIN

Paul H. Aoyagi and R. Mittra

Coordinated Science Laboratory
College of Engineering
UNIVERSITY OF ILLINOIS AT URBANA-CHAMPAIGN

SECURITY CLASSIFICATION OF THIS PAGE

REPORT DOCUMENTATION PAGE

Form Approved
OMB No. 0704-0188

1a. REPORT SECURITY CLASSIFICATION Unclassified	1b. RESTRICTIVE MARKINGS None
2a. SECURITY CLASSIFICATION AUTHORITY	3. DISTRIBUTION / AVAILABILITY OF REPORT Approved for public release; distribution ulimited
2b. DECLASSIFICATION / DOWNGRADING SCHEDULE	
4. PERFORMING ORGANIZATION REPORT NUMBER(S) UILU-ENG-92-2221	5. MONITORING ORGANIZATION REPORT NUMBER(S)
6a. NAME OF PERFORMING ORGANIZATION Coordinated Science Lab University of Illinois 6b. OFFICE SYMBOL (*If applicable*) N/A	7a. NAME OF MONITORING ORGANIZATION Office of Naval Research
6c. ADDRESS (*City, State, and ZIP Code*) 1101 W. Springfield Ave. Urbana, IL 61801	7b. ADDRESS (*City, State, and ZIP Code*) Arlington, VA 22217
8a. NAME OF FUNDING / SPONSORING ORGANIZATION Joint Services Electronics Program 8b. OFFICE SYMBOL (*If applicable*)	9. PROCUREMENT INSTRUMENT IDENTIFICATION NUMBER N00014-90-J-1270
8c. ADDRESS (*City, State, and ZIP Code*) Arlington, VA 22217	10. SOURCE OF FUNDING NUMBERS PROGRAM ELEMENT NO. / PROJECT NO. / TASK NO / WORK UNIT ACCESSION NO.

11. TITLE (*Include Security Classification*)
On the Efficient and Accurate Application of Partial Differential Equation Solvers of Maxwell's Equations in the Time Domain.

12. PERSONAL AUTHOR(S)
Paul H. Aoyagi and R. Mittra

13a. TYPE OF REPORT	13b. TIME COVERED	14. DATE OF REPORT (*Year, Month, Day*)	15. PAGE COUNT
Technical	FROM _____ TO _____	1992, July 14	106

16. SUPPLEMENTARY NOTATION

17. COSATI CODES			18. SUBJECT TERMS (*Continue on reverse if necessary and identify by block number*)
FIELD	GROUP	SUB-GROUP	Finite-difference Time Domain; Transients; Electromagnetics; Fourier Analysis; Transmission Line Matrix

19. ABSTRACT (*Continue on reverse if necessary and identify by block number*)

A new field/voltage relation for use with the symmetric condensed node transmission line matrix (TLM) method is introduced. It is found that there is no rigorous mathematical proof which demonstrates the consistency and convergence of the symmetric condensed node TLM method under the field/voltage relation originally introduced. It is proposed that other field/voltage relations may exist which may be more consistent with Maxwell's equations and more accurate than the previous relation. The new field/voltage relation given is derived qualitatively by comparing the symmetric condensed node TLM algorithm with the Yee algorithm (commonly referred to as the finite difference time domain (FDTD)). It is demonstrated numerically that this new relation eliminates nonphysical spurious oscillations introduced by the conventionally used field/voltage relation near the source region.

The presence, cause and correction of a dc anomaly generated by modeling time limited sources using the Yee algorithm are discussed. It is shown mathematically that the Yee algorithm will preserve the divergence relation at any given time, t_0, for all time $t > t_0$. It

20. DISTRIBUTION / AVAILABILITY OF ABSTRACT ☐ UNCLASSIFIED/UNLIMITED ☐ SAME AS RPT. ☐ DTIC USERS	21. ABSTRACT SECURITY CLASSIFICATION
22a. NAME OF RESPONSIBLE INDIVIDUAL	22b. TELEPHONE (*Include Area Code*) / 22c. OFFICE SYMBOL

DD Form 1473, JUN 86 *Previous editions are obsolete.* SECURITY CLASSIFICATION OF THIS PAGE

is demonstrated that this will result in the presence of fictitious static charges in the system even after charges have been removed from the system. Numerical results are given to verify the analysis.

The optimum time step with which to operate the Yee algorithm is given. Fourier analysis is used to derive the discretization and truncation errors and the mathematical conditions for reducing these errors are given. It is found that the Yee algorithm in unbounded space will be the most accurate when the discretization is fine enough and the simulations are run at the largest time step rather than at the smallest time step allowed by the CFL stability criterion. In addition, quantitative descriptions of the eigenfunction spectrum are given which demonstrate the nondissipative nature of the Yee algorithm and the filtering effect caused by discretization. Numerical simulations of a perfect electricl conducting (pec) are given to verify various aspects of the analysis.

A higher-order explicit differencing scheme of Maxwell's equation is considered. In particular, a second order accurate in time and fourth order accurate in space differencing scheme, i.e., 2-4 scheme, using central differencing is studied using Fourier analysis. The stability criterion for the 2-4 scheme is derived as well as expressions for the discretization and truncation errors. It is found that these errors can be made fourth order by reducing the time step or by using an effective dielectric constant concept. Comparisons with the Yee algorithm (2-2 scheme) are made to determine the relative merits of each method. It is found that the 2-4 scheme is more computationally intensive than for the 2-2 scheme, i.e., stricter stability criterion, twice as many computations per iteration, but that the accuracy can be made significantly better than the 2-2 scheme at higher frequencies. In addition, the 2-4 scheme is found to have less grid anisotropy but less spatial resolution than for the 2-2 scheme. Numerical results using a pec cavity are used to verify various aspects of the mathematical analysis.

A hybrid Yee/scalar-wave algorithm is introduced. The new method is designed to economically simulate the time-domain response of planar circuit geometries while generating results which are numerically identical to the Yee algorithm but at approximately one-half the computation time and two-thirds the memory. The method consists of modeling nondivergence-free regions using the Yee algorithm and divergence-free regions using the finite difference form of the scalar-wave equation. Since the scalar-wave equation, unlike the Yee algorithm, uncouples the field components from one another, the number of computations and memory can be reduced in the divergence-free regions by keeping track of only two of the six electric and magnetic field components. In addition, the application of Engquist-Majda absorbing boundary conditions (ABC) and the problems associated with using a reduced number of fields are discussed.

Finally, the feasibility of using the hybrid Yee/scalar-wave algorithm method is demonstrated by computing the far-field radiation patterns of several tapered slot antennas (TSA). In particular, the several radiation patterns of the linear tapered slot and the Vivaldi are computed using the far-field time-domain transformations and compared with measured results from the published literature. It is found that the E-plane results are in good agreement with measured results but that the H-plane results are greatly affected by the modeling of the antenna feed.

TABLE OF CONTENTS

CHAPTER 1

INTRODUCTION

1.1 A Brief History of the Finite Difference Method

Finite difference techniques have been of interest to mathematicians and physicists as far back as 1910 [1]. Two of the more essential aspects of finite differencing schemes, namely convergence and stability, were considered as far back as 1928 in the landmark paper by Courant, Friedrichs and Lewy [2]. Despite the tremendous generality and simplicity of the finite difference approach in solving general ordinary and partial differential equations, the approach was rarely used since the computer did not exist at that time. Consequently, much of the work on the finite difference technique prior to the 1960s tended to be analytical rather than application oriented in nature. Examples of the mathematical nature of the research are given in the innumerable references contained in [3] and [4].

In the early 1960s with the gradual proliferation of automatic computing came a revitalized interest in the finite difference technique. No longer the exclusive property of mathematicians, the physicists and engineers of the 1960s began to concentrate more and more on the application of the finite difference method in hopes of numerically solving problems previously too intractable. Perhaps no group began investigating the finite difference method more than those researchers with an urgent need to solve physical problems involving shock and turbulence: phenomena which had always traditionally been too complicated to solve using standard analytical techniques. Consequently, the researchers in fluid dynamics, geoscience, acoustics and atmospheric science had little choice but to consider numerical techniques such as the finite difference method even before the existence of the computer.

The growing popularity of the finite difference technique within the engineering and physics community in the 1960s rekindled interest within the mathematics community. With the utility of the approach being vindicated by the invention of the computer, more and more funding became available for its study allowing mathematicians to analyze the method in greater detail than before. This culminated in a number of publications on various aspects of the finite difference technique in the late 1960s through the mid-1970s such as absorbing boundary conditions [5], grid anisotropy

[6], errors introduced by inhomogeneities [7], the application of higher-order schemes [8] and subgridding [9]. The interest in finite difference techniques by the mathematics community only lasted until the mid-1980s when attention was gradually shifted to the finite element method.

1.2 The Finite Difference Method and the Electromagnetics Community

During its years of popularity in the mathematics community, the finite difference method also became of some interest to the electrical engineering electromagnetics community. However, prior to the 1980's, interest in the finite difference method was restricted almost exclusively to the frequency domain rather than time domain. Examples of this interest are given in a number of papers published in the *IEEE Transactions on Microwave Theory and Technique* special issue on computer-oriented microwave practices published in August 1969. Though a great deal of mathematical theory had been developed for the finite difference approach in the time domain, the computer resources were so limited that only the frequency domain problem using the scalar-wave equation could be solved. According to [10], for example, it was predicted that a finite-difference time-domain solution of a two-dimensional 100x100 uniform mesh could require anywhere from 3-4 days of computer time just to obtain modest accuracy. Moreover, there was a belief, perhaps somewhat exaggerated, that the time domain solution of three-dimensional problems could take hundreds to thousands of years! Regardless of whether these estimates are indeed correct, it can be stated that the limitations on the computer technology prevented the finite difference method in the time domain from being a practical tool in electromagnetics prior to the mid-1980s There were, however, two papers published in 1966 which went against the conventional wisdom and investigated in some detail the use of the finite difference in the time domain in solving Maxwell's equations in the time domain.

The first paper was published by Roberts and Weiss in 1966 [11]. In particular, they discussed how explicit finite difference schemes could be used to solve Maxwell's equations in the time domain for magnetohydrodynamic problems. What distinguishes this paper from other works is the number of topics presented that were later to be the subject of study in both the mathematics and the engineering communities many years later. Some of these topics include 1) the implementation of 2-2 and 2-4 differencing schemes of Maxwell's equations (using leap-frog and angled differencing), 2) the mathematical equivalence between contour integrations and finite differencing, 3) the

topology of the finite difference mesh, i.e., the Yee lattice, 4) analysis of higher-order differencing schemes.

Later that same year, a paper by Yee introduced an explicit form of the finite difference method in the time domain to the electrical engineering electromagnetics community [12]. Unlike the paper by Roberts and Weiss, Yee's paper considered the finite-difference solution of Maxwell's equations without the convective derivative of the magnetic field. This resulted in a simplification of the partial differential equation and a more compact finite difference scheme than that proposed by Roberts and Weiss. The sole focus of the Yee paper was on the practical application of an explicit 2-2 (second-order accurate differencing of the space and time derivatives) leap-frogging scheme in determining the scattered fields from a perfect electrically conducting cylinder. Though there was very little in the way of mathematical analysis, Yee's paper was the first to introduce the pertinent difference equations as well as the self-consistent topology for the discretization of the electromagnetic fields commonly referred to within the electrical engineering electromagnetics community as the Yee lattice. Yee's work was reintroduced into the community in 1972 by Taflove [13] where it was named the "finite difference time domain" or "FDTD" method: the name most commonly associated with it in the electrical engineering electromagnetics community today.

It was not, however, until the proliferation of the supercomputer in the 1980s with its tremendous memory capacity of several million words and computation speed of several million floating-point operations per second that researchers in the electrical engineering electromagnetics community at large began to take notice of the FDTD method. With the increase in memory and speed, more and more practical electromagnetics problems ranging from radar cross-section problems to microwave circuits could be routinely solved with enough efficiency to rival and even surpass existing numerical methods of the day, i.e., method of moments (MoM). Moreover, the vector nature of the FDTD method allowed one to model nonseparable geometries and boundaries giving it a distinct advantage over the frequency-domain finite-difference approach using the scalar Helmholtz equation. (We note, parenthetically, that the finite-difference frequency-domain solution of the scalar Helmholtz equation was obsolete within the electromagnetics community shortly after its introduction in 1967) It was at this time that researchers also began to recognize the advantages that partial differential equation solvers, such as the FDTD and the finite element method, had over many of the integral equation techniques.

Eventually, with the ever-increasing improvements in the performance of the supercomputer as well as the advent of the work station and parallel computing, the FDTD method has grown to rival and in some cases surpass many of the integral equation techniques as well as analytical techniques in the solution of many electromagnetics problems. With the focus of the community turning towards the characterization of increasingly more complicated geometries in a radar cross section and, particularly, in high speed digital circuits, integral equation techniques have become more cumbersome if not impossible to use. In contrast, the simplicity and generality of the FDTD method have made the solution of even the most complicated electromagnetics problems fairly routine. A single computer program, for example, can handle virtually every conceivable isotropic geometry, whereas many MoM codes must be customized into solving a specific class of problems. The time-domain nature of the FDTD method also allows one to compute the broadband frequency response of a system with a single simulation as opposed to running a frequency-domain simulation many times. These advantages coupled with the remarkable simplicity of the method have resulted in a meteoric rise in popularity of the FDTD method over the past several years. In the joint 1986 URSI/IEEE Antennas and Propagation Symposium, for example, the total number of papers presented on the FDTD method was only four. Six years later in 1992, the number increased to over sixty. The growing applications of the FDTD along with the ever-increasing improvements in computer technology have even led some researchers to predict that the FDTD method may gradually displace many of the other commonly used numerical techniques in electromagnetics.

1.3 Purpose of This Thesis

Though there has been a great deal of published research generated within the electrical engineering electromagnetics community regarding the FDTD community as of late, most of the work can be classified as an application of the FDTD method rather than as a study of the method itself. With the possible exceptions of brief mathematical overviews presented in [11],[14], [15], there is very little in the electrical engineering literature on the mathematical aspects of the FDTD method. Moreover, an examination of the references in many published works as well as the state of some of the research being done, shows that, with the exception of the work on absorbing boundary conditions, much of the finite difference research done in the mathematics community some 20 years ago on difference methods is still relatively unknown in the electromagnetics community. One of the objectives of this work is to provide a bridge

between some of the work done in the mathematics community and the electrical engineering electromagnetics community in the hopes of 1) preventing unnecessary duplication of work, 2) providing quantitative insight into how the FDTD method works, i.e., its limitations and how to improve it . Many of the ideas of this work are extensions of the research done by the mathematics community in the mid 1970s. Much of the analytical work, in Chapters 4, 5, in particular, can be traced to the works of von Neumann [16], Vichnevetsky [17], Trefethen [18], Roberts and Weiss [11]. The presentation in this thesis assumes that the reader is knowledgeable with the numerical implementation of the FDTD algorithm, the use of absorbing boundary conditions and the concept of stability.

1.4 Note about the Terminology

Though the algorithm introduced by Yee is most commonly referred to in the electrical engineering electromagnetics community as the "FDTD method," we will generally avoid using this term throughout the rest of this thesis. This is due to the fact that it is possible to have many finite difference schemes in the time domain that are different than that proposed by Yee. In Chapter 5, for example, we will be considering a higher-order differencing scheme that is markedly different than the algorithm introduced by Yee. To avoid ambiguities, we will refer to the explicit leap-frog finite-differencing scheme commonly referred to as the "FDTD method" as the "Yee algorithm" or, as it is referred to by mathematicians, a "2-2 scheme." We will reserve the term "FDTD" to describe the general class of explicit differencing schemes in the time domain.

1.5 Outline of the Thesis

In the past several years, the symmetric condensed node transmission line matrix (TLM) method has also been gaining popularity in the engineering community as an alternative to the Yee algorithm. The TLM method is also a time-domain solver based on the discretization of a system in space and time; however, unlike the Yee algorithm, space is discretized into a network of transmission lines. Voltages, rather than field values, are monitored on the transmission line and the electromagnetic fields are computed using a simple field/voltage relationship. Though the utility of the methods has been demonstrated in a number of different publications, Chapter 2 shows that the symmetric condensed node TLM simulation is susceptible to anomalous high-frequency oscillation in the simulation of the transient electromagnetic fields near the source. The cause of this

phenomenon is believed to be related to the fact that the original field/voltage relationship was derived qualitatively without insuring the mathematical equivalence between the symmetric condensed node TLM algorithm and Maxwell's curl equation. Chapter 2 presents a new field/voltage relationship which is found to eliminate the spurious oscillations generated by the original field/voltage relationship.

It has been known for some time that the Yee algorithm can generate a non-physical dc offset in the transient response of the electromagnetic fields. Chapter 3 investigates the mathematical reason for this phenomenon. It is found that Maxwell's curl equations can represent a complete time-domain description of the fields if and only if the divergence relations are known to be constant for all time. If the divergence relations are time varying, i.e., time-varying charges, the Yee algorithm will artificially maintain and superimpose static charges in the system. The result is the presence of dc modes inside closed cavities and the presence of fictitious dc fields even after sources have been turned off.

Chapter 4 mathematically determines the optimum time step with which to run the Yee algorithm. In the past there has been empirical evidence which showed that the Yee algorithm is most accurate when run at the largest time step. This is a somewhat counterintuitive result, particularly, when considering that finite difference approximations generally tend to become better as the discretization is made smaller. However, by determining the eigenfunctions of the finite difference solution, one can show mathematically that the truncation and the discretization error must necessarily be reduced if the time step is chosen near the stability limit. In particular, it is found that the errors introduced by the space and time discretizations will cancel each other as the time step is made larger resulting in a smaller overall error. Fourier analysis is also found to provide unique insight into the accuracy of the Yee algorithm by providing quantitative details regarding the spectral bandwidth of the finite difference solutions and its relationship with the continuous solution. Simple numerical simulations are run to verify the analysis.

Presently, the Yee algorithm is the standard form of FDTD used by engineers in the electromagnetics community. In mathematics, the Yee algorithm would be classified as a 2-2 scheme (second-order accurate space and time difference). An alternate differencing which has been looked at extensively by mathematicians in the past in regard to differencing schemes of hyperbolic partial differential equations is a 2-4 scheme. It is

a higher-order scheme which has been considered by some researchers to be the optimum differencing scheme for use in approximating the wave equation. In Chapter 5, a Fourier analysis is performed to determine the eigenfunctions of a 2-4 differencing scheme of Maxwell's equations. A comparison with the standard Yee algorithm is then made and the relative advantages of each discussed in detail. It is found that the 2-4 scheme suffers less from grid anisotropy than the 2-2 scheme and that the accuracy of the method can be increased from second order to fourth order by using smaller time steps or an effective dielectric constant concept.

Chapter 6 introduces a new and efficient formulation of the Yee algorithm. In particular, the Yee algorithm is combined with the finite-difference scalar-wave equation to reduce the number of computations and computer memory needed per iteration. Mathematical conditions for the application of this algorithm are presented. It is found that this hybrid approach is optimal for planar structures and geometries resulting in more than twice the speed of the standard Yee algorithm while using one-third less memory. Moreover, the numerical results can be shown (both mathematically and numerically) to be identical to the Yee algorithm. A discussion on how to modify the Engquist-Majda absorbing boundary conditions (ABC) for use in the hybrid algorithm is presented along with simple numerical examples.

Chapter 7 applies the hybrid Yee/scalar wave algorithm in solving the E-plane radiation patterns of the Vivaldi and the linear tapered slot antennas. The far-field patterns were computed using the recently introduced far-field time-domain transformations. The results are compared with the published measured data to verify the accuracy of the FDTD approach. In general, the agreement was found to be good.

Finally, Chapter 8 summarizes some of the important results of this work and suggests topics for future study.

1.6 References

[1] L.F. Richardson, "The approximate solution of physical problems involving differential equations using finite differences, with application fo the stress in a masonry dam," *Philos. Trans. Roy. Soc., London, Ser. A*, vol. 210, pp. 307-357, 1910.

[2] R. Courant, K. O. Friedrichs, and H. Lewy, "*Uber die partiellen diferenzengleichungen der mathematischen phsik*," Math. Ann., vol. 100, pp. 32-74, 1928.

[3] R. D. Richtmyer and K.W. Morton, *Difference Methods for Initial-Value Problems*, 2nd ed. New York: Interscience Publishers, 1967.

[4] W. F. Ames, *Numerical Methods for Partial Differential Equations*, 2nd ed. New York: Academic Press, Inc., 1977.

[5] B. Engquist, and A. Majda, "Absorbing boundary conditions for the numerical simulation of waves," *Math. Comp.*, vol. 31, no. 139, pp. 629-651, July 1977.

[6] G. Birkhoff, and V. A. Dougalis, "Numerical solution of hydrodynamic problems," *Proc. of the of the AICA International Symposium on Computer Methods for Advances in Partial Differential Equations*, R. Vichnevetsky, ed., New Brunswick, AICA, pp. 7-13, June 1975.

[7] D. L. Brown, "A note on the numerical solution of the wave equation with piecewise smooth coefficients," *Math. Comp.*, vol. 42, no. 166, pp. 369-391, April 1984.

[8] J. Oliger, "Fourth order difference methods for the initial boundary-value problem for hyperbolic equations," *Math. Comp.*, vol. 28, no. 125, pp. 15-25, Jan. 1974.

[9] G. Browning, H.-O. Kreiss, and J. Oliger, "Mesh refinement," *Math. Comp.*, vol. 27, no. 121, pp. 29-39, January 1973.

[10] A. Wexler, "Computation of electromagnetic fields," *IEEE Trans. Microwave Theory Tech.*, vol. MTT-17, no. 8, pp. 416-439, August 1969.

[11] K.V. Roberts and N.O. Weiss, "Convective difference schemes," *Math. Comp.*, vol. 20, pp. 272-299, 1966.

[12] K.S. Yee, "Numerical solution of initial boundary value problems involving Maxwell equations in isotropic media," *IEEE Trans. Antennas Propagat.*, AP-14, pp. 302-307, 1966.

[13] A. Taflove and M. E. Brodwin, "Numerical solution of steady state electromagnetic scattering problems using the time-dependent Maxwell's equations," *IEEE Trans. Microwave Theory Tech.*, vol. MTT-23, pp. 623-630, 1975.

[14] A.C. Cangellaris, C.C. Lin, and K.K. Mei, "Point-matched time domain finite element methods for electromagnetic radiation and scattering," *IEEE Trans. Antennas Propagat.*, vol. AP-35, pp. 1160-1173, October 1966.

[15] A. Taflove and K.R. Umashankar, "The finite-difference time-domain method for numerical modeling of electromagnetic wave interactions with arbitrary structures," *PIER 2: Finite Element and Finite Difference Methods in Electromagnetic Scattering*, J.A. Kong (chief) and M.A. Morgan, Eds. New York: Elsevier, 1990.

[16] J. Von Neumann and R.D. Richtmyer, "A method for the numerical calculation of hydrodynamic shocks," *J. App. Phys.*, vol. 21, pp. 232-237, March 1950.

[17] R. Vichnevetsky and J.B. Bowles, *Fourier Analysis of Numerical Approximations of Hyperbolic Equations*. Philedelphia: SIAM, 1982.

[18] L.N. Trefethen, "Group velocity in finite difference schemes," *SIAM Rev.*, vol. 24, pp. 113-136, 1982.

CHAPTER 2

AN IMPROVED FIELD/VOLTAGE RELATION FOR USE IN THE SYMMETRIC CONDENSED NODE TLM METHOD

2.1 Introduction

Recently, the symmetric condensed node transmission line matrix (TLM) method has been receiving some attention as a method for solving electromagnetic scattering problems in the time domain. Though sharing many of the same advantages as the Yee algorithm, the symmetric condensed node TLM method requires at least three times the memory and twice the computation for what appears to be the same order of accuracy. In addition, unlike the Yee algorithm, there is no mathematical analysis which shows that the voltage pulse propagation in the symmetric condensed node TLM network will converge to a solution to Maxwell's equation as the discretization is made smaller. If one could mathematically establish such a convergence for the TLM method it may be possible to 1) determine the order of accuracy, 2) determine whether it is possible to increase the accuracy, and 3) rewrite the algorithm to reduce the memory and computation time. These are important issues since they will to a large extent determine if the TLM method is better or worse than other competing time domain techniques, most notably, the Yee algorithm, for a given application. A potentially important clue in determining the mathematical relation between the condensed node TLM algorithm and Maxwell's equations is in the relationship between the voltage pulses in the TLM method and the electric and magnetic fields they are trying to model. Hence, it is with this purpose that we investigate any potential errors in this field/voltage relationship.

The goals of this chapter are to show that the field/voltage relation given in [1] can generate spurious oscillations in the time domain and propose new field/voltage relations based heuristically on the Yee algorithm that eliminate the spurious oscillations and potentially provide a more accurate relationship between the voltages and the fields.

2.2 Description of the Symmetric Condensed Node TLM Method

The TLM method is based on modeling transient electromagnetic wave propagation using a network of transmission lines which was introduced by Johns [1]. Though there are other time domain techniques that exist based on a transmission line analogy such as the

Bergeron and Spatial Network Method (SNM) and several different versions of the TLM method that exist, the symmetric condensed node TLM method appears to be the most commonly used of these transmission line based techniques. Briefly, the symmetric node TLM method is based on discretizing space into a network of cells that have 12 input and output ports represented by transmission lines. A typical cell is shown in Fig. 2.1. The pulses entering a cell through a transmission line arm are assumed to be uncoupled as they travel to the center of the cell but are then coupled to other lines through what is known as a scattering matrix. To illustrate, the scattering matrix for the homogeneous free space is

$$\frac{1}{2}\begin{bmatrix} 0 & 1 & 1 & 0 & 0 & 0 & 0 & 0 & 1 & 0 & -1 & 0 \\ 1 & 0 & 0 & 0 & 0 & 1 & 0 & 0 & 0 & -1 & 0 & 1 \\ 1 & 0 & 0 & 1 & 0 & 0 & 0 & 1 & 0 & 0 & 0 & -1 \\ 0 & 0 & 1 & 0 & 1 & 0 & -1 & 0 & 0 & 0 & 1 & 0 \\ 0 & 0 & 0 & 1 & 0 & 1 & 0 & -1 & 0 & 1 & 0 & 0 \\ 0 & 1 & 0 & 0 & 1 & 0 & 1 & 0 & -1 & 0 & 0 & 0 \\ 0 & 0 & 0 & -1 & 0 & 1 & 0 & 1 & 0 & 1 & 0 & 0 \\ 0 & 0 & 1 & 0 & -1 & 0 & 1 & 0 & 0 & 0 & 1 & 0 \\ 1 & 0 & 0 & 0 & 0 & -1 & 0 & 0 & 0 & 1 & 0 & 1 \\ 0 & -1 & 0 & 0 & 1 & 0 & 1 & 0 & 1 & 0 & 0 & 0 \\ -1 & 0 & 0 & 1 & 0 & 0 & 0 & 1 & 0 & 0 & 0 & 1 \\ 0 & 1 & -1 & 0 & 0 & 0 & 0 & 0 & 1 & 0 & 1 & 0 \end{bmatrix} \begin{bmatrix} V_{1i}^n \\ V_{2i}^n \\ V_{3i}^n \\ V_{4i}^n \\ V_{5i}^n \\ V_{6i}^n \\ V_{7i}^n \\ V_{8i}^n \\ V_{9i}^n \\ V_{10i}^n \\ V_{11i}^n \\ V_{12i}^n \end{bmatrix} = \begin{bmatrix} V_{1r}^{n+1} \\ V_{2r}^{n+1} \\ V_{3r}^{n+1} \\ V_{4r}^{n+1} \\ V_{5r}^{n+1} \\ V_{6r}^{n+1} \\ V_{7r}^{n+1} \\ V_{8r}^{n+1} \\ V_{9r}^{n+1} \\ V_{10r}^{n+1} \\ V_{11r}^{n+1} \\ V_{12r}^{n+1} \end{bmatrix} \tag{2.1}$$

where

V_{ki}^n = incident voltage pulse at node k at time n

V_{kr}^{n+1} = reflected voltage pulse at node k at time (n + 1).

The simulation is initiated by releasing a voltage pulse in the network and updating the voltages at each cell using the scattering matrix at each iteration. A field/voltage relationship is then used to relate the voltages to the fields. A salient yet important characteristic of the TLM method is that the speed of the electromagnetic wave is one-half the speed of the voltage pulses in the transmission line network. This means that two iterations of the algorithm are required to advance one time step, Δt, where

$$\Delta t = \frac{\Delta l}{c}$$

where Δl = cell length, c = speed of light.

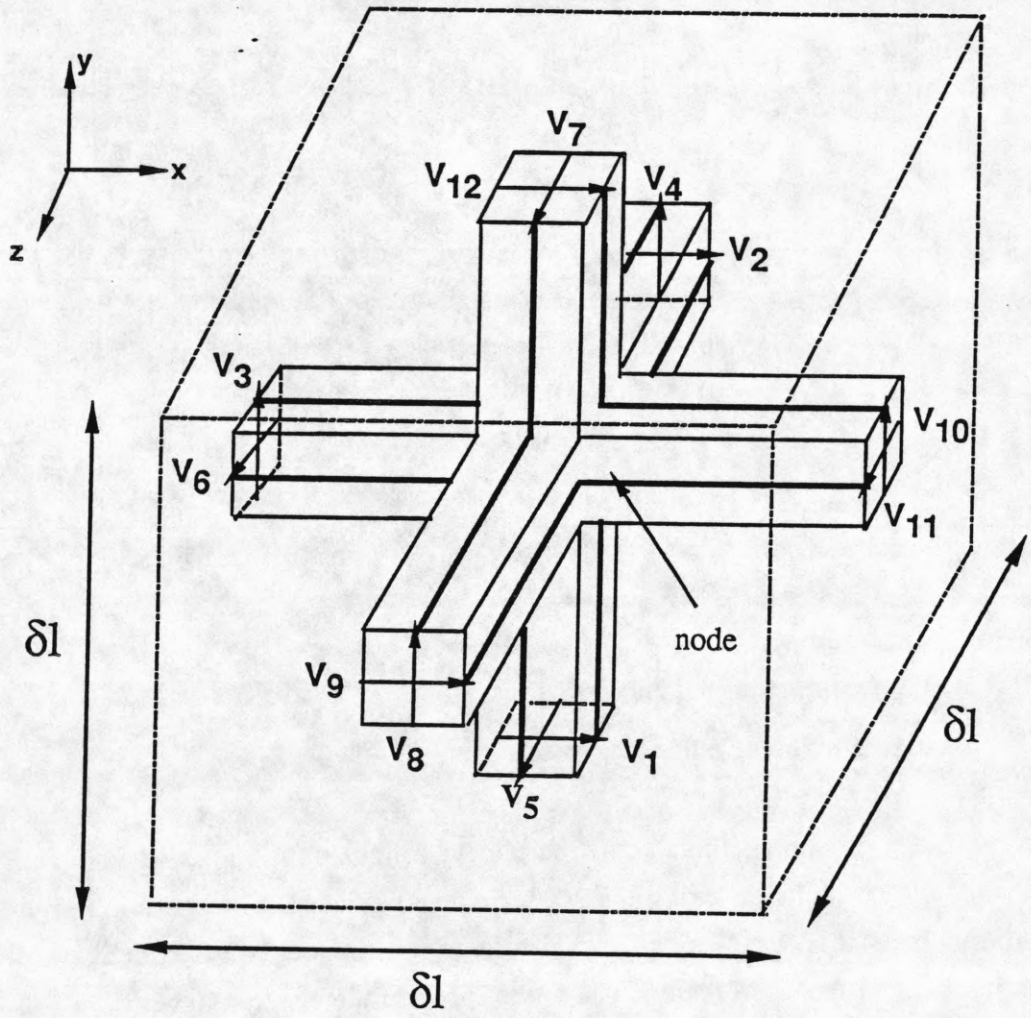

Fig. 2.1 The symmetric condensed node TLM cell.

2.3 The Presence of Spurious Time-Domain Oscillations

An interesting characteristic of the symmetric condensed node TLM method is the presence of spurious oscillations in the time domain. To illustrate, we consider the impulse response of a point electric field source inside a 3x4x6 pec cavity. It is found that the impulse response has spurious oscillations near the source region (Fig. 2.2). Only two cells away from the source region, however, these oscillations are found to disappear abruptly (Fig. 2.3). Because these results are not consistent with our physical intuition nor with results obtained using the Yee algorithm (Fig. 2.4), we conclude that the symmetric condensed node TLM cannot be entirely correct.

2.4 Possible Causes of Spurious Oscillations

It is believed that there are two probable explanations for the spurious oscillations exhibited in Fig. 2.2. The first is that there is an error or deficiency in the formulation of the symmetric condensed node TLM algorithm itself. That is, because there is no mathematical proof which demonstrates a consistency between the TLM approach and Maxwell's equations, the symmetric condensed node TLM as given in [1] may not be a true solver of Maxwell's equation. A second explanation would be to assume that the basic formulation is correct but that the mathematical translation of the voltage information in the TLM network into the electromagnetic fields is in error. In this work we will investigate the second possibility and leave the investigation of the first to a later work.

2.5 The Field/Voltage Relation

The field/voltage relation given in [1] is constructed using a static analysis. Each transmission line arm in Fig. 2.1 is approximated as a lumped capacitance and the capacitances for the same polarization added. The total electric field in the cell for a given polarization is then assumed to be proportional to the total voltage induced on this lumped capacitance. (A parallel assumption is made to relate the total magnetic field with the total current entering the cell for a given magnetic polarization.) An example of the field/voltage relation is given for the x component of the electric field, i.e.,

$$E_x^n = \frac{1}{2}(V_{1i}^n + V_{2i}^n + V_{9i}^n + V_{12i}^n) \tag{2.2}$$

where i denotes incident voltages.

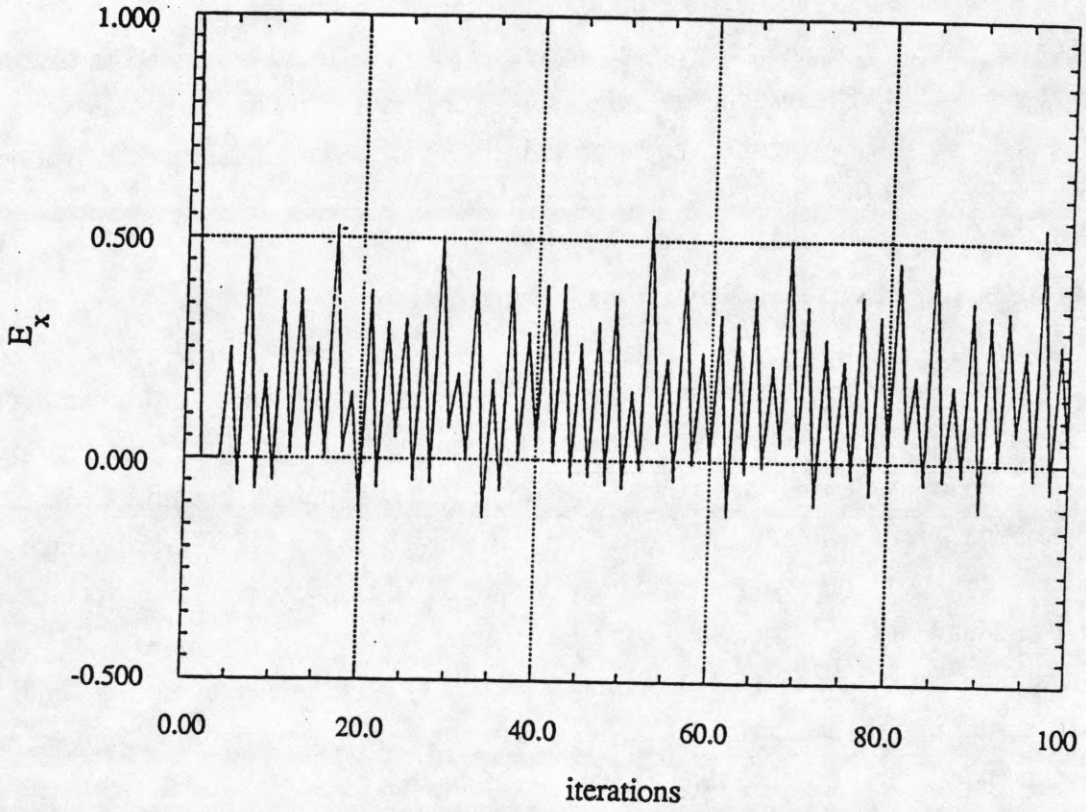

Fig. 2.2 Symmetric condensed node TLM impulse response of the x-directed electric field for a 3x4x6 cell pec cavity using the voltage field relation given in [1]. The source was a single cell x-directed electric field located at (2,3,4). The observation point was also located at (2,3,4).

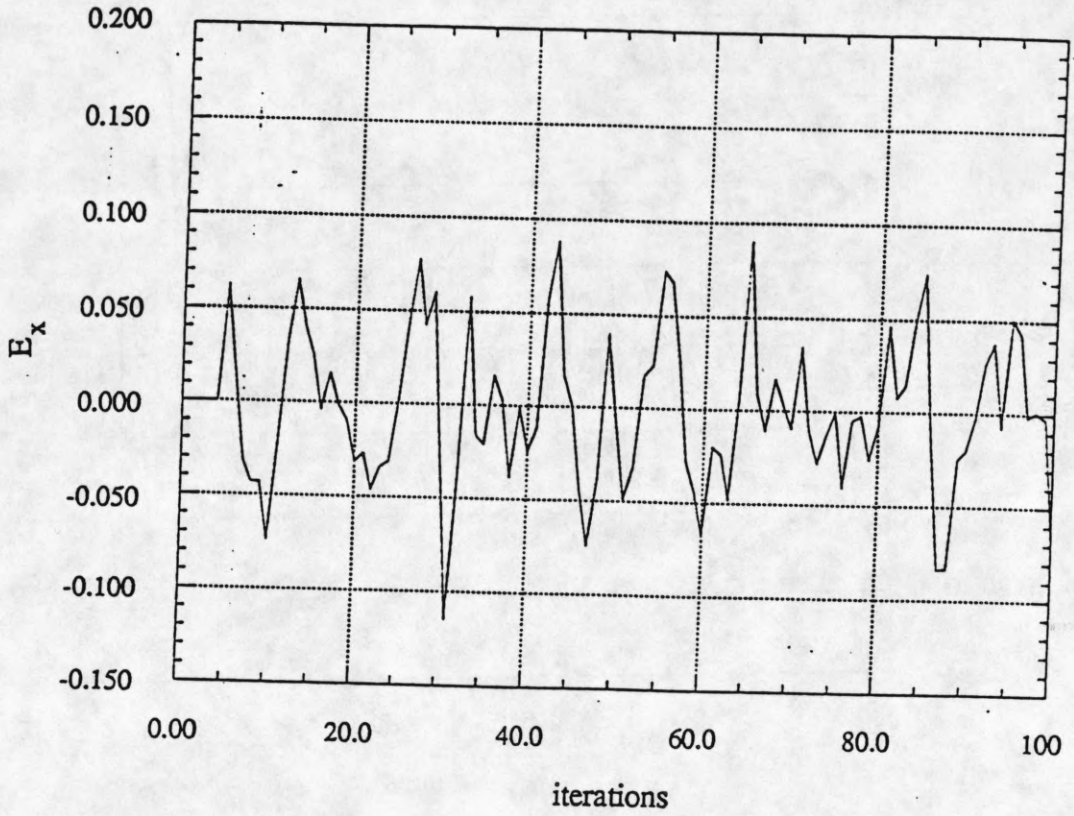

Fig. 2.3 Symmetric condensed node TLM impulse response of the x-directed electric field for a 3x4x6 cell pec cavity using the voltage field relation given in [1]. The source was a single cell x-directed electric field located at (2,3,4). The observation point was located at (3,2,2).

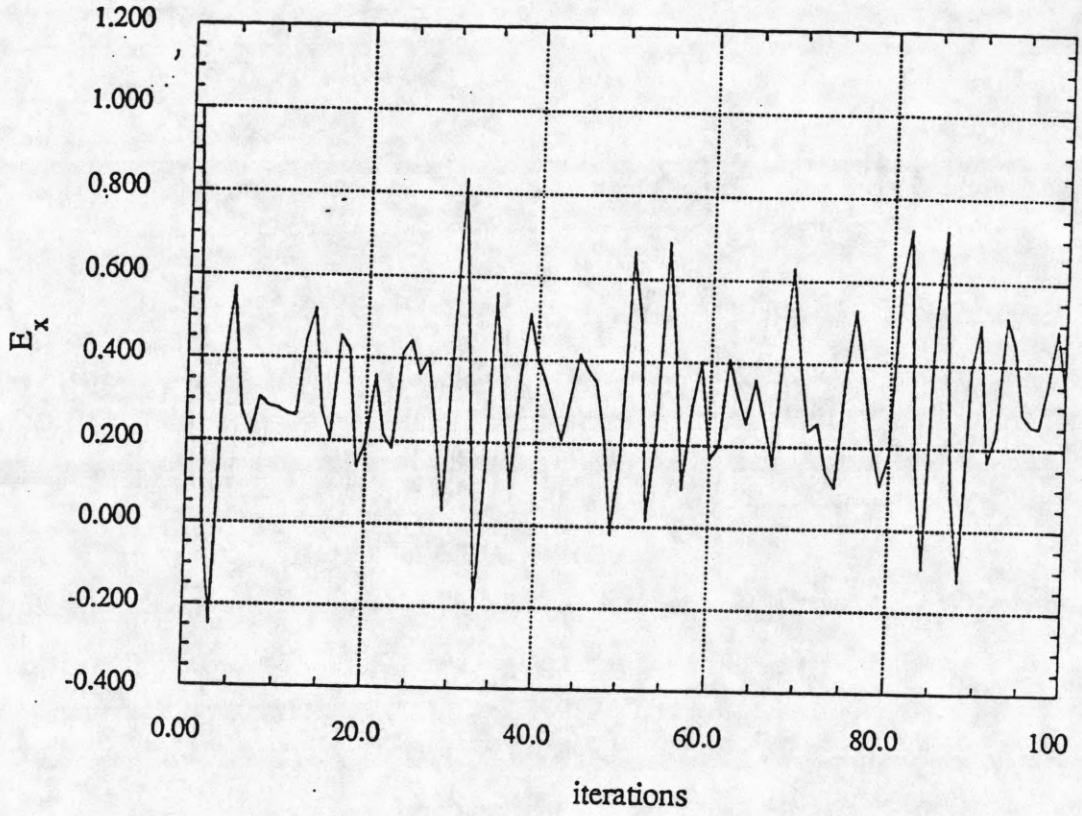

Fig. 2.4 Yee algorithm impulse response of the x-directed electric field for a 3x4x6 cell pec cavity. The source was a single cell x-directed electric field located at (2,3,4). The observation point was also located at (2,3,4).

2.6 On an Improved Field/Voltage Relation

We note that though it seems intuitively reasonable for the analysis and (2.2) to be correct, i.e., that the electric field would be proportional to the sum of voltages, there is no rigorous mathematical basis for this to be necessarily true. In particular, there is no mathematical analysis which shows that the derivation and its resultant field/voltage relation will insure that the symmetric condensed node TLM method will be a rigorous transmission line analogy of Maxwell's equations. In light of this deficiency, we consider constructing several new field/voltage relation that are potentially more accurate and perhaps just as valid.

Our construction of a new field/voltage relation begins by first noting that the TLM algorithm is very similar in form and concept to the Yee algorithm, i.e., both are explicit time domain schemes designed to solve Maxwell's equations by discretizing space and time. In addition, it has been empirically found that both algorithms have approximately the same accuracy. A significant difference between the two, however, is that the Yee algorithm can be proven mathematically to be consistent with Maxwell's equations, whereas the symmetric condensed node TLM method presently cannot. If we assume that the TLM method is also consistent with Maxwell's equations, then it must also be equivalent in some sense to the Yee algorithm. (Such an equivalence has been demonstrated between the expanded node TLM algorithm and the Yee algorithm [2].) Consequently, we will use the Yee algorithm to determine a field/voltage relationship. We first note that the fields at any given time, t, using the Yee algorithm can be generated using field information from t-Δt and t-2Δt. In addition, we note that the fields are based strictly on the nearest neighbor information. In the same manner, one can make the fields computed using the TLM algorithm have a similar dependence. Taking into account Equation (2.1) and assuming that nearest neighbor information will be conveyed by the nearest voltage pulses, we assume the field/voltage relation to take the general form of

$$E_x^n = \alpha_1 E_x^{n-1} + \alpha_2 E_x^{n-2} + \sum_{k=1}^{12} \beta_{ki} V_{ki}^n + \sum_{k=1}^{12} \beta_{kr} V_{kr}^n + \sum_{k=1}^{12} \chi_{ki} V_{ki}^{n-1} + \sum_{k=1}^{12} \chi_{kr} V_{kr}^{n-1} + \sum_{k=1}^{12} \gamma_{ki} V_{ki}^{n-2} + \sum_{k=1}^{12} \gamma_{kr} V_{kr}^{n-2} \qquad (2.3)$$

where α_1, α_2, β_{ki}, β_{kr}, χ_{ki} , χ_{kr}, γ_{ki}, γ_{kr} = real constants.

Having determined roughly what information may be needed to establish an equivalence between the Yee algorithm and the TLM method, we have to determine more precisely how to combine this information. From the published literature it been has demonstrated that the field/voltage Equation (2.2) appears to yield results that are comparable to those of the Yee algorithm. Therefore, we can assume that the form of the field/voltage expressions given in [1] is at least partially correct and subsequently simplify (2.3), i.e.,

$$E_x^n = \alpha_1 E_x^{n-1} + \alpha_2 E_x^{n-2} + \alpha_3 \sum_k V_{ki}^n + \alpha_4 \sum_k V_{ki}^{n-1} + \alpha_5 \sum_k V_{ki}^{n-2} \qquad (2.4)$$

where k = 1, 2, 9, 12, and α_p= real constant for p =1, 2, 3, 4, 5.

2.7 Discussion and Results

Through trial and error it was determined through computer simulation that the following relations will eliminate spurious oscillations near the source region of a 3x4x6 pec cavity:

$$E_x^n = E_x^{n-1} + \frac{1}{2}\left[\sum_k V_{ki}^n - \sum_k V_{ki}^{n-2}\right] \qquad (2.5)$$

$$E_x^n = \frac{1}{2}\left[E_x^{n-1} + \sum_k V_{ki}^n - \sum_k V_{ki}^{n-2}\right] \qquad (2.6)$$

$$E_x^n = \frac{1}{2}\left[E_x^{n-1} - E_x^{n-2} + \sum_k V_{ki}^n\right] \qquad (2.7)$$

$$E_x^n = E_x^{n-1} + \frac{1}{2}\left[-E_x^{n-2} + \sum_k V_{ki}^n\right] \qquad (2.8)$$

$$E_x^n = \frac{1}{2}\sum_k V_{ki}^n + \frac{1}{4}\left[E_x^{n-1} - E_x^{n-2}\right] \qquad (2.9)$$

where k=1, 2, 9, 12, and the coefficients of each formula were chosen to produce the same value for the electric field for the same initial incident voltages.

Though all four expressions were found to reduce the spurious oscillations to one degree or another, Equations (2.5) and (2.6) were found to be most like the Yee algorithm

results of Fig. 2.3. The results for (2.5) and (2.6) are shown in Fig. 2.5. It can be seen that both (2.5) and (2.6) eliminate most if not all of the spurious oscillations observed earlier. Though both results are similar, one finds that the time domain response of (2.5) appears to be most like the Yee algorithm (Fig. 2.4) due primarily to the presence of a dc offset. In Fig. 2.6 we compare the results obtained using (2.5) with those obtained using the field/voltage relationship given in [1]. It can be seen that despite the spurious oscillations, the two results are quite similar and, in particular, one notes that the time domain response of (2.5) appears to outline the oscillatory response computed using [1]. Mathematically, it appears that we can approximate their relationship as

$$f_{[1]}[n] = f_{2.5}[n] + K \cos \omega_{osc} n \tag{2.10}$$

where $f_{[1]}[n]$ = time domain response using [1],
$f_{2.5}[n]$ = time domain response using Eq. (2.5),
ω_{osc} = frequency of the spurious oscillation,
K = magnitude of the spurious oscillation
n = iteration.

A similar relation can also be used to relate (2.6) with (2.2). Therefore, it is apparent that the frequency domain response computed using (2.5) and (2.2) will be very nearly identical except near the frequency of the spurious oscillation. Figure 2.7 compares the time domain response of (2.5) versus (2.2) for regions away from the source region. It can be seen that their time domain responses are virtually identical and, consequently, one would expect their frequency responses also to be similar. Thus, we conclude that using (2.5) will improve the time domain response near the source region, but will not change the frequency domain response of the system compared to (2.2). Due to the similarity with (2.5), a similar conclusion can be extended to the field/voltage relationship of (2.6).

2.8 Conclusions

It has been shown that using the standard field/voltage relation given in [1] causes the symmetric condensed node TLM algorithm to have nonphysical spurious oscillations near the source region and that these results are not consistent with those obtained using the Yee algorithm. It is believed that a possible cause for this problem is an error in the field/voltage relation which resulted from ignoring mathematical conditions necessary to

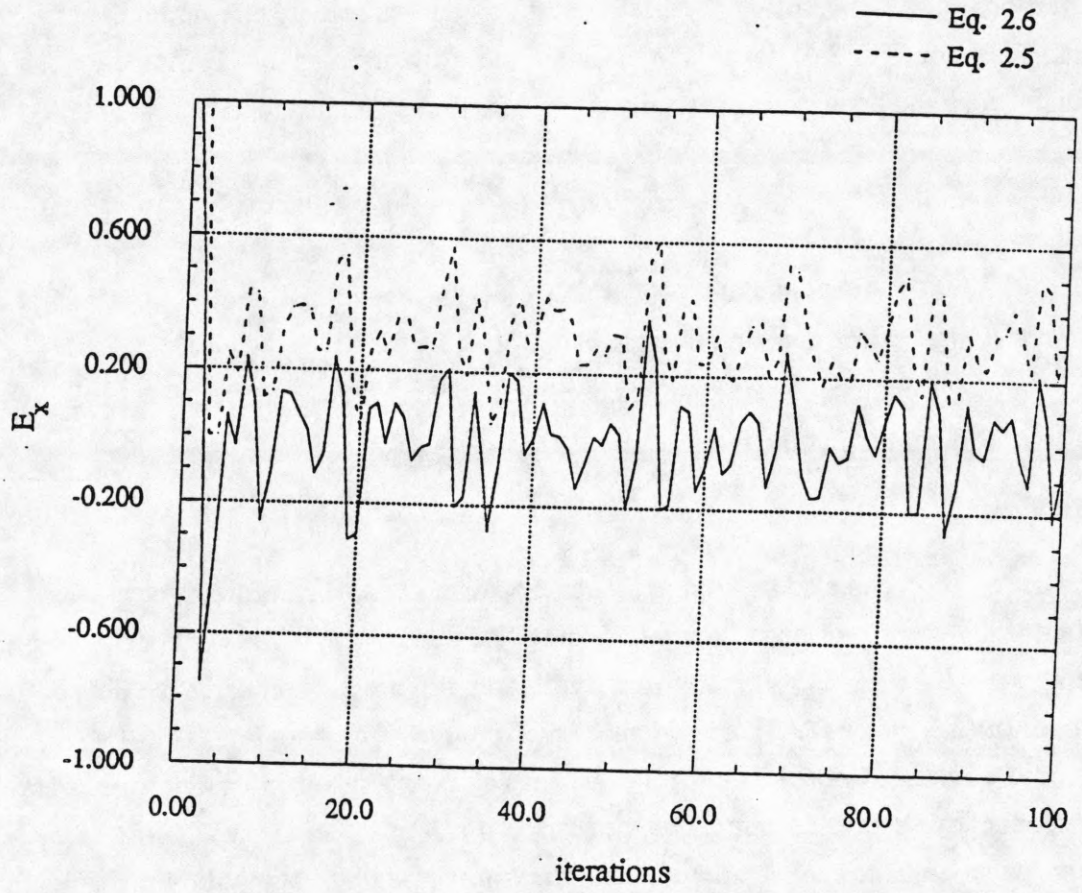

Fig. 2.5 Symmetric condensed node TLM impulse response of the x-directed electric field for a 3x4x6 cell pec cavity using the voltage field relation given in Equations (2.5) and (2.6). The source was a single cell x-directed electric field located at (2,3,4). The observation point was also located at (2,3,4).

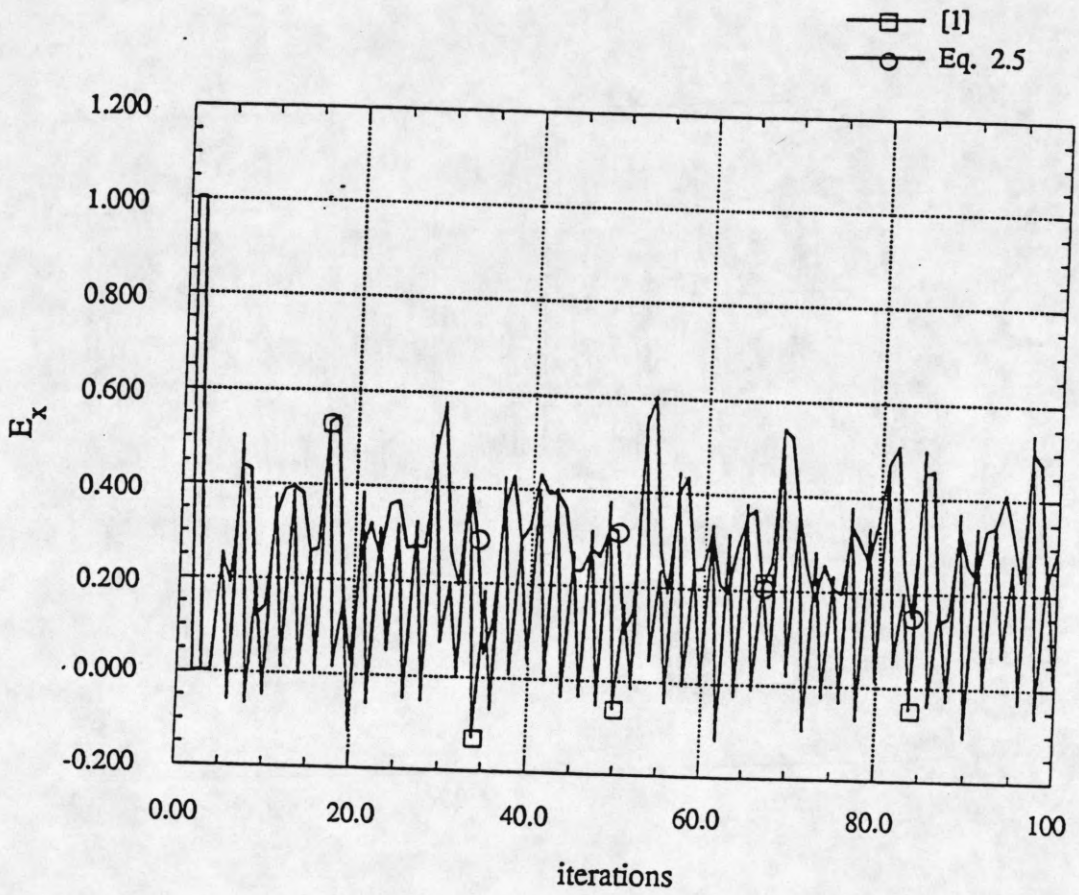

Fig. 2.6 Symmetric condensed node TLM impulse response of the x-directed electric field for a 3x4x6 cell pec cavity using the voltage field relation given in Equation (2.5) and the relation given in [1]. The source was a single cell x-directed electric field located at (2,3,4). The observation point was also located at (2,3,4).

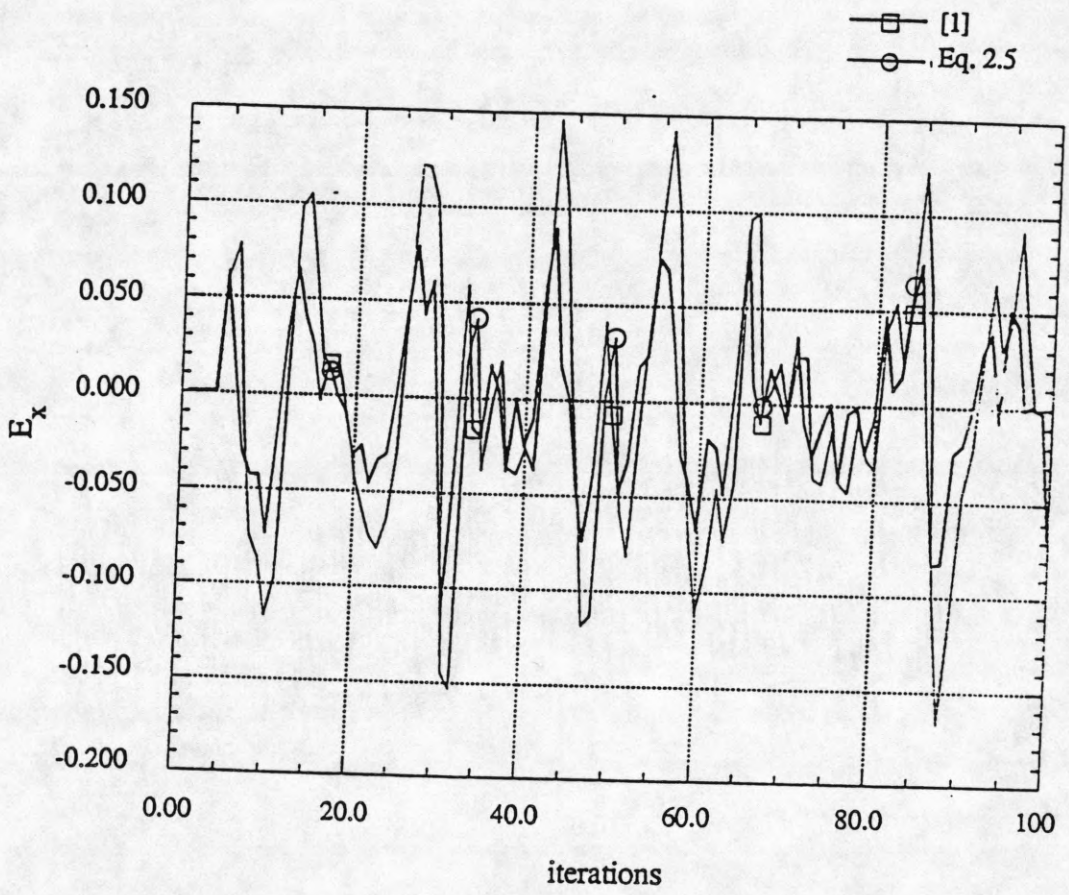

Fig. 2.7 Symmetric condensed node TLM impulse response of the x-directed electric field for a 3x4x6 cell pec cavity using the voltage field relation given in Equation (2.5) and the relation given in [1]. The source was a single cell x-directed electric field located at (2,3,4). The observation point was also located at (3,2,2).

make the TLM algorithm a mathematically rigorous analogy of Maxwell's equations. To correct for possible errors in the original field/voltage relation, several new field/voltage relations, based qualitatively on the Yee algorithm, were proposed. Two new relations were presented which eliminated the spurious oscillations in the time domain near the source region while retaining the reported frequency domain accuracy of the field/voltage relationship in [1].

2.9 References

[1] P. B. Johns, "A symmetrical condensed node for the TLM method," *IEEE Trans. Microwave Theory Tech.*, vol. MTT-35, no. 4, pp. 370-377, April 1987.

[2] P. B. Johns, "On the relationship between the TLM and finite-difference methods for Maxwell's equations," *IEEE Trans. Microwave Theory Tech.*, vol. MTT-35, no. 1, pp. 60-61, Jan. 1987.

CHAPTER 3

ON THE APPLICABILITY OF MODELING THE ZERO FREQUENCY COMPONENT USING THE YEE ALGORITHM

3.1 Introduction

The possibility of a dc error in the finite difference solution of Maxwell's equations on a staggered grid was mentioned as early as 1966 [1]. Since then its existence appears to have been known empirically for sometime in the electromagnetics community; however, it was not until recently that the presence of residual dc fields was reported to be generated by the Yee algorithm [2]. In particular, it was found that the Yee algorithm simulations of a transient source can generate electric and/or magnetic fields that converge to nonzero dc values even as time goes to infinity. Interestingly, a similar phenomenon can also be observed in the symmetric condensed node transmission line matrix method. At present there appears to be some debate in the electrical engineering electromagnetics community on what the actual cause of this dc offset is or if such an offset is the result of actual physics.

The purpose of this section is to mathematically determine whether the Yee algorithm is capable of modeling dc fields of a time-dependent source and to explain the dc offset which is present in the transient fields. In particular, we discuss the physical meaning of using arbitrary field distributions as sources to generate the transient response. In addition, we also investigate how the initial conditions affect the modeling of the dc fields. It is found that using fields as sources is physically equivalent to creating point charge pairs. It is demonstrated that the Yee algorithm will correctly model the dc fields generated by these point charges. Numerical experiments are used to validate the analysis.

3.2 The Applicability of Modeling the Direct Current Component

3.2.1 Enforcing the divergence relations in the frequency domain

To determine whether the Yee algorithm is capable of modeling the dc term or not, we first consider the conditions under which Maxwell's curl equations can be used.

To correctly model the electromagnetic fields in a sourceless homogeneous medium, Maxwell's curl equations and the divergence relations must be enforced, i.e.,

$$\nabla x\overline{E} = -\mu\frac{\partial\overline{H}}{\partial t} \tag{3.1}$$

$$\nabla x\overline{H} = \varepsilon\frac{\partial\overline{E}}{\partial t} \tag{3.2}$$

$$\nabla\cdot\overline{E} = 0 \tag{3.3}$$

$$\nabla\cdot\overline{H} = 0 \tag{3.4}$$

where ε, μ = constant electric permittivity and magnetic permeability of the media. By taking the divergence of (3.1) and (3.2), it can be seen that the curl equations given by (3.1) and (3.2) will have the divergence relation built in provided the time derivatives are nonzero. In such cases, only the curl equations have to be solved to obtain the electromagnetic field distribution. In contrast, when the time derivatives are zero the curl equations reduce to the following form

$$\nabla x\overline{E} = 0 \tag{3.5}$$

$$\nabla x\overline{H}=0. \tag{3.6}$$

Clearly, Equations (3.5) and (3.6) do not have the proper divergence relations included in them; consequently, it appears that the divergence relations given by (3.3) and (3.4) must be enforced *in addition* to the curl equations. Mathematically, we can view this as specifying the gauge of Equations (3.6) and (3.7), which, in turn, makes the fields unique.

3.2.2 Enforcing the divergence relations in the time domain

Because the Yee algorithm is based on the curl equations, one might expect difficulty in modeling the dc fields due to problems associated with the divergence relation. The conclusions of the previous analysis, however, are not entirely applicable to the time domain since the evolution of the divergence relation with respect to time was not considered. To see if the divergence relations at dc are being handled properly, we can rewrite the curl equations by taking their divergence, i.e.,

$$\frac{\partial}{\partial t}(\nabla\cdot\overline{H}) = 0 \tag{3.7}$$

$$\frac{\partial}{\partial t}(\nabla \cdot \overline{E}) = 0. \tag{3.8}$$

If Equations (3.7) and (3.8) are considered in the context of an initial value problem (IVP), it is clear that at if $\nabla \cdot \overline{H} = \rho_m$ and $\nabla \cdot \overline{E} = \rho_e$ at $t = t_0$, where ρ_m, ρ_e are constants, then $\nabla \cdot \overline{H} = \rho_m$ and $\nabla \cdot \overline{E} = \rho_e$ for all $t > t_0$. Hence, a constant divergence relation can be implicitly enforced for all $t > t_0$ by specifying the divergence at $t = t_0$.

3.3 Numerical Validation

A simple check of the above analysis is to see if the divergence relation at $t = t_0$ is being kept constant by the Yee algorithm for $t > t_0$. This was verified by computing the transient response of an electric field point source, i.e.,

$$E_{xs}(n) = \begin{pmatrix} 1 & n = 1 \\ 0 & n > 1 \end{pmatrix} \tag{3.9}$$

where n = iteration number, $t = n\Delta t$, Δt=time step, and computing the divergence of the electric field just above and below the source (see Fig. 3.1). It was found that the divergence remained equal to one even after the source had been turned off. Physically speaking, this constant divergence implies that there are static charges in the system which give rise to residual dc fields (Fig. 3.2).

Now we consider changing the time dependence of the previous source to a half sinusoid, i.e.,

$$E_{xs}(n) = \begin{bmatrix} \sin\dfrac{(n-1)}{N}\pi & 1 \le n \le N+1 \\ 0 & elsewhere \end{bmatrix} \tag{3.10}$$

where N = integer > 0. According to the previous analysis, every time a new charge is introduced by the source it will be preserved for all of time. The result will be a superposition of all the charges introduced over time. From Fig. 3.1, it can be seen that the charge introduced by a field source will be given by

$$\rho_{above}[n] = -\sum_n E_{xs}[n] \tag{3.11}$$

$$\rho_{below}[n] = \sum_n E_{xs}[n] \tag{3.12}$$

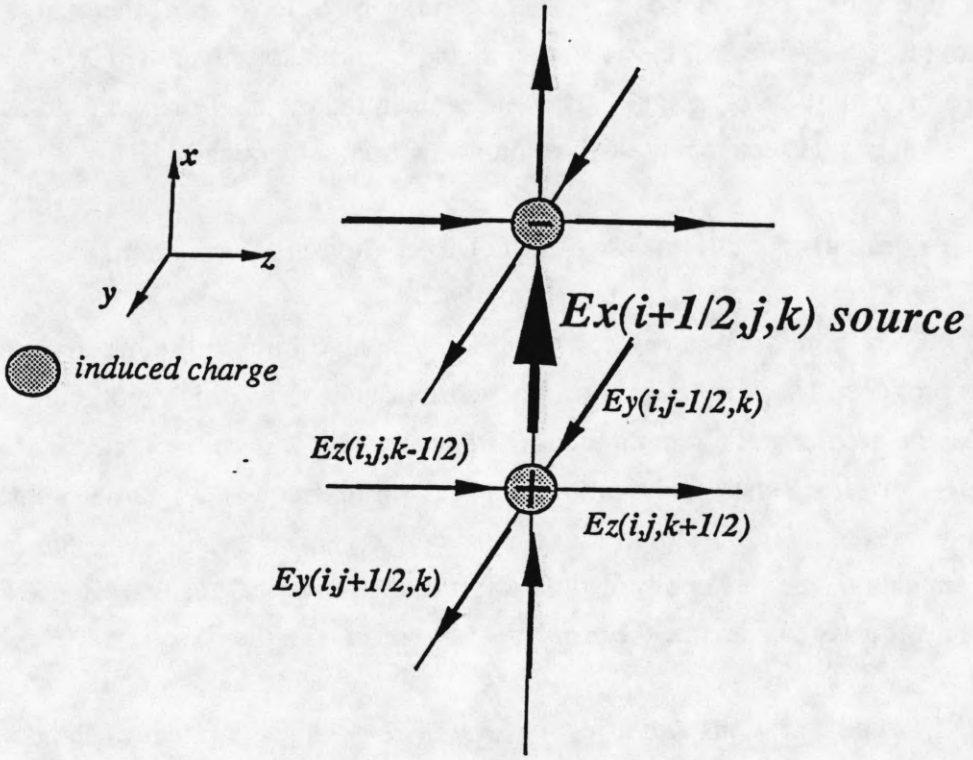

Fig. 3.1 Diagram of the charges introduced by using a single electric field as a source in the Yee algorithm. The values of the charges are governed by the central difference approximation of the divergence relation.

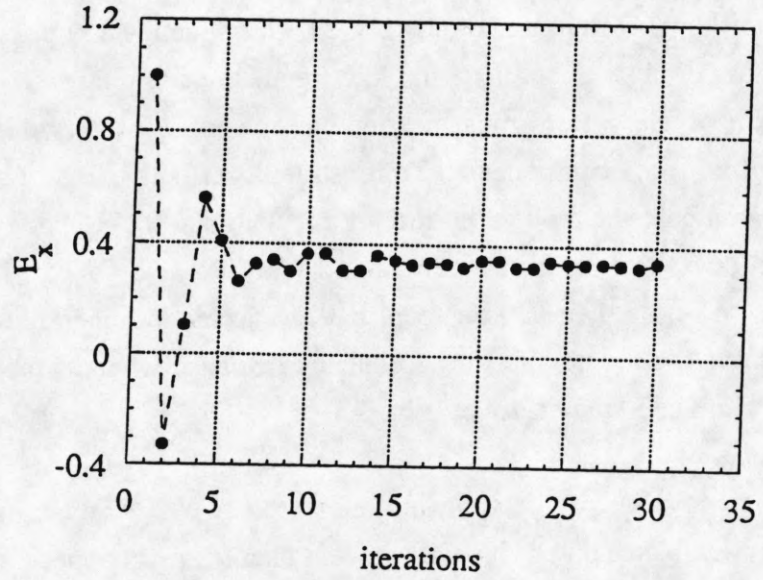

Fig. 3.2 Time domain impulse response of a single cell E_x field radiating in free space generated by the Yee algorithm. The observation point is equal to the source point.

where the subscripts "above" and "below" refer to the location of the charge relative to the source. In Figure 3.3, the predicted divergence relation given by (3.11) and (3.12) is compared with the electric field divergence generated by the Yee algorithm as a function of time. It can be seen that the two results are virtually identical.

3.4 Eliminating Difficulties with the Direct Current Component

Even though we have shown that the Yee algorithm will correctly model the dc fields produced by constant charges, there are occasions in which modeling the dc term can have a detrimental effect on the low frequency response of the system. In particular, if a large dc term exists, its effect on the neighboring frequencies can be substantial and many iterations may be required to obtain convergence. In addition, the presence of constant charges add a nonphysical dc offset to the numerical results. Consequently, we will look at ways to alleviate the problems associated with the dc term.

The most obvious and effective way of removing the effect of the dc term is to use a source with no dc term [3]. Physically, such a source would introduce constant charges into the system which would eventually cancel each other. It is important to note that, strictly speaking, this approach is applicable if and only if the system is linear. Because the Yee algorithm is a nonlinear system which couples high frequency components into low frequency components (see Chapter 4 and [1]), we stipulate that a zero dc source will be effective if and only if the high frequency components of the finite difference solution do not contaminate the low frequency components. This means that the discretization of the system must be fine enough to accurately describe the most significant high frequency components. To illustrate its effectiveness of removing the dc component, we compare the mode spectrum of a rectangular 3x4x6 pec cavity generated by using a zero dc source with that generated by an impulse source, i.e., nonzero dc component. From Fig. 3.4, it can be seen that the dc mode generated by an impulse source is contaminating the neighboring frequency response whereas the zero dc source appears to have eliminated the dc effect (Fig. 3.5).

Another way to remove dc source contributions is to use a divergence-free initial field distribution. Physically speaking, this will prevent charges from appearing in the source even if the source has a nonzero dc component. An example of such a source is a line source connecting two pec plates. Figure 3.6 demonstrates the effectiveness of this approach for the pec cavity problem. In contrast to the previous approach, it provides

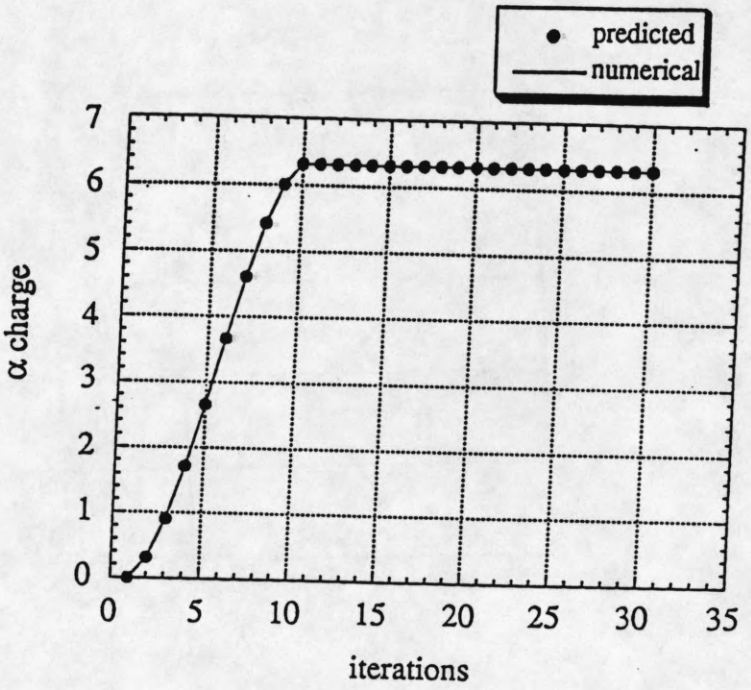

Fig. 3.3 Comparison between the predicted charge accumulation and the numerical charge accumulation generated by the Yee algorithm simulation for a transient E_x point source radiating in free space. The excitation was a half sinusoid with a period of 20 iterations.

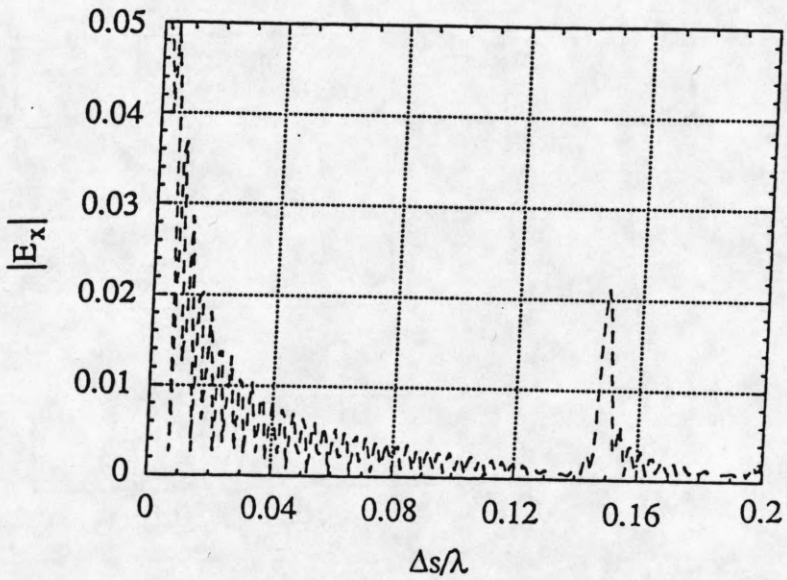

Fig. 3.4 The resonant mode spectrum of a 3x4x6 rectangular pec cavity generated by the Yee algorithm using an impulse E_x point source (500 iterations).

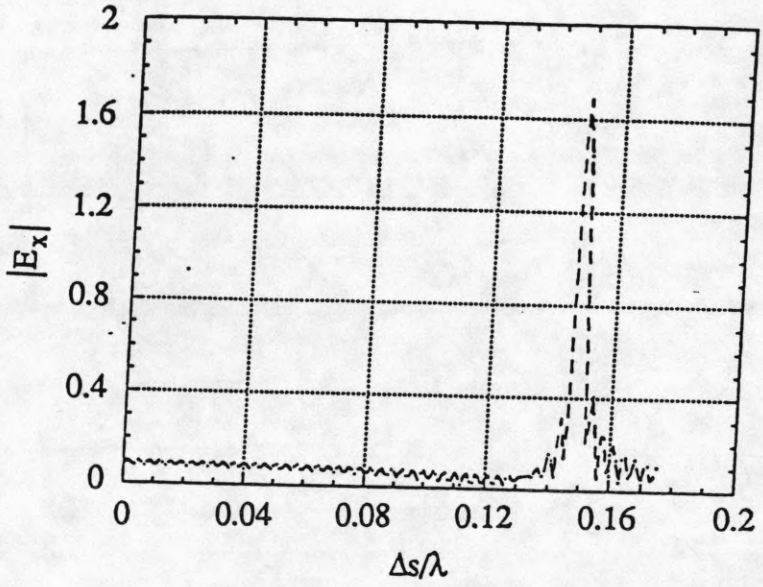

Fig. 3.5 The mode spectrum of a 3x4x6 cavity generated by the Yee algorithm using an E_x point source. The source was a half-cosine with a period of 20 iterations and no zero dc component (500 iterations).

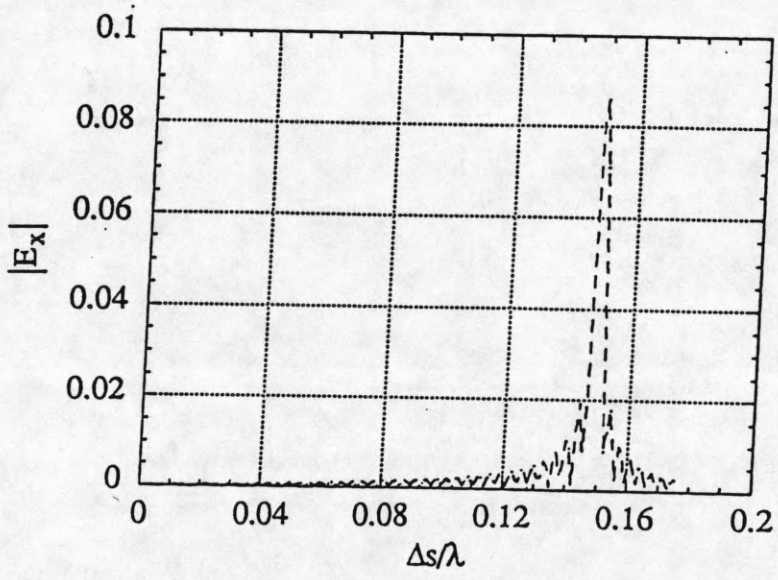

Fig. 3.6 The mode spectrum of a 3x4x6 cavity generated by the Yee algorithm using a divergence free impulse E_x line source (500 iterations).

freedom in choosing the time dependence of the source but restricts the spatial distribution.

Other ways of removing the dc component are filtering techniques. Essentially, one post processes the time data in order to remove the effects of the dc term. Two of these methods include removing the dc average from the time data and using the time derivative to obtain the frequency response. Although these filtering techniques allow a great deal of freedom in choosing both the time and spatial dependencies of the initial sources, these techniques are not effective unless a sufficient number of iterations are taken. In contrast, the effectiveness of the nonfiltering techniques will be relatively insensitive to the number of iterations. Moreover, post processing requires additional computations whereas the previous methods of dealing with the dc terms require no additional overhead.

3.5 Conclusions

The validity of using the Yee algorithm to model a dc electromagnetic field is discussed. It is shown mathematically that the divergence relations at dc are enforced by the initial conditions. It is found that the charges that are introduced into the system during a time domain simulation do not disappear when time goes to infinity. Consequently, the divergence relation at any given point in space and time is governed by the superposition of the previous charges. Numerical simulations were presented to verify the analysis.

Ways to remove the constant charges generated by an arbitrary field source were given. The recommended way to remove the effect of the charge is to use a source with zero dc. It is believed that this will allow the user the most flexibility in choosing the source distribution and time dependence while still effectively eliminating the effects of the dc charges. Another way to remove the constant charge terms that was discussed was to use a divergence-free source. Though quite effective, it is not always possible to find a divergence-free source for some problems. Moreover, divergence-free sources will not take care of the dc charges that may build up in objects other than the source, i.e., pec edges. Numerical results were given which demonstrated the applicability of both methods.

3.6 References

[1] K.V. Roberts and N.O. Weiss, "Convective difference schemes," *Math. Comp.*, vol. 20, pp. 272-299, 1966.

[2] C.M. Furse, S.P. Mathur, and O.P. Gandhi, "Improvements to the finite-difference time domain method for the radar cross section of a perfectly conducting target," *IEEE Trans. Microwave Theory Tech.*, vol. MTT-38, no. 7, pp. 919-927, July 1990.

[3] W.C. Chew, private communication.

CHAPTER 4

ON IMPROVING THE ACCURACY OF THE YEE ALGORITHM USING LARGER TIME STEPS

4.1 Introduction

The Yee algorithm (more commonly referred to as the finite difference time domain (FDTD)) is a central difference approximation in time and space of Maxwell's curl equations written in explicit form. One advantage of the Yee algorithm over the symmetric condensed node TLM method is that it can be shown mathematically to be consistent with Maxwell's equations. In particular, the Lax equivalence theorem insures that a finite difference solution to Maxwell's equation will always converge to the continuous solution as the space and time increments approach zero provided the system is stable [1]. We note that there is no analogous theorem regarding the symmetric condensed node TLM solution.

Though more accurate finite difference solutions will be generated by using smaller space and time discretizations, in practice, one can ill afford to make the discretizations too small due to limitations on computer time and memory. For efficiency, one would ideally like to use the largest discretization possible to obtain satisfactory results. It is therefore of practical as well as academic interest that we examine the effect that finite discretization (in time and space) has on the accuracy of finite difference schemes such as the Yee algorithm.

In the past, there has been work which considered the existence of time steps for explicit finite difference solutions of general partial differential equations which result in an optimal balance between accuracy and computations [2]. Regarding the Yee algorithm specifically, there has been empirical evidence which suggests paradoxically that the optimal time step may correspond to the largest time step allowed under the stability criterion rather than the smallest time step [3], [4]. The purpose of this work is to provide mathematical evidence to substantiate this phenomenon. To do this, we will follow the methodology given in [5]-[7]. In particular, Fourier transform representations of the continuous and finite difference solutions will be used to derive expressions for the truncation and discretization errors. The mathematical conditions which minimize these errors are then determined. It is found that, provided the differencing scheme is stable

and the spatial discretization fine enough, the truncation and discretization errors of the Yee algorithm will be reduced whenever the time step corresponds to the largest time step allowed by the stability limit. Numerical simulations of a resonant cavity are used to verify various aspects of the analysis.

4.2 Decomposition of the Continuous Solution of Maxwell's Equations into Spectral Components

We begin by assuming that our problem is a properly posed initial value problem in an infinite, homogeneous, isotropic space. In addition, we will be excluding the effect of the source and the presence of absorbing boundary conditions. Maxwell's equation can then be rewritten as six independent scalar wave equations of the following form

$$\nabla^2 U(x,y,z,t) - \frac{1}{c^2}\frac{\partial^2}{\partial t^2} U(x,y,z,t) = 0 \tag{4.1}$$

where $U(x,y,z,t) \in$ electric and magnetic fields,

c = speed of light in free space.

We next assume that any solution to (4.1) is expressible in terms of the Fourier transform, i.e.,

$$U(x,y,z,t) = \int_{-\infty}^{\infty}\int_{-\infty}^{\infty}\int_{-\infty}^{\infty}\int_{-\infty}^{\infty} \bar{U}(k,\omega) e^{-jk\cdot r} e^{j\omega t} dk_x dk_y dk_z d\omega \tag{4.2}$$

where

$$k = k_x\hat{x} + k_y\hat{y} + k_z\hat{z}$$

This expression can be simplified by noting that only those spectral components that satisfy (4.1) are needed to construct a general solution to (4.1). These are the so-called eigenfunctions of the system [8]. Substituting (4.2) into (4.1) shows that these components must satisfy the dispersion relation, i.e.,

$$\omega(k) = c\sqrt{k_x^2 + k_y^2 + k_z^2} \tag{4.3}$$

Therefore, we can conclude that only three of the four variables of integration are truly independent. This implies that Equation (4.2) can be reduced to a triple integral, i.e.,

$$U(x,y,z,t) = \int_{-\infty}^{\infty}\int_{-\infty}^{\infty}\int_{-\infty}^{\infty}\tilde{U}'(k)e^{-jk\cdot r}e^{j\omega(k)t}dk_x dk_y dk_z \tag{4.4}$$

or in discretized form

$$U(m\Delta x, n\Delta y, p\Delta z, l\Delta t) = \int_{-\infty}^{\infty}\int_{-\infty}^{\infty}\int_{-\infty}^{\infty}\tilde{U}'(k)e^{-jk\cdot r_{mnp}}e^{j\omega(k)l\Delta t}dk_x dk_y dk_z \tag{4.5}$$

where $r_{mnp} = m\Delta x\hat{x} + n\Delta y\hat{y} + p\Delta z\hat{z}$, $\Delta s = \Delta x = \Delta y = \Delta z =$ space discretization, $\Delta t =$ time discretization, and m,n,p,l are integers.

At this point, one might be tempted to simplify (4.5) even further by noting that the discretization of any complex exponential will result in periodicity of the spectrum. This periodicity implies that the infinite spectrum of $e^{jk_x m\Delta x}$, for example, can be entirely represented by a finite spectrum, $-\pi \le k_x\Delta x \le \pi$. However, to use this property to simplify (4.5), each spectral component given by

$$e^{-jk\cdot r_{mnp}}e^{j\omega(k)l\Delta t} \tag{4.6}$$

must be periodic with respect to $k_x\Delta x$, $k_y\Delta y$, $k_z\Delta z$. Specifically, this would require that

$$\rho^{1/2}\sqrt{(N_1\pi + k_x\Delta s)^2 + (N_2\pi + k_y\Delta s)^2 + (N_3\pi + k_z\Delta s)^2} = \omega\Delta t + N_4\pi \tag{4.7}$$

where N_1, N_2, N_3, N_4 are integers for all $k_x\Delta x, k_y\Delta y, k_z\Delta z, \omega\Delta t \in [-\pi, \pi]$. Clearly (4.7) will not be satisfied leading to the conclusion that the limits of integration in (4.5) cannot be reduced to triple integral form. This implies that the exact solution to the wave equation, even in discretized form, can only be represented using an infinite spectrum of plane waves.

4.3 Decomposition of the Finite Difference Solution to Maxwell's Equations into Spectral Components

Analogous to the spectral representation of the continuous solution to the scalar wave equation, we now wish to represent the solution to its central difference approximation using a similar superposition of spectral components. To do this, we must determine the eigenfunctions of the difference equation given by

$$u_{m,n,p,l} = 2u_{m,n,p,l} - u_{m,n,p,l-1} + \rho\{u_{m+1,n,p,l} + u_{m-1,n,p,l} + u_{m,n+1,p,l} + u_{m,n-1,p,l} + u_{m,n,p+1,l} + u_{m,n,p-1,l} - 6u_{m,n,p,l}\} \tag{4.8}$$

where $u_{m,n,p,l} = u(m\Delta x, n\Delta y, p\Delta z, l\Delta t)$, $\rho = (c\Delta t/\Delta s)^2$. If we assume that a Fourier transform representation of $u(x,y,z,t)$ exists. we can begin by writing

$$u(m\Delta x, n\Delta y, p\Delta z, l\Delta t) = \int_{-\infty}^{\infty}\int_{-\infty}^{\infty}\int_{-\infty}^{\infty}\int_{-\infty}^{\infty} \tilde{u}(k,\Omega) e^{j\Omega l\Delta t} e^{-jk\cdot r_{mnp}} dk_x dk_y dk_z d\Omega \tag{4.9}$$

Analogous to what was done previously, we note that (4.9) can be simplified by noting that only those spectral components which satisfy (4.8) are needed to represent any general solution to (4.8). By substituting (4.9) into (4.8) one can derive the dispersion relation [7], [9],[10]

$$\sin\frac{\Omega\Delta t}{2} = \rho^{1/2}\left(\sin^2\frac{k_x\Delta s}{2} + \sin^2\frac{k_y\Delta s}{2} + \sin^2\frac{k_z\Delta s}{2}\right)^{1/2} \tag{4.10}$$

In order to find an explicit expression for Ω, one can use the analysis outlined in [10]. In particular, one can use the series expansion of the sine terms in conjunction with the following representation for the inverse sine

$$\sin^{-1}\theta = \theta + \frac{1}{2\cdot 3}\theta^3 + \frac{1\cdot 3}{2\cdot 4\cdot 5}\theta^5 + \frac{1\cdot 3\cdot 5}{2\cdot 4\cdot 6\cdot 7}\theta^7 + \ldots. \tag{4.11}$$

to derive the following expression

$$\Omega(k) = \omega(k) + \varepsilon_p(k, \Delta s, \rho) \tag{4.12}$$

where

$$\varepsilon_p(k, \Delta s, \rho) = -\frac{1}{24}\frac{\omega(k)^3}{c^2}((\cos^4\alpha + \cos^4\beta + \cos^4\gamma) - \rho)(\Delta s)^2 + O((\Delta s)^4) \tag{4.13}$$

$$\cos\alpha = \frac{ck_x}{\omega(k)},\ \cos\beta = \frac{ck_y}{\omega(k)},\ \cos\gamma = \frac{ck_z}{\omega(k)} \tag{4.14}$$

It is important to note that Equation (4.12) is valid if and only if (4.11) is valid, i.e., $\theta^2 < 1$. From (4.10), we can conclude that this will require that the finite difference equation must be stable, i.e., $\rho < 1/3$. In all subsequent analysis, we will assume stability unless otherwise stated. Parenthetically, we point out that (4.13) can also be derived by using a simple adaptation of the overstability analysis [11].

Equation (4.10) shows that only three of the four variables of integration in (4.9) are truly independent. Hence, we can rewrite (4.9) as a triple integral, i.e.,

$$u(m\Delta x, n\Delta y, p\Delta z, l\Delta t) = \int_{-\infty}^{\infty}\int_{-\infty}^{\infty}\int_{-\infty}^{\infty} \tilde{u}'(k) e^{j\varepsilon_p(k,\Delta s,\rho)l\Delta t} e^{j\omega(k)l\Delta t} e^{-jk\cdot r_{mnp}}\, dk_x dk_y dk_z \tag{4.15}$$

Simplifying further, we note that each spectral component given by

$$e^{j\varepsilon_p(k,\Delta s,\rho)l\Delta t} e^{j\omega(k)l\Delta t} e^{-jk\cdot r_{mnp}} \tag{4.16}$$

is periodic with respect to k_x, k_y, k_z, i.e.,

$$\sin\frac{\Omega\Delta t + 2N_4\pi}{2} = \rho(\sin^2\frac{k_x\Delta s + 2N_1\pi}{2} + \sin^2\frac{k_y\Delta s + 2N_2\pi}{2} + \sin^2\frac{k_z\Delta s + 2N_3\pi}{2})^{1/2} \tag{4.17}$$

where N_1, N_2, N_3, N_4 are integers and $k_x\Delta x, k_y\Delta y, k_z\Delta z, \Omega\Delta t \in [-2\pi, 2\pi]$. Unlike the analogous transform expression of the previous case, this periodicity can be exploited to reduce the limits of integration, i.e.,

$$u(m\Delta x, n\Delta y, p\Delta z, l\Delta t)$$

$$= \int_{-a}^{a}\int_{-a}^{a}\int_{-a}^{a} \tilde{u}''(k) e^{j\varepsilon_p(k,\Delta s,\rho)l\Delta t} e^{j\omega(k)l\Delta t} e^{-jk\cdot r_{mnp}} dk_x dk_y dk_z \qquad (4.18)$$

where $a=2\pi/\Delta s$. An engineering way to interpret the representation of (4.18) is that the finite difference solution is a low-pass filtered version of the continuous solution given by (4.5) [12]. We note, however, that though the spectral components of the finite difference solution are nonattenuating (indicating that the scheme is nondissipative) the presence of an additional phase term, ε_p, will affect the fidelity of this low-pass filter. In particular, the finite difference solution will introduce a phase error into the exact solution which will depend not only on the discretization of time, space but on the direction of propagation.

4.4 Increasing the Accuracy of the Finite Difference Solution by Using the Time Step

There are two different ways commonly used to quantify the accuracy of a finite difference solution 1) the discretization error and 2) the truncation error. Though there are several definitions for discretization and truncation errors which are used [12], for the purposes of this work, we will define the discretization error to be the difference between the continuous solution and the finite difference solution and the truncation error to be the error between the partial differential equation and the finite difference equation. Though the truncation error is commonly used in the electromagnetics community as a means of comparing the relative accuracy of a finite difference approximation, the discretization error is actually a much more significant quantity. This discretization error, for example, aside from being a more direct measure of how close the approximate solution is to the exact solution, takes into account the stability of the finite difference solution whereas the truncation error does not. In this section, we will examine the effect of the time step on both types of error.

4.5 The Effect of the Time Step on Truncation Error

The simplest way to determine the effect of the time step on accuracy is to consider the truncation error. It can be easily shown using the Taylor series expansion that the truncation error for (4.8) is of second order, i.e.,

$$\varepsilon_{trunc}(r,\Delta s,\rho) = -\frac{(\Delta s)^2}{12}[(\frac{\partial^4}{\partial x^4}+\frac{\partial^4}{\partial y^4}+\frac{\partial^4}{\partial z^4})-\frac{\rho}{c^4}\frac{\partial^4}{\partial t^4}]U(x,y,z,t)+O((\Delta s)^4) \tag{4.19}$$

Substituting (4.5) into (4.19) we obtain

$$\varepsilon_{trunc}(r,\Delta s,\rho) = -\frac{(\Delta s)^2}{12}\int_{-\infty}^{\infty}\int_{-\infty}^{\infty}\int_{-\infty}^{\infty}\tilde{U}'(k)e^{j\omega(k)t}e^{jk\cdot r}$$
$$\times(\frac{\omega(k)}{c})^4[(\cos^4\alpha+\cos^4\beta+\cos^4\gamma)-\rho]dk_x dk_y dk_z.+O((\Delta s)^4) \tag{4.20}$$

Because the time error and the space error terms are of opposite sign, it is possible to cancel ε_{trunc} to some extent. In particular, if

$$[(\cos^4\alpha+\cos^4\beta+\cos^4\gamma)-\rho]=0 \tag{4.21}$$

ε_{trunc} will become fourth order. Unfortunately, it is clear that for a fixed ρ, Equation (4.21) can only hold for certain angles of incidence. However, by choosing a ρ which is in the range of values of the direction cosines, i.e.,

$$\frac{1}{3}\le(\cos^4\alpha+\cos^4\beta+\cos^4\gamma)\le 1 \tag{4.22}$$

ε_{trunc} can be reduced. If we recall that ρ must also be constrained by the stability criterion, i.e., $\rho < 1/3$, we can conclude that the truncation error will be minimized when the time step is chosen closest to the stability limit.

4.6 The Effect of the Time Step on the Discretization Error

Though computing the truncation error is a very expedient way of evaluating the error of a finite difference scheme, it does not tell us specifically how error will manifest itself in the actual solution to the difference equation. To do this, we now consider the discretization error, ε_{disc}. The discretization error is typically defined to be the difference between the continuous solution and the finite difference solution. Using the transform expressions derived earlier, we can write

$$\varepsilon_{disc}(r_{mnp},l\Delta t,\Delta s,\rho) = \varepsilon_a(r_{mnp},l\Delta t,\Delta s,\rho)+\varepsilon_\infty(r_{mnp},l\Delta t,\Delta s)+\varepsilon_{-\infty}(r_{mnp},l\Delta t,\Delta s) \tag{4.23}$$

where

$$\varepsilon_a(r_{mnp}, l\Delta t, \Delta s, \rho)$$

$$= \int_{-a}^{a}\int_{-a}^{a}\int_{-a}^{a}(\tilde{U}'(k) - \tilde{u}''(k)e^{j\varepsilon_p(k,\Delta s,\rho)l\Delta t})e^{j\omega(k)l\Delta t}e^{-jk\cdot r_{mnp}}dk_x dk_y dk_z \quad (4.24)$$

$$\varepsilon_\infty(r_{mnp}, l\Delta t, \Delta s) = \int_{a}^{\infty}\int_{a}^{\infty}\int_{a}^{\infty}\tilde{U}'(k)e^{j\omega(k)l\Delta t}e^{-jk\cdot r_{mnp}}dk_x dk_y dk_z \quad (4.25)$$

$$\varepsilon_{-\infty}(r_{mnp}, l\Delta t, \Delta s) = \int_{-\infty}^{-a}\int_{-\infty}^{-a}\int_{-\infty}^{-a}\tilde{U}'(k)e^{j\omega(k)l\Delta t}e^{-jk\cdot r_{mnp}}dk_x dk_y dk_z \quad (4.26)$$

From Equations (4.24)-(4.26) it can be seen that the discretization error is made up of essentially two different types of error. The first type, given by (4.25), is the error associated with the inaccuracies of modeling k-space components within the finite spectrum of the finite difference solution given by (4.21). The second type, given by (4.25) and (4.26), is the error associated with the presence of large k-space components in the continuous solution which lie outside this finite spectrum. Consequently, a necessary condition for the finite difference solution to be an accurate approximation to the continuous solution is that the spectral content of the continuous solution be approximately band limited to within [-a,a]. Practically speaking, this translates into making sure that the discretization is made fine enough to accurately model the most significant high frequency components [6]. If the discretization is not made fine enough aliasing between the large k-space components and the small k-space components will cause $\tilde{u}''$ to differ from $\tilde{U}'$. This means that the discretization error will not decrease even if there is no phase error, i.e., $\varepsilon_p = 0$. Under these circumstances, it is possible to have a coarser mesh result in finite difference solutions which paradoxically satisfy the continuous wave equation to a higher degree of accuracy than a finer mesh but are solutions to a problem different than what was originally intended.

If we assume that the discretization is made fine enough, however, we can make the following approximations

$$\int_{-a}^{a}\int_{-a}^{a}\int_{-a}^{a}(\tilde{U}(k) - \tilde{u}''(k)e^{j\varepsilon_p(k,\Delta s,\rho)l\Delta t})e^{j\omega(k)l\Delta t}e^{-jk\cdot r_{mnp}}dk_x dk_y dk_z \quad (4.27)$$

$$\varepsilon_{-\infty}(r_{mnp}, l\Delta t, \Delta s), \varepsilon_\infty(r_{mnp}, l\Delta t, \Delta s) \cong 0 \quad (4.28)$$

$$\varepsilon_p(k,\Delta s,\rho) \to 0 \Rightarrow \tilde{u}'' \to \tilde{U}'' \tag{4.29}$$

This implies that a necessary and sufficient condition for reducing the discretization error is to reduce the phase error, $\varepsilon_p(k,\Delta s,\rho)$. By comparing $\varepsilon_p(k,\Delta s,\rho)$ with the expression for the truncation error (4.20) it can be seen that the discretization error will also be minimized when ρ corresponds to the stability limit given by $\rho=1/3$.

4.7 Numerical Verification of the Analysis

As a partial verification of the analysis, the resonant frequencies of a pec rectangular waveguide were computed using the Yee algorithm to compute the impulse response. The simulations were run using seven different time steps while keeping the total time of simulation fixed. The frequency response was then computed using a discrete time Fourier transform (DTFT). Results for four TE modes, i.e., (0,1,1), (0,2,2), (0,2,1), (0,1,2), of the cavity were then compared with analytic solutions. To magnify the effects of the time step on the accuracy of the finite difference algorithm, a coarse grid was chosen to model the cavity. The results are shown in Fig. 4.1 and Fig. 4.2. Increasing the time step does indeed increase the accuracy. Furthermore, we note that the gains obtained by increasing the time step are significantly reduced as the space discretization, Δs, becomes smaller compared to the wavelength. This corresponds to the reduction of the error given in (4.12). In addition, we note another trend which appears to verify the previous analysis. To understand the nature of this verification, we begin by noting that the truncation error and the phase error given by (4.20) and (4.27), respectively, will converge to a constant maximum value as Δt approaches zero. This simple observation implies that the finite difference solution will also converge to a solution possessing the largest possible error . Moreover, it can be deduced from the sign of the phase error given in Equation (4.13) that this should result in computed resonant frequencies which are slightly lower than the exact solution. These are trends clearly exhibited by both Figs. 4.1 and 4.2.

4.8 Conclusions

This work has provided heuristic evidence based on Fourier decomposition of the finite difference solution to the wave equation that the solution to the Yee algorithm can

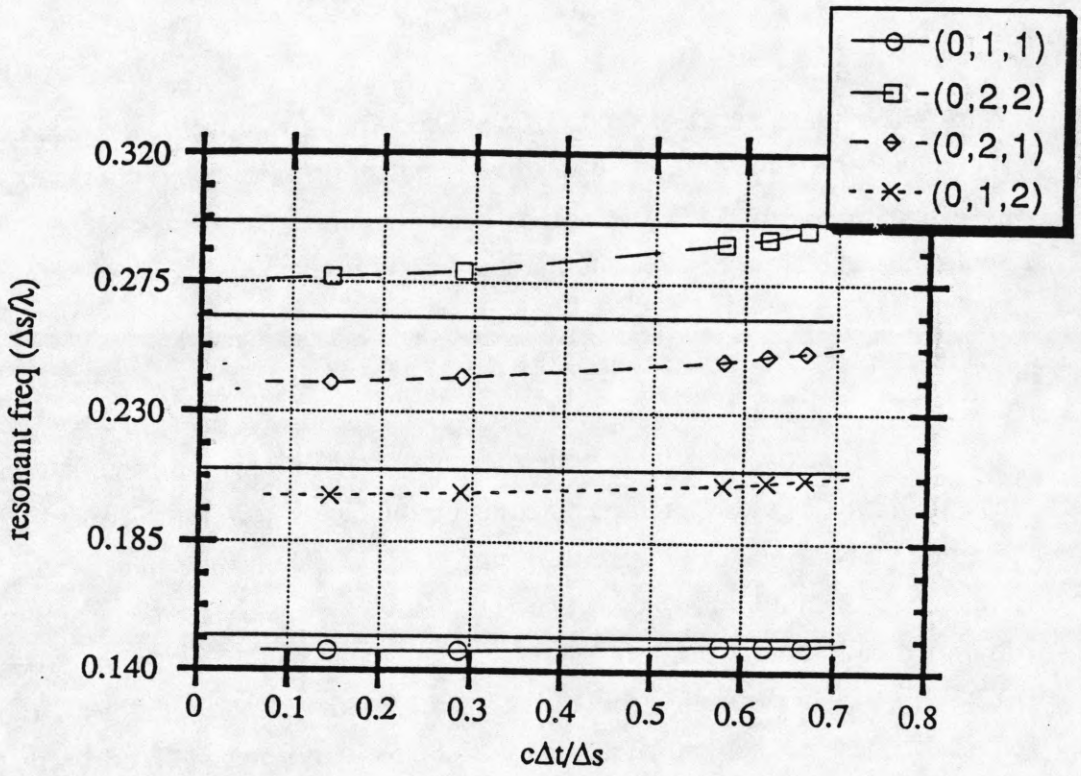

Fig. 4.1 Plot of the FDTD resonant frequencies for a (3,4,6) pec cavity vs. the time step for different modes. The straight lines represent the exact solutions.
Note $\rho^{1/2} = c\Delta t/\Delta s =$ 0.714: 810 iterations
0.667: 870 iterations
0.625: 925 iterations
0.578: 1000 iterations
0.288: 2000 iterations
0.144: 4000 iterations
0.072: 8000 iterations.

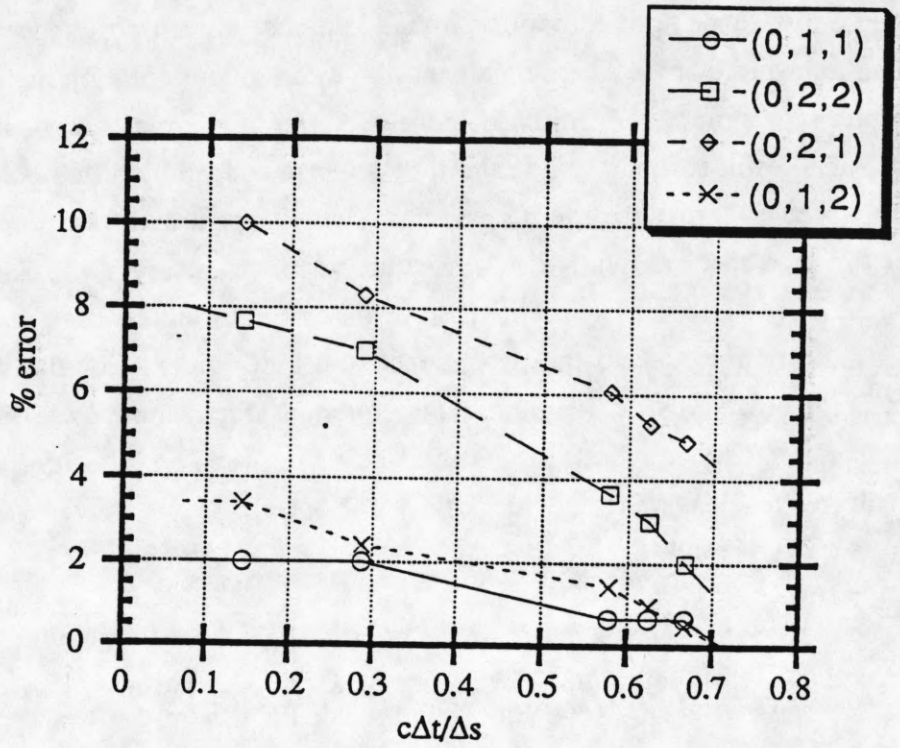

Fig. 4.2 Plot of the percentage error of the computed resonant frequencies vs. time step using the FDTD for various modes in a (3,4,6) pec cavity.
Note $\rho^{1/2} = c\Delta t/\Delta s =$ 0.714: 810 iterations
0.667: 870 iterations
0.625: 925 iterations
0.578: 1000 iterations
0.288: 2000 iterations
0.144: 4000 iterations
0.072: 8000 iterations.

be improved by increasing the time step rather than decreasing it. In particular, it is found that a larger time step can reduce both the truncation and discretization errors of the finite difference approximation provided the discretization of space and time is fine enough to insure that the spectral content of the continuous solution lies primarily within the finite spectrum of the finite difference solution. The mathematical reason for this paradoxical result is found to be caused by an error cancellation that occurs between the leading (second-) order error terms associated with the central differencing approximation of the time and space derivatives. As the time step is made larger, the cancellation can be shown to increase thereby reducing the overall error. Complete cancellation in 2-D and 3-D is not possible due to the dependence and independence of the spatial and time differencing errors, respectively, on the direction of propagation. Various aspects of the mathematical analysis were then verified by using the Yee algorithm to compute the resonant frequencies of a rectangular cavity.

4.9 References

[1] R.D. Richtmyer and K.W. Morton, *Difference Methods for Initial-Value Problems*. 2nd ed., New York: Interscience Publishers, 1967.

[2] J. Gary, "On the optimal time step and computational efficiency of difference schemes for PDE," *J. Comp. Phys.*, vol. 16, pp. 298-303, 1974.

[3] I.S. Kim and W.R.J. Hoefer, "Effect of the stability factor on the accuracy of two-dimensional TD-FD simulations," *IEEE AP-S International Symposium Digest,* vol 2, pp. 1108-1111, June 1989.

[4] R.C. Booten, "The accuracy of wave solutions with the finite-difference time domain method," *URSI Radio Science Meeting Digest*, p. 221, May 1990.

[5] H.-O. Kreiss and J. Oliger, "Comparison of accurate methods for the integration of hyperbolic equations," *Tellus*, vol. 24, no. 3, 1972.

[6] R. Vichnevetsky and J.B. Bowles, *Fourier Analysis of Numerical Approximations of Hyperbolic Equations*. Philedelphia: SIAM, 1982.

[7] L.N. Trefethen, "Group velocity in finite difference schemes," *SIAM Rev.*, vol. 24, pp. 113-136, 1982.

[8] L.B. Felsen, "Propagation and diffraction of transient fields in non-dispersive and dispersive media," *Transient Electromagnetic Fields*, L.B. Felsen, ed., vol. 10, New York: Springer-Verlag, pp. 16-22, 1976.

[9] A. Taflove and K.R. Umashankar, "The finite-difference time-domain for numerical modeling of electromagnetic wave interactions," *Electromagnetics*, vol. 10, no. 1, pp. 105-126, 1990.

[10] W.C. Chew, *Waves and Fields in Inhomgeneous Media.* New York: Van Nostrand Reinhold, 1990.

[11] F.B. Hildebrand, *Finite Difference Equations and Simulations.* Englewood Cliffs: Prentice-Hall, Inc., 1968.

[12] G.D. Smith, *Numerical Solutions of Partial Differential Equations,* 2nd ed. Oxford: Clarendon Press, 1978.

CHAPTER 5

COMPARISON OF 2-2 SCHEMES VS. 2-4 SCHEMES IN THE FINITE DIFFERENCE TIME DOMAIN SOLUTIONS OF MAXWELL'S EQUATIONS

5.1 Introduction

Presently, the Yee algorithm is the most commonly used form of the finite difference time domain (FDTD) scheme being used to solve Maxwell's equations. The Yee algorithm is what mathematicians call a 2-2 differencing scheme, i.e., second-order accurate finite differencing of the time and space derivatives, respectively. Despite its proven utility in the solution of transient electromagnetic problems, the Yee algorithm may not be the most efficient form of FDTD available. There have been studies which purport that 2-4 differencing schemes (second-order accurate differencing of the time derivative, fourth-order accurate differencing of the space derivative) possess the optimal balance between accuracy and computation [1]-[4]. Yet despite the presence of such literature there has been, aside from a brief abstract [5], very little published mathematical or numerical work within the electromagnetics community on the application of 2-4 schemes in the solution of Maxwell's equation.

The purpose of this work is to discuss the possible mathematical advantages and disadvantages of using a 2-4 differencing scheme rather than the standard Yee algorithm to solve Maxwell's equations. To do this we will determine the 3-D and 2-D stability conditions for a 2-4 scheme of the Maxwell's equation and derive expressions for the truncation and discretization error using Fourier analysis. Various ways to decrease the truncation and discretization errors are then considered. It is found that the 2-4 scheme has a stability criterion that is slightly stricter than that of a 2-2 scheme but that a 2-4 scheme will suffer from less grid anisotropy than a 2-2 scheme. It is also found that the truncation error of a 2-4 scheme can be made fourth-order accurate by successively decreasing the time step or, in the some cases, by using an effective dielectric concept. On the downside, the 2-4 scheme is found to require twice as much computation as the Yee algorithm. Moreover, the 2-4 scheme is found to have less spatial resolution than the Yee algorithm and, consequently, may be more susceptible to errors caused by aliasing between spectral components. Numerical simulations of a small cavity resonator are used to verify various aspects of the analysis.

5.2 Derivation of the 2-4 Stability Condition of the Scalar-Wave Equation

Though the stability criterion for a 2-2 differencing scheme of the scalar-wave equation is well-known, i.e., [6], there is very little if anything in the published literature regarding the stability of a 2-4 differencing scheme of Maxwell's equations. In this section we will use the von Neumann stability analysis [7] to derive the 2-4 stability condition. For brevity, we will assume the variable conventions of the previous chapter without explicitly stating them. We begin by assuming wave propagation in unbounded, homogeneous, isotropic free space excluding the sources. Thus, we can simplify Maxwell's equations to six scalar-wave equations. By using the Taylor series expansion to approximate the derivatives, one obtains the following 2-4 difference scheme, i.e.,

$$u_{m,n,p,l+1} = 2u_{m,n,p,l} + u_{m,n,p,l-1} - (\frac{c\Delta t}{\Delta s})^2\{-\frac{1}{12}(u_{m+2,n,p,l} + u_{m,n+2,p,l} + u_{m,n,p+2,l} + u_{m-2,n,p,l} + u_{m,n-2,p,l} + u_{m,n,p-2,l}) + \frac{4}{3}(u_{m+1,n,p,l} + u_{m,n+1,p,l} + u_{m,n,p+1,l} + u_{m-1,n,p,l} + u_{m,n-1,p,l} + u_{m,n,p-1,l}) - \frac{15}{2}u_{m,n,p,l}\} \tag{5.1}$$

We now assume that any solution to the finite difference equation can be represented using an infinite superposition of spectral components of the following form

$$\xi^l(k, \Delta s, \rho)e^{jk\cdot r_{mnp}} \tag{5.2}$$

where ξ is called the amplification factor. Substituting (5.2) into (5.1) and using trigonometric identities, we can obtain the following equation,

$$\xi^2 - B\xi + 1 = 0 \tag{5.3}$$

where

$$B = -(2 + \rho[-\frac{1}{6}(\cos 2k_x\Delta x + \cos 2k_y\Delta y + \cos 2k_z\Delta z) + \frac{8}{3}(\cos k_x\Delta x + \cos k_y\Delta y + \cos k_z\Delta z) - \frac{15}{2}]) \tag{5.4}$$

Consequently,

$$\xi = \frac{-B \pm \sqrt{B^2 - 4}}{2} \tag{5.5}$$

Using the identity

$$cos2\theta = -1 + 2cos^2\theta \tag{5.6}$$

(5.4) can be rewritten as

$$B = -(2 - \frac{\rho}{3}\{(cos k_x \Delta x - 7)(cos k_x \Delta x - 1) + (cos k_y \Delta y - 7)(cos k_y \Delta y - 1) + (cos k_z \Delta z - 7)(cos k_z \Delta z - 1)\} \tag{5.7}$$

It can be seen that the largest value of B will occur when all cosine terms are equal to zero. This implies that

$$|B|_{max} = |2 - 16\rho| \tag{5.8}$$

For stability, ξ must be less than or equal to 1 or, equivalently, from (5.5) $|B|_{max} \leq 2$. Consequently, the stability condition becomes

$$\rho = (\frac{c\Delta t}{\Delta s})^2 \leq \frac{1}{4} \qquad \text{(for 3-D)} \tag{5.9}$$

Similarly, the 2-D stability criterion is

$$(\frac{c\Delta t}{\Delta s})^2 \leq \frac{3}{8} \qquad (for\ 2\text{-}D) \tag{5.10}$$

5.3 Spectral Decomposition of the Finite Difference Solution

We begin by assuming that any solution to (5.1) can be represented as a Fourier transform, i.e.,

$$u(m\Delta x, n\Delta y, p\Delta z, l\Delta t)$$

$$= \int_{-\infty}^{\infty}\int_{-\infty}^{\infty}\int_{-\infty}^{\infty}\int_{-\infty}^{\infty} \bar{u}(k,\Omega) e^{j\Omega l\Delta t} e^{-jk\cdot r_{mnp}} dk_x dk_y dk_z d\Omega \tag{5.11}$$

By substituting (5.11) into (5.1), we can derive the following dispersion relation

$$\sin(\frac{\Omega\Delta t}{2}) = (\rho[\frac{1}{24}(\cos 2k_x\Delta x + \cos 2k_y\Delta y + \cos 2k_z\Delta z) - \frac{2}{3}(\cos k_x\Delta x + \cos k_y\Delta y + \cos k_z\Delta z) + \frac{15}{8}])^{1/2} \tag{5.12}$$

If we assume stability, the binomial expansion in conjunction with the series expansions of sine and inverse sine can be used to derive an explicit expression for Ω, i.e.,

$$\Omega(k) = \omega(k) + \varepsilon_p(k, \Delta s, \rho) \tag{5.13}$$

where

$$\varepsilon_p(k,\Delta s,\rho) = \frac{1}{24}\rho\frac{\omega(k)^3}{c^2}(\Delta s)^2 - \frac{1}{20}\frac{\omega(k)^5}{c^4}[\frac{1}{9}(\cos^6\alpha + \cos^6\beta + \cos^6\gamma) - \frac{3}{32}\rho^2](\Delta s)^4 + O((\Delta s)^6) \tag{5.14}$$

and $\omega(k)$ and the direction cosines are defined in the previous chapter.

Equation (5.12) shows that only three of the four components of integration in (5.11) are truly independent. Consequently, (5.11) can be reduced to a triple integral. Moreover, because the dispersion relation is periodic with respect to k_x, k_y, k_z, i.e.,

$$\sin(\frac{\Omega\Delta t + N_1\pi}{2}) = (\rho[\frac{1}{24}(\cos 2(k_x\Delta x + N_2\pi) + \cos 2(k_y\Delta y + N_3\pi) + \cos 2(k_z\Delta z + N_4\pi)) - \frac{2}{3}(\cos(k_x\Delta x + N_2\pi) + \cos(k_y\Delta y + N_3\pi) + \cos(k_z\Delta z + N_4\pi)) + \frac{15}{8}])^{1/2} \tag{5.15}$$

where N_1, N_2, N_3, N_4 are integers and $k_x\Delta x, k_y\Delta y, k_z\Delta z \in [-\pi, \pi], \Omega\Delta t \in [-2\pi, 2\pi]$, we may also reduce the limits of integration, i.e.,

$$u(m\Delta x, n\Delta y, p\Delta z, l\Delta t)$$

$$= \int_{-a}^{a}\int_{-a}^{a}\int_{-a}^{a} \tilde{u}''(k) e^{j\varepsilon_p(k,\Delta s,\rho)l\Delta t} e^{j\omega(k)l\Delta t} e^{-jk\cdot r_{mnp}} dk_x dk_y dk_z \tag{5.16}$$

where $a=\pi/\Delta s$.

5.4 The Relationship Between Higher-Order Schemes and Bandwidth

By examining the bandwidth of the spatial domain and comparing it with the bandwidth of the time domain, we can substantiate a rule of thumb used by finite difference practitioners. Specifically, it has been stated that higher-order differencing schemes are generally not recommended due to the possibility of spurious solutions [8]. Equation (5.15) demonstrates that the 2-4 differencing scheme has resulted in a decrease in the plane wave spectrum compared to that of the 2-2 differencing scheme (see Chapter 4). In particular, we note that even though their frequency bandwidths are equivalent their k-space bandwidths are not. Consequently, a 2-4 scheme will possess the same time resolution as the 2-2 scheme but less spatial resolution. This, in turn, implies that the 2-4 scheme will be more susceptible to errors due to aliasing than a lower order 2-2 scheme for identical time and space discretizations. This suggests, in general, that higher-order differencing approximations of either the space or time derivatives will result in a drastic decrease in its spectral bandwidth, i.e, those plane waves which can be modeled uniquely. We conclude that a disadvantage of using higher order schemes, in general, is that finer discretization may be required to the suppress spurious solutions caused by aliasing. Further work needs to be done on determining, in practice, how detrimental the reduction in bandwidth will affect a 2-4 differencing scheme of Maxwell's equations.

5.5 Reduction of the Truncation Error

From the Taylor series expansion of (5.1) the truncation error, ε_{trunc}, is

$$\varepsilon_{trunc}(r,\Delta s,\rho)$$
$$= [\frac{\rho(\Delta s)^2}{12c^4}\frac{\partial^4}{\partial t^4} + (\Delta s)^4(-\frac{1}{90}(\frac{\partial^6}{\partial x^6}+\frac{\partial^6}{\partial y^6}+\frac{\partial^6}{\partial z^6}) + \frac{\rho^2}{360c^6}\frac{\partial^6}{\partial t^6})]U(x,y,z,t) + O((\Delta s)^6)$$

(5.17)

Substituting the spectral representation of the continuous solution given in the previous chapter, we find that

$$\varepsilon_{trunc}(r,\Delta s,\rho) = (\Delta s)^2 C_{time2}(r,\rho) + (\Delta s)^4[-C_{space4}(r,\rho) + C_{time4}(r,\rho)] + O((\Delta s)^6)$$

(5.18)

where

$$C_{time2} = \frac{1}{12}\int_{-\infty}^{\infty}\int_{-\infty}^{\infty}\int_{-\infty}^{\infty}\tilde{U}'(k)e^{j\omega(k)t}e^{jk\cdot r}(\frac{\omega(k)}{c})^4\rho dk_x dk_y dk_z \qquad (5.19)$$

$$C_{time4} = \frac{-1}{360}\int_{-\infty}^{\infty}\int_{-\infty}^{\infty}\int_{-\infty}^{\infty}\tilde{U}'(k)e^{j\omega(k)t}e^{jk\cdot r}(\frac{\omega(k)}{c})^6\rho^2 dk_x dk_y dk_z \qquad (5.20)$$

$$C_{space4} = \frac{-1}{90}\int_{-\infty}^{\infty}\int_{-\infty}^{\infty}\int_{-\infty}^{\infty}\tilde{U}'(k)e^{j\omega(k)t}e^{jk\cdot r}(\frac{\omega(k)}{c})^6(\cos^6\alpha+\cos^6\beta+\cos^6\gamma)dk_x dk_y dk_z$$

(5.21)

where $U'(k)$ is the transform of the continuous solution, C_{time2}, C_{time4}, are the second- and fourth-order error contributions due to the time differencing and C_{space4} is the fourth-order error contributions due to the space differencing. Unlike the 2-2 scheme analyzed in the previous chapter, it can be seen that decreasing rather than increasing the time step will reduce the truncation error, because the spatial differencing and the time differencing are of different orders of accuracy. As the time step is made smaller, however, the second-order error can be made to vanish leaving only the fourth-order spatial error. Unfortunately, in practice, one can ill afford to make the time step too small due to the associated increase in computation time. Consequently, it is useful to know the largest time step that can be used to produce a fourth-order truncation error. To determine this time step, we simply equate the largest value of the fourth-order space error with the second-order time error and solve for the time step, i.e., ρ. One finds that

$$\rho^{1/2} \le 2.3(\frac{\Delta s}{\lambda}) \qquad (5.22)$$

where $\lambda = \frac{2\pi}{\omega(k)}$.

Equation (5.21) shows that the condition for fourth-order accuracy is actually dependent on the frequency of the spectral component. That is, any frequency, $\omega(k)$, greater than that specified by (5.21) will result in fourth-order truncation error whereas any frequency less than that will result in second-order truncation error. It is, however, possible to make the finite difference equation appear to be completely fourth-order accurate at lower frequencies provided the time step is made small enough, i.e., $\Delta s/\lambda < 1/20$, because, in practice, the observable difference between a second- and a fourth-order error will become increasingly less noticeable [1].

5.6 Reduction of the Discretization Error

Using (5.14) and the results from the previous chapter, the discretization error of the 2-4 scheme can be written as

$$\varepsilon_{disc}(r_{mnp}, l\Delta t, \Delta s, \rho) = \varepsilon_a(r_{mnp}, l\Delta t, \Delta s, \rho) + \varepsilon_\infty(r_{mnp}, l\Delta t, \Delta s) + \varepsilon_{-\infty}(r_{mnp}, l\Delta t, \Delta s) \tag{5.23}$$

where

$$\varepsilon_a(r_{mnp}, l\Delta t, \Delta s, \rho) = \int_{-a}^{a}\int_{-a}^{a}\int_{-a}^{a}(\tilde{U}'(k) - \tilde{u}''(k)e^{j\varepsilon_p(k,\Delta s,\rho)l\Delta t})e^{j\omega(k)l\Delta t}e^{-jk\cdot r_{mnp}}dk_x dk_y dk_z \tag{5.24}$$

$$\varepsilon_\infty(r_{mnp}, l\Delta t, \Delta s) = \int_{a}^{\infty}\int_{a}^{\infty}\int_{a}^{\infty}\tilde{U}'(k)e^{j\omega(k)l\Delta t}e^{-jk\cdot r_{mnp}}dk_x dk_y dk_z \tag{5.25}$$

$$\varepsilon_{-\infty}(r_{mnp}, l\Delta t, \Delta s) = \int_{-\infty}^{-a}\int_{-\infty}^{-a}\int_{-\infty}^{-a}\tilde{U}'(k)e^{j\omega(k)l\Delta t}e^{-jk\cdot r_{mnp}}dk_x dk_y dk_z \tag{5.26}$$

If we assume that the discretization is fine enough so that the spectral content of the continuous solution lies within [-a,a], the discretization error can be decreased by reducing the phase error, ε_p. By comparing (5.14) and (5.18), it can be seen that the same condition that minimizes the truncation error, i.e., (5.21), will also minimize the discretization error.

So far we have only considered ways to reduce the truncation and discretization errors of the transient finite difference solution. Often, however, one is interested in the

frequency response rather than the actual transient response of a system. Consequently, it is important to also consider ways to reduce the truncation and discretization errors at individual frequencies. One way to do this is to use an effective dielectric concept. To elaborate further, we note that the leading order term of ε_p , unlike that of the 2-2 schemes, is independent of direction. If we assume a homogeneous, isotropic environment, the effect of this error will be to add extra phase to each spectral component at every time step. This additional phase, however, is identical to the presence of a dielectric constant, ε_{eff} , not specified in the original problem. Therefore, most of the phase error can in fact be removed simply by changing our perception of the system we are solving. In order to use this information to improve the accuracy of the finite difference solution to the original problem, i.e., without ε_{eff}, one simply scales the frequency response accordingly.

To compute the effective dielectric constant, ε_{eff}, we begin by redefining $\omega(k)$, i.e.,

$$\omega(k) = \frac{c}{\sqrt{\varepsilon_{eff}}}\sqrt{(k_x^2 + k_y^2 + k_z^2)} \tag{5.27}$$

Substituting (5.26) into (5.15) and (5.17) one obtains

$$\Omega = \omega\sqrt{\varepsilon_{eff}} + \frac{1}{24}\frac{\rho(\Delta s)^2}{c^2}(\omega)^3(\sqrt{\varepsilon_{eff}})^3 + O((\Delta s)^4) \tag{5.28}$$

For the phase error (5.17) to be of fourth-order, $\Omega=\omega$. This implies that

$$(\sqrt{\varepsilon_{eff}})^3 + \frac{24}{(\omega\Delta t)^2}\sqrt{\varepsilon_{eff}} - \frac{24}{(\omega\Delta t)^2} = 0 \tag{5.29}$$

Equation (5.28) is a standard cubic equation with respect to $\sqrt{\varepsilon_{eff}}$. It can be shown that it will always have two complex roots and one real root. Assuming propagation in a lossless media we consider only the real solution. This is given analytically by

$$\sqrt{\varepsilon_{eff}} = (\frac{b}{2} + K)^{3/2} - (-\frac{b}{2} + K)^{3/2} \tag{5.30}$$

where

$$b = \frac{24}{(\omega \Delta t)^2} = \frac{24}{(2\pi)^2 \rho} \left(\frac{\lambda}{\Delta s}\right)^{-2} \tag{5.31}$$

$$K = \sqrt{\frac{b^2}{4} + \frac{b^3}{27}} \tag{5.32}$$

Having determined the effective dielectric constant, it is important to determine how much improvement in accuracy can be achieved. By lumping the effect of the second-order phase error into an effective dielectric constant, clearly the phase error given by (5.14) will be of fourth-order. This, in turn, implies that the discretization error at each frequency will inevitably decrease. To determine what the resulting improvement in the truncation error is we note, from previous analyses of the 2-2 and 2-4 schemes, that in every case the order of the phase error has been equal to the order of the truncation error. On the basis of this qualitative observation, it is believed that the effective dielectric constant approach will make both the phase error and truncation error fourth-order.

5.7 The 2-4 vs. 2-2 Differencing Schemes of the Wave Equation

By comparing the stability criterion for the 2-4 scheme, i.e., (5.9), with that of the 2-2 scheme it is clear that the latter is a more stable scheme. Therefore, one can deduce that the 2-2 scheme can be run at a larger time step thereby reducing the number of computations required to reach a steady state. This result accentuates the relative computational efficiency of the 2-2 scheme especially since a 2-2 scheme already requires half the computation of a 2-4 scheme per iteration regardless of the time step.

Perhaps, the most important difference between the 2-2 and 2-4 schemes is in accuracy. Though mathematically, both schemes are of second-order truncation error, the accuracy of both schemes may be improved beyond this through proper choice of the time step. In particular, the truncation error of a 2-4 scheme can be made fourth-order provided the time step is decreased to zero, whereas the truncation error of the 2-2 scheme can also be reduced but to a lesser degree by choosing the largest time step allowed by stability. In general, we conclude that the 2-4 scheme is more accurate under the condition that a sufficiently small time step is chosen. If the time step is not chosen small enough, it is possible for the 2-2 scheme to actually be more accurate than the 2-4 scheme; consequently, the choice of time step is essential in justifying the use of the more

computationally intensive 2-4 scheme over the less intensive 2-2 scheme. An important exception to this statement is found when the frequency response of a homogeneous, isotropic system is being computed. As outlined earlier, in such cases the effective dielectric constant concept can be used to increase the accuracy of the 2-4 scheme, i.e., fourth-order truncation error, regardless of the time step.

A subtle difference between the 2-2 and the 2-4 schemes which may have an important effect on the relative accuracies of each method, involves the domain of their bandwidths. Though both schemes have periodic dispersion relations in k-space, the spectrum of the 2-2 scheme is twice as broad as that of the 2-4 scheme in the spatial domain. This implies that the 2-2 scheme will be less sensitive to aliasing errors than the 2-4 scheme for the same space discretization. Therefore, a 2-4 scheme may require a finer space discretization than a 2-2 scheme as well as a smaller time step to achieve better accuracy. Another way to reduce the inaccuracies due to aliasing, which we mention only briefly, is to introduce a diffusion term in the 2-4 scheme which will attenuate the large k-space components of the continuous solution [3], [9]. This approach, however, has the drawback of increasing the number of computations.

Another important difference between the 2-2 scheme and the 2-4 scheme is in their grid anisotropy. In the context of the analysis given in this work, grid anisotropy is caused by the spatial dependence of the phase error introduced into each spectral component by the finite differencing of time and space. The effect is to advance or retard the phase or wave fronts of an electromagnetic field depending on the direction of propagation, which, in turn, causes an artificial distortion of the field. Though the phase error of both the 2-4 and 2-2 schemes are mathematically of second-order, the phase error of the 2-2 scheme turns out to be more dependent on direction due to the presence of second-order spatial differencing than the phase error of the 2-4 scheme. Consequently, a 2-4 scheme will suffer from much less grid anisotropy than a 2-2 scheme. It is important to note, however, that less grid anisotropy does not necessarily imply that the 2-4 scheme will be more accurate relative to the exact solution than the 2-2 scheme; it means that a 2-4 scheme will tend to preserve the physical shape of the fields better.

5.8 Numerical Verification of the Analysis

To verify the analysis presented previously, the impulse response of a perfect electrical conductor (pec) rectangular cavity was computed using a 2-4 differencing

scheme of Maxwell's equations and compared with that for the exact solution. An example of a 2-4 difference scheme consistent with the Yee mesh is given by

$$E_x^{l+1}(m+1/2,n,p) = E_x^{l+1}(m+1/2,n,p)+\frac{c\Delta t}{\Delta s}\eta(\frac{9}{8})\{H_z^{l+1/2}(m+1/2,n+1/2,p) - H_z^{l+1/2}(m+1/2,n-1/2,p) - H_y^{l+1/2}(m+1/2,n,p+1/2) + H_y^{l+1/2}(m+1/2,n,p-1/2) - \frac{1}{27}[H_z^{l+1/2}(m+1/2,n+3/2,p) - H_z^{l+1/2}(m+1/2,n-3/2,p) - H_y^{l+1/2}(m+1/2,n,p+3/2) + H_y^{l+1/2}(m+1/2,n,p-3/2)]\} \tag{5.33}$$

Similar formulas for the other electric and magnetic field components may also be derived but are omitted for brevity.

We begin by numerically verifying the 3-D stability criterion given by Equation (5.9). To do this, we place an electric field point source (Gaussian time dependence) inside a large pec cavity and plot the transient fields around the source using different time steps (see Fig. 5.1). It is found that time steps that are only slightly greater than (5.9), i.e., $\rho = 0.251$, will result in instability whereas time steps which are slightly less than (5.9), i.e., $\rho = 0.242$, will be stable after 1000 iterations. When ρ is equal to the theoretical stability limit of 0.250, the algorithm becomes unstable after several hundred iterations. We can conclude that the empirical stability limit is slightly stricter (3.0%) than that given by (5.9). The discrepancy can be attributed to the combination of round-off error and approximations in the physical constants.

To study the effect of time step on accuracy, the numerical simulations were run using several different time steps while keeping the total time of the simulation fixed. The frequency response was then computed using a discrete time Fourier transform (DTFT). Results for four TE modes, (0,1,1), (0,2,2),(0,2,1), (0,1,3), (0,1,2), of the cavity were then compared with the analytical solutions. The result are shown in Fig. 5.2. It is found that virtually all of the behaviour exhibited in this figure can be predicted by the previous analysis. Most notably, (5.23) dictates quantitatively the manner in which the accuracy of the computation will be improved. In particular, for large time steps it can be

seen that the dominant error term of the 2-4 scheme will be the second-order time error given by (5.19), i.e.,

$$\text{for large } \rho: \quad \varepsilon(k,\rho) \cong \varepsilon_{time}(\rho) \tag{5.34}$$

Because the sign of this error is positive, the phase of the exact solution can be shown to be larger after each iteration resulting in resonances which are higher than what they should be. On the other hand, for very small time steps, it can be seen that the dominant phase error will correspond to the fourth-order space error given by (5.18), i.e.,

$$\text{for small } \rho: \quad \varepsilon(k,\rho) \cong \varepsilon_{space}(k,\rho) \tag{5.35}$$

Unlike the time error term, however, this error has a negative sign associated with it and will cause the phase of the exact solution to be retarded slightly after each iteration. It can be shown that this retardation will result in computed resonances which are slightly lower than what they should be. It can be seen from Fig. 5.2 that this behaviour is indeed observed in all cases except for the first two resonances. Specifically, though there is increased in accuracy as the time step is made smaller, the limiting values of the first two resonances appear to be slightly higher than the exact solution rather than lower. A likely explanation for this phenomenon is the aliasing due to the finite bandwidth of the finite difference solutions.

One of the most important windfalls that one would expect from a higher-order scheme is an increase in the accuracy of the high frequency components. For time steps which satisfy the fourth-order criterion of (5.20) it is clear that the computed resonances shown in Fig. 5.2 are not only in very good agreement with those for the exact solution but that the high frequency agreement is much better than that of the 2-2 scheme (see Chapter 4). According to the effective dielectric concept, however, it should also be possible to make the larger time step solutions fourth-order accurate. To test this idea, the solutions of a 2-4 simulation which take into account an effective dielectric constant are compared with the exact solution. The results are again shown in Fig. 5.3. It can be seen that the effective dielectric concept results in a reasonably accurate prediction of the resonance curves. In theory, they should be within fourth-order error of each other with the numerical results being slightly less than the predicted.

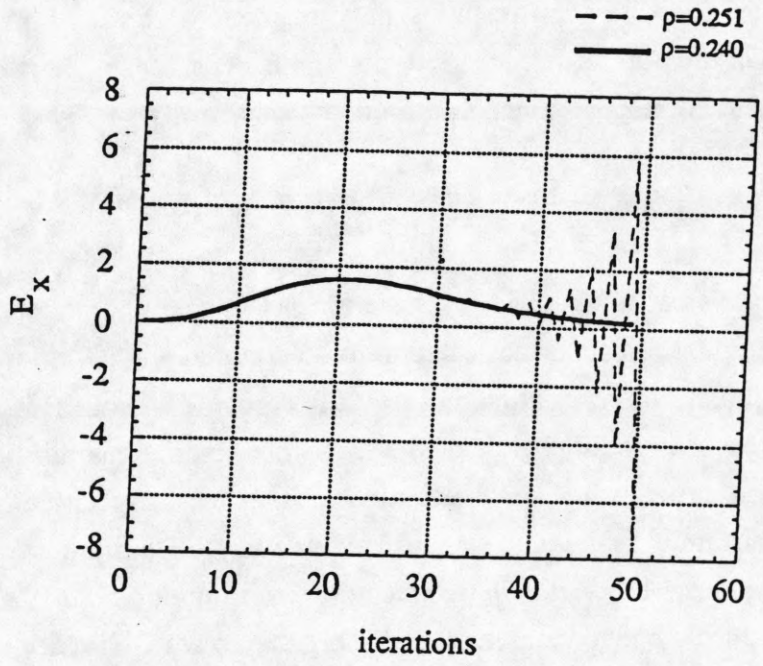

Fig. 5.1 Numerical validation of the 2-4 scheme stability criterion for Maxwell's equations. The excitation is a point source E_x field with a Gaussian time dependence located in the middle of a (60,60,60) cell pec cavity. The observation point is equal to the source point. The predicted stability limit is $\rho = 0.250$.

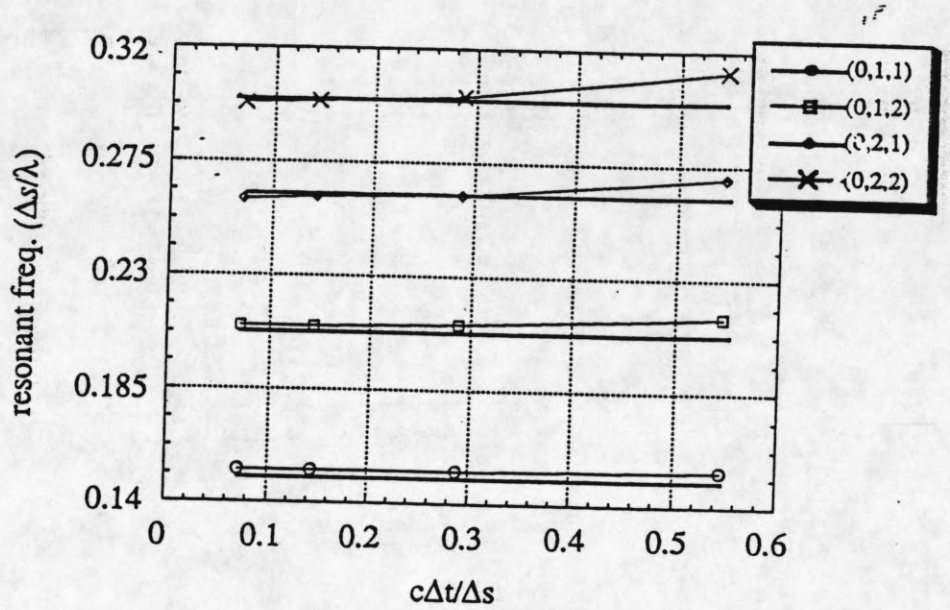

Fig. 5.2 Plot of the FDTD resonant frequencies for a (3,4,6) pec cavity vs. the time step for different modes. The straight lines represent the exact solutions.
Note $\rho^{1/2} = c\Delta t/\Delta s =$ 0.546: 1000 iterations
0.288: 2000 iterations
0.144: 4000 iterations
0.072: 8000 iterations.

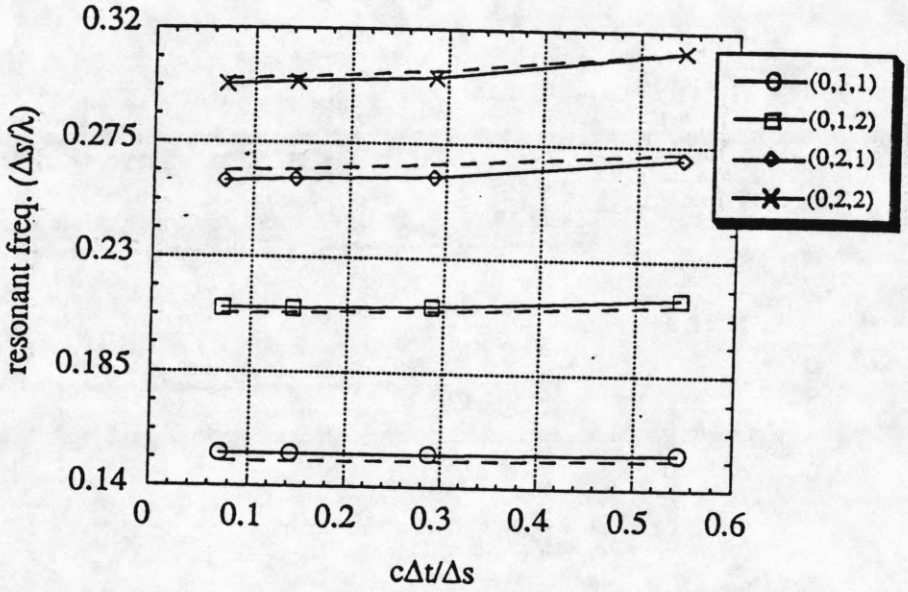

Fig. 5.3 Comparison of the 2-4 FDTD results with analytically predicted resonances using the effective dielectric constant concept (dotted line).

5.9 Conclusions

In this chapter, a quantitative comparison of the stability and accuracy of the 2-2 difference scheme and the 2-4 difference scheme of the wave equation in homogeneous, isotropic space was made. The stability condition for the 2-D and 3-D 2-4 difference schemes was derived and compared with that of the 2-2 scheme. It was found that the 2-4 stability condition is slightly stricter than that of the 2-2 scheme (approximately 15%). Analysis was also done to determine the relationship between time step and accuracy of a 2-4 scheme particularly in comparison with the 2-2 scheme. Under the assumption that the spectral content of the continuous solution was primarily within the finite spectrum of the finite difference solution, it was found that unlike the 2-2 scheme the discretization error of the 2-4 scheme can be made fourth-order as the time step is made smaller. In addition, it was found that the 2-4 scheme is much less anisotropic than the 2-2 scheme. It was shown that this isotropy can be exploited by using the concept of an effective dielectric constant to make the 2-4 scheme fully fourth-order accurate regardless of the size of the time step. Simple numerical results of a small rectangular cavity were given to verify the analysis and its conclusions.

5.10 References

[1] K.V. Roberts and N.O. Weiss, "Convective difference schemes," *Math. Comp.*, vol. 20, pp. 272-299, 1966.

[2] H.-O. Kreiss and J. Oliger, "Comparison of accurate methods for the integration of hyperbolic equations," *Tellus*, vol. 24, no. 3, 1972.

[3] D. Gottlieb and E. Turkel, "Disspative two-four methods for time-dependent problems," *Math. Comp.*, vol. 30, no. 136, pp. 703-723, Oct. 1976.

[4] J. Oliger, "Fourth-order difference methods for the initial boundary-value problem for hyperbolic equations," *Math. Comp.*, vol. 28, no. 125, pp. 15-25, Jan. 1974.

[5] J. Fang and K.K. Mei, "A higher-order finite difference scheme for the solution of Maxwell's equations in the time domain," presented at *IEEE Antennas Propagat. Soc. Int. Symp.*, San Jose, CA, p. 228, June 1989.

[6] A. Taflove and K.R. Umashankar, "The finite-difference time-domain for numerical modeling of electromagnetic wave interactions," *Electromagnetics*, vol. 10, no. 1, pp. 105-126, 1990.

[7] J. Von Neumann and R.D. Richtmyer, "A method for the numerical calculation of hydrodynamic shocks," *J. App. Phys.*, vol. 21, pp. 232-237, March 1950.

[8] W.H. Press, B.P. Flannery, S.A. Teukolsky, and W.T. Vetterling, *Numerical Recipes*. New York: Cambridge University Press, pp. 642-643, 1986.

CHAPTER 6

A HYBRID YEE ALGORITHM/SCALAR-WAVE EQUATION APPROACH

6.1 Introduction

In the past few years the Yee algorithm has been demonstrated to be a viable technique for solving electromagnetic scattering problems. However, it suffers from two drawbacks, computer time and computer memory. Though there are other formulations of Maxwell's equations which can be mathematically equivalent, namely, the finite difference approximation of the vector-wave equation and the scalar-wave equation, it appears that only the scalar-wave equation can provide a possible computational and memory advantage over the Yee algorithm. Though commonly used in two-dimensional frequency domain problems in the late 1960s and early 1970s , with the exception of [1], there have been very few applications of the scalar-wave equation in three dimensions in the time domain. The purpose of this work is to study the applicability of the scalar-wave equation formulation in reducing the memory and computation of the finite difference algorithm for 3-D open region problems. The major objectives of this work are 1) to show the mathematical conditions under which a finite difference scalar-wave equation may be used in three dimensions and to demonstrate its mathematical and numerical equivalencies to the Yee algorithm, 2) show that the scalar-wave equation can be combined with the Yee algorithm (and the vector-wave equation) as a means of reducing the memory by at least 33% and the computations by at least 40% in simulating many planar geometry problems while being numerically equivalent to a full Yee algorithm, and 3) show how absorbing boundary conditions may be effectively applied to components normal to the outer boundary using the divergence relation and the vector-wave equation.

6.2 Different Types of FDTD Formulations

6.2.1 The Yee algorithm

The Yee algorithm is a central difference approximation of Maxwell's curl equations written in explicit form. Typical examples of the electric and magnetic field finite difference equations for lossless media are listed below.

$$E_x^{l+1}(m+1/2,n,p) = E_x^l(m+1/2,n,p) + \frac{\Delta t}{\varepsilon(m+1/2,n,p)\Delta s}$$
$$\bullet[H_z^{l+1/2}(m+1/2,n+1/2,p) - H_z^{l+1/2}(m+1/2,n-1/2,p)$$
$$+H_y^{l+1/2}(m+1/2,n,p-1/2) - H_y^{l+1/2}(m+1/2,n,p+1/2)] \quad (6.1)$$

$$H_y^{l+1/2}(m+1/2,n,p+1/2) = H_y^{l-1/2}(m+1/2,n,p+1/2)$$
$$+\frac{\Delta t}{\mu(m+1/2,n,p+1/2)\Delta s} \bullet [E_z^l(m+1/2,n,p+1/2)$$
$$-E_z^l(m+1/2,n-1/2,p) + E_x^l(m+1/2,n,p-1/2)$$
$$-E_x^l(m+1/2,n,p+1/2)] \quad (6.2)$$

where m, n, p are defined such that $x = m\Delta x$, $y = n\Delta y$, $z = p\Delta z$

$\Delta s = \Delta x = \Delta y = \Delta z$ = uniform space discretization

l = time index such that $t = l\Delta t$

Δt = time discretization

ε=electric permittivity

μ=magnetic permeability.

A characteristic of these equations is that they are coupled, i.e., one cannot compute any single field component independently from the other components. Consequently, in order to advance the fields a single time step, 24 additions and subtractions and 6 multiplications per cell must be performed per cell. In addition, this also means that one must store six real numbers corresponding to the six field components to implement the algorithm.

6.2.2 The vector-wave equation

It is apparent from (6.1) and (6.2) that the Yee algorithm has a redundancy built into its formulation. In particular, one notes that it is possible to substitute all of the magnetic field terms in Equation (6.1), for example, strictly in terms of electric field expressions. By performing similar manipulations on the E_y and E_z equations one can reduce the total number of difference equations from 6 to 3. A complementary reduction can, of course, also be done with the magnetic fields expressions. This brings up the possibility of eliminating some of the additions and multiplications as well as reducing the memory requirements. To illustrate, replacing the magnetic field components in (6.1) will result in the following expression

$$E_x^{l+1}(m+1/2,n,p) = (2-4\left(\frac{v(m+1/2,n,p)\Delta t}{\Delta s}\right)^2)E_x^l(m+1/2,n,p)$$
$$-E_x^{l-1}(m+1/2,n,p)+\left(\frac{v(m+1/2,n,p)\Delta t}{\Delta s}\right)^2(E_x^l(m+1/2,n+1,p)$$
$$+E_x^l(m+1/2,n-1,p)+E_x^l(m+1/2,n,p+1)+E_x^l(m+1/2,n,p-1)$$
$$-E_y^l(m+1,n+1/2,p)+E_y^l(m+1,n-1/2,p)-E_z^l(m+1,n,p+1/2)$$
$$+E_z^l(m+1,n,p-1/2)+E_y^l(m,n+1/2,p)-E_y^l(m,n-1/2,p)$$
$$+E_z^l(m,n,p+1/2)-E_z^l(m,n,p-1/2)) \tag{6.3}$$

It can be shown that these equations are equivalent to the central difference approximation of the vector-wave equation, i.e.,

$$\nabla x\nabla x\overline{E}+\frac{1}{v^2}\frac{\partial^2}{\partial t^2}\overline{E}=0 \tag{6.4}$$

where $v^2 = c^2/\varepsilon_r(m+1/2,n,p)$, c=speed of light in free space, ε_r = relative permittivity

Because (6.3) is derived directly from the Yee algorithm, (essentially a discrete manipulation of the continuous vector identities) their solutions will be identical (a fact verified by computer simulation). However, despite having eliminated the explicit computation of the magnetic fields, we have actually increased the total number of additions per iteration from 24 to 39 per cell. Moreover, since values at l and l -1 must be stored, the memory requirements turn out to be exactly the same as for the Yee algorithm. We conclude that a fully explicit finite difference vector-wave formulation will provide little, if any, practical advantage over the commonly used Yee algorithm.

6.2.3 The scalar-wave equation

To further simplify the Yee algorithm we can make the common assumption that the fields will be divergence free. The corresponding central difference approximation of this condition is

$$E_x^l(m+1/2,n,p)-E_x^l(m-1/2,n,p)+E_y^l(m,n+1/2,p)$$
$$-E_y^l(m,n-1/2,p)+E_z^l(m,n,p+1/2)-E_z^l(m,n,p-1/2)=0 \tag{6.5}$$

Substituting this expression into (6.3) we obtain

$$E_x^{l+1}(m+1/2,n,p) = (2-6\left(\frac{v\Delta t}{\Delta s}\right)^2)E_x^l(m+1/2,n,p)$$
$$-E_x^{l-1}(m+1/2,n,p)+\left(\frac{v\Delta t}{\Delta s}\right)^2(E_x^l(m+1/2,n+1,p)$$
$$+E_x^l(m+1/2,n-1,p)+E_x^l(m+1/2,n,p+1)+E_x^l(m+1/2,n,p-1)$$
$$-E_x^l(m+3/2,n,p)+E_x^l(m-1/2,n,p)) \tag{6.6}$$

where to legitimately substitute (6.5) into (6.3) the permittivity, ε, was made constant. It can be shown that the resulting expression (6.6) is the central difference approximation of the scalar-wave equation, i.e.,

$$\nabla^2\overline{E}+\frac{1}{v^2}\frac{\partial^2}{\partial t^2}\overline{E}=0 \tag{6.7}$$

where v is a constant.

Unlike the finite difference approximation of the vector-wave equation one notes that there is a modest computational savings in its implementation over the Yee algorithm. In particular, the scalar-wave equation formulation requires only 21 additions and 6 multiplications per cell as opposed to 24 addition and 6 multiplications while possessing the same memory requirements. However, the true advantage of a scalar-wave approach is not just confined to these meager savings but in the potential flexibility it offers. To be specific, the Yee algorithm and the finite difference vector-wave algorithm are made up of coupled equations in which one cannot omit computation of any field components. The scalar-wave formulation, on the other hand, consists of a set of uncoupled equations in which a given field component may be computed without necessarily having to compute the other field components. Hence, by making use of the scalar-wave formulation, it may be possible to reduce the computation and memory of the algorithm simply by omitting some of the field quantities and retaining a reduced number of fields. Since the scalar-wave formulation is directly derivable from the Yee algorithm, one would expect this reduced field formulation to generate results that are identical to that of the Yee algorithm provided the fields are divergence free.

6.2.4 On implementing a finite difference scalar-wave equation

Though there may be some advantage in using a finite difference scalar-wave formulation, one must exercise some care in implementation, because the scalar-wave equation, unlike the Yee algorithm or the equivalent vector-wave formulation, is valid if and only if the fields are divergence free. This poses some restriction on its application since this condition is not always true throughout the system. Furthermore, even if the physics of the problem dictates divergence free fields, it is not clear whether iterating a scalar-wave formulation will necessarily preserve the divergence-free condition as time is advanced. It turns out that it can be shown that if the initial conditions are such that the fields are divergence free at time, t_0, the scalar-wave formulation will in fact preserve the divergence-free condition for all time, $t > t_0$. A short mathematical proof of this is given in Appendix A. Hence, we conclude that the two conditions that are required to properly apply the scalar-wave formulation are 1) that the electric and magnetic field source distributions be divergence free for all time, 2) that the physics of the problem dictate that the resulting fields also be divergence free for all time.

6.3 A Hybrid Approach

6.3.1 Preliminary validation

Considering the previous discussion, the application of the scalar-wave formulation to simulate transient electromagnetic radiation, in general, appears to be somewhat limited. A notable exception to this statement is the scalar-wave formulations in two dimensions, because one can always formulate the 2-D problem in such a way that at least one of the field components will be divergence free regardless of the presence of dielectric interfaces and pec structures. In addition, it can be shown that one can always find a divergence-free source/initial condition in such cases. For 3-D problems, the applicability of the scalar-wave formulation is much more restricted. One can extend the applicability of the scalar-wave formulation in 3-D by partitioning the system into regions that are divergence free and other regions in which they are not. One can then apply the scalar-wave formulation in the divergence-free regions and in the remaining regions apply an alternate algorithm, such as the Yee algorithm or the FDTD vector-wave equation,. To verify the feasibility of this concept, a nondivergence free source radiating in a (50,50,50) isotropic, homogeneous space was simulated. The source was chosen to be a single cell electric field sinusoidal excitation with the problem domain partitioned

into two regions (Fig. 6.1). Region 1 was chosen to be a small nondivergence-free volume around the source and region 2 was chosen to consist of the remaining volume. The vector-wave equation formulation was used to simulate the fields in region 1 and the scalar-wave equation formulation was used to simulate the field in region 2. To lessen the effects of the outer boundary, the number of iterations was limited to 60. The resulting field distribution in the plane of the source was then compared with that obtained using a full Yee algorithm over the entire problem. A typical sampling is given in Table 6.1. It can be seen that the results are virtually identical to one another, i.e., within 0.1% of each other with discrepancies attributable to machine error and to the inconsistencies between the physical constants used in each formulation. Parenthetically, it should be noted that identical results could also have been produced if we had replaced the vector-wave equation in region 1 with the Yee algorithm.

6.3.2 Partitioning the problem into planar regions

Despite having demonstrated the validity of a hybrid scheme, one notes that for problems partitioned in the previous manner, there is actually little to be gained by using a hybrid approach, because the number of field components in the scalar-wave formulation used in region 2 could not be reduced to properly interface the field information with region 1. Obviously, one of the major factors in determining how much can be gained from a scalar formulation is how one partitions the system. If one partitions the problem in such a way that the divergence-free regions may be completely interfaced with the nondivergence free regions without having to use all three field components, one can omit field components from the algorithm and reduce the computation and memory. An example of such a scheme is to partition the problem into planar volumes. Since each interface is two dimensional in nature, the uniqueness theorem tells us that the fields within each region will be completely characterized by the two tangential components on that planar interface. Consequently, one may neglect the normal component and use the scalar-wave equation formulation on the two tangential components in each divergence free region. The result is a reduction in the number of computations compared to those for the Yee algorithm from 24 additions and 6 multiplications to 14 additions and 4 multiplications. For the special case of modeling free space, however, the number of additions can be reduced to just 12 additions simply by choosing the time step to be near the stability limit. (We note that although it can be shown that choosing such a time step will increase the accuracy, care must be taken in doing this due to the danger of instability. For all of the simulations given in this work,

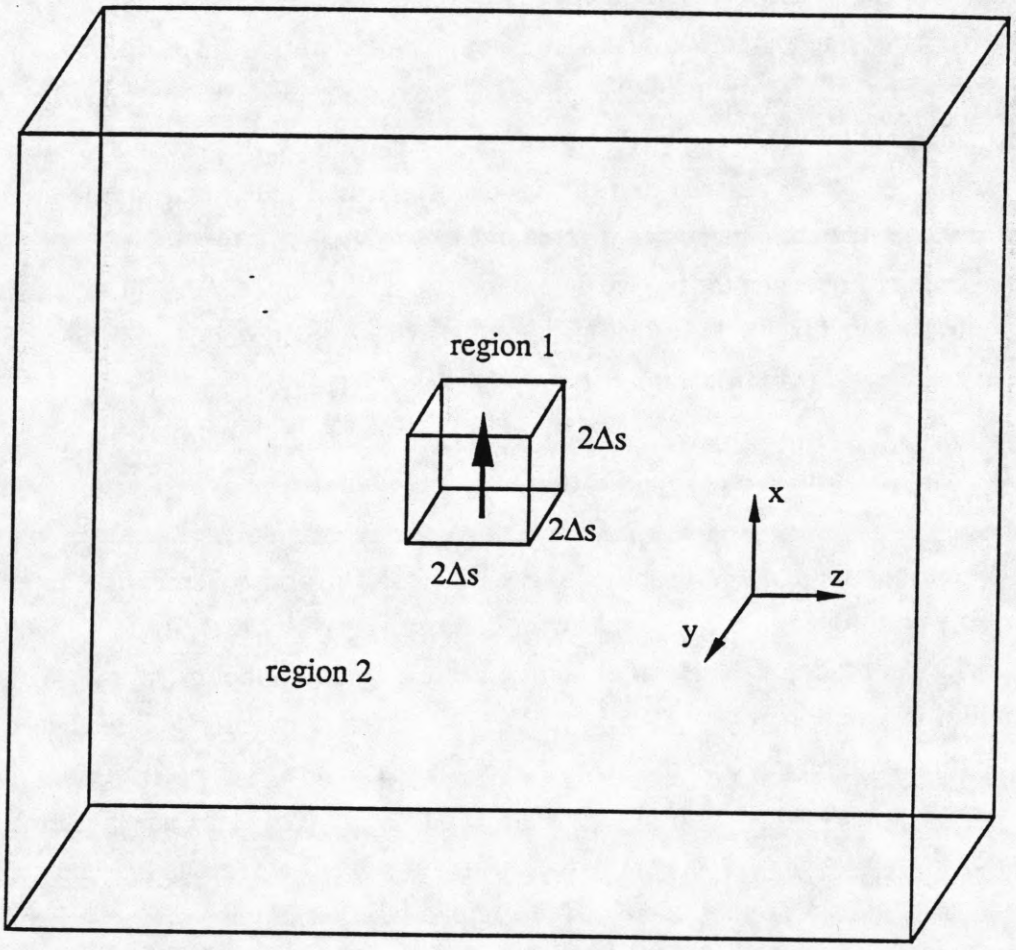

Fig. 6.1 Partitioning scheme used to apply a combined finite difference vector-wave equation/scalar-wave equation formulation for a single cell E_x-field excitation radiating in infinite, isotropic free space. Region 1 is defined to be a cubic volume around the source of (2Δs, 2Δs, 2Δs) in which the vector-wave formulation is to be applied, where Δs = cell size. Region 2 is defined to be all of the remaining space in which the scalar-wave formulation is applied to all electric field components.

Table 6.1 Comparison of the E_x field values in the xz plane (y=25) for an x-directed sinusoidal point dipole inside a 50,50,50 FDTD uniform mesh using a) the combined wave equation/vector-wave equation, b) the standard Yee algorithm. The number of iterations was 60, $c\Delta t/\Delta s = 0.5$.

z axis →

x axis ↓	23	24	25	26	27
22	2.3350e-02	3.3226e-02	3.7026e-02	3.3226e-02	2.3350e-02
23	2.9875e-02	4.2894e-02	5.0536e-02	4.2894e-02	2.9875e-02
24	3.4206e-02	4.9644e-02	7.8578e-02	4.9644e-02	3.4206e-02
25	3.2808e-02	3.7923e-02	2.4610e-09	3.7923e-02	3.2808e-02
26	3.4206e-02	4.9644e-02	7.8578e-02	4.9644e-02	3.4206e-02
27	2.9875e-02	4.2894e-02	5.0536e-02	4.2894e-02	2.9875e-02
28	2.3350e-02	3.3226e-02	3.7026e-02	3.3226e-02	2.3350e-02

a)

z axis →

x axis ↓	23	24	25	26	27
22	2.3353e-02	3.3235e-02	3.7036e-02	3.3235e-02	2.3353e-02
23	2.9883e-02	4.2906e-02	5.0553e-02	4.2906e-02	2.9883e-02
24	3.4214e-02	4.9661e-02	7.8604e-02	4.9661e-02	3.4214e-02
25	3.2818e-02	3.7933e-02	2.4610e-09	3.7933e-02	3.2818e-02
26	3.4214e-02	4.9661e-02	7.8604e-02	4.9661e-02	3.4214e-02
27	2.9883e-02	4.2906e-02	5.0553e-02	4.2906e-02	2.9883e-02
28	2.3353e-02	3.3235e-02	3.7036e-02	3.3235e-02	2.3353e-02

b)

the time step will be chosen to be near the stability limit.) Although partitioning the problem into planar regions can always be done, the final determining factor on how much time and memory can be saved clearly depends on the relative volumes of the divergence-free region compared to the nondivergence-free region. To minimize the computation and the memory, the volume of the nondivergence-free regions should be made as small as possible, thus, increasing the computation of the fields using the scalar-wave formulation and decreasing the application of the more computationally and memory intensive Yee algorithm. Fortunately, for an important class of problems this can be easily done. In particular, if we consider planar circuit structures or stratified media geometries, the nondivergence-free regions can often be restricted to very thin planar volumes, i.e., two cells thick, which are sufficient to take care of the nondivergence-free fields. Such a region would be placed around planar dielectric interfaces and planar pec edges. The remaining volume would then be divergence free and amenable to a scalar-wave formulation. For a moderately discretized system of 20 cells, this means that only 10 percent of the problem has to be simulated using the Yee algorithm. Therefore, for all practical purposes, a hybrid Yee algorithm/scalar-wave formulation of many planar circuit geometries will often provide a memory and computational savings that is approximately equivalent to that provided by a complete scalar-wave formulation based on just two field components. Table 6.2 summarizes and compares all of the computational and memory requirements of the Yee algorithm, the vector-wave equation and the hybrid Yee algorithm/scalar-wave equation approaches for the planar circuit geometries.

6.3.3 Verification of a hybrid-formulation using planar region partitioning

To demonstrate the validity and effectiveness of using planar partitioning to reduce the computation and the memory of a system we consider the previous problem partitioned into three planar volumes (Fig. 6.2). Region 2 was chosen to be a planar volume two cells thick surrounding the source. Regions 1, 3 were chosen to consist of the remaining planar volumes. A reduced field scalar-wave formulation, i.e., computation and storage of the normal field component omitted, was then applied to regions 1 and 3 and the Yee algorithm applied to region 2. Results of the simulation are given in Table 6.3. As before, the number of iterations was limited to 60 in order to eliminate the effects of the outer boundary. It is once again found that the numerical results are virtually identical with those produced by a full Yee algorithm of the system.

Table 6.2 Comparison of the minimum computation and memory costs of the various differencing techniques for a) general geometries, b) planar circuit geometries.

	additions	mult.	memory/cell
Yee algorithm	24	6	6
vector wave FDTD	36	6	6
hybrid Yee/scalar wave (3 component formulation)	21	6	6

a)

	additions	mult.	memory/cell
Yee algorithm	24	6	6
vector wave FDTD	36	6	6
hybrid Yee/scalar wave (2 component formulation)	14(12)*	4(2)*	4

* indicates the potential cost of the algorithm for use in free space

b)

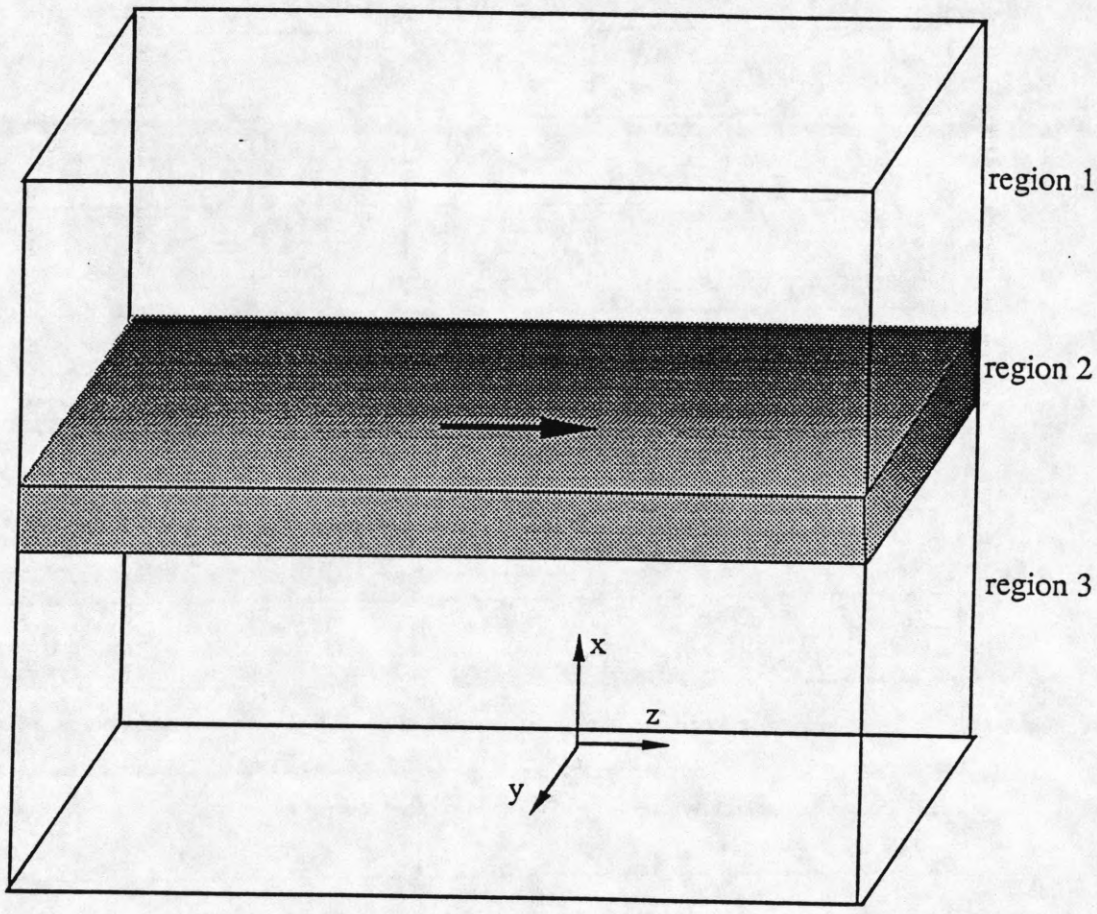

Fig. 6.2 Planar partitioning scheme used to apply a combined Yee algorithm/scalar-wave equation formulation with a single cell E_y-field excitation radiating in infinite, isotropic free space. Region 2 is defined to be a planar volume around the source of thickness $2\Delta s$ in which the Yee algorithm is applied, where Δs = cell size. Regions 1, 3 are defined to be the remaining spaces in which the scalar-wave algorithm is applied to the E_y, E_z fields.

Table 6.3 Comparison of the E_y component in the xz plane (y=25) for a y-directed sinusoidal point dipole inside a 50,50,50 uniform mesh using a) the hybrid Yee/scalar wave algorithm, b) the standard Yee algorithm. The number of iterations was 60, $c\Delta t/\Delta s = 0.577$.

z axis →

x axis ↓	23	24	25	26	27
22	1.0908e-02	1.4751e-02	1.5943e-02	1.4751e-02	1.0908e-02
23	1.7291e-02	2.1596e-02	2.2541e-02	2.1596e-02	1.7291e-02
24	2.1596e-02	2.5251e-02	2.3452e-02	2.5251e-02	2.1596e-02
25	2.2541e-02	2.3452e-02	2.4610e-09	2.3452e-02	2.2541e-02
26	2.1595e-02	2.5250e-02	2.3452e-02	2.5250e-02	2.1595e-02
27	1.7291e-02	2.1595e-02	2.2540e-02	2.1595e-02	1.7291e-02
28	1.0908e-02	1.4751e-02	1.5943e-02	1.4751e-02	1.0908e-02

a)

z axis →

x axis ↓	23	24	25	26	27
22	1.0903e-02	1.4753e-02	1.5938e-02	1.4753e-02	1.0903e-02
23	1.7294e-02	2.1591e-02	2.2544e-02	2.1591e-02	1.7294e-02
24	2.1591e-02	2.5253e-02	2.3448e-02	2.5253e-02	2.1591e-02
25	2.2544e-02	2.3448e-02	2.4610e-09	2.3448e-02	2.2544e-02
26	2.1591e-02	2.5253e-02	2.3448e-02	2.5253e-02	2.1591e-02
27	1.7294e-02	2.1591e-02	2.2544e-02	2.1591e-02	1.7294e-02
28	1.0903e-02	1.4753e-02	1.5938e-02	1.4753e-02	1.0903e-02

b)

Discrepancies can, as before, be attributed to machine error and inconsistencies in the physical constants used in each formulation.

6.4 Application of an Absorbing Boundary Condition to a Hybrid Approach

In the previous examples, the validity of the hybrid approach using planar partitioning was verified by restricting the number of iterations in order to ignore the effect of the outer boundaries. However, many problems of interest, i.e., planar circuit antennas, spurious microstrip line radiation, are open region in nature and require thousands of iterations. Consequently, one must consider how to apply an absorbing boundary condition (ABC) to the hybrid approach. Usually when using the Yee algorithm one applies the ABC directly on the two tangential components of the outer boundary. Unfortunately, if one uses a reduced scalar-wave formulation one does not always have access to both tangential components but rather one tangential component and the normal component, which leads to a novel predicament. Since a single tangential component on the outer boundary cannot provide enough information to uniquely compute all of the interior fields one must adapt the commonly used ABC to compute the normal field components on the outer boundary. There are several possible ways to do this: 1) apply the ABC to the normal component on the outer boundary, 2) set the normal component on the outer boundary equal to zero, 3) use the divergence relation to translate the normal component information into tangential field information and then apply the ABC. (It will be shown that this can be accomplished in two different ways.) We now examine each approach using the first-order Engquist-Majda ABC to illustrate the results.

6.4.1 Applying the ABC to the normal component

The most obvious solution to the problem is to apply the ABC as is, directly to the normal component. To test this approach, a sinusoidal electric line source distribution ten cells long was placed inside a 50x50x50 volume of free space and the resulting field distribution studied (Fig. 6.3). The results are then compared with those obtained by applying the same ABC on the tangential components of the outer boundary using the Yee algorithm (Fig. 6.4). It can be seen that the resulting field pattern obtained by applying the ABC on the normal component in the hybrid algorithm appears to be comparable to those obtained using the ABC on the tangential components. However, for more complicated systems, one finds that the effectiveness of this approach is severely degraded. Figure. 6.5 shows the field plot of a truncated slot line radiating in

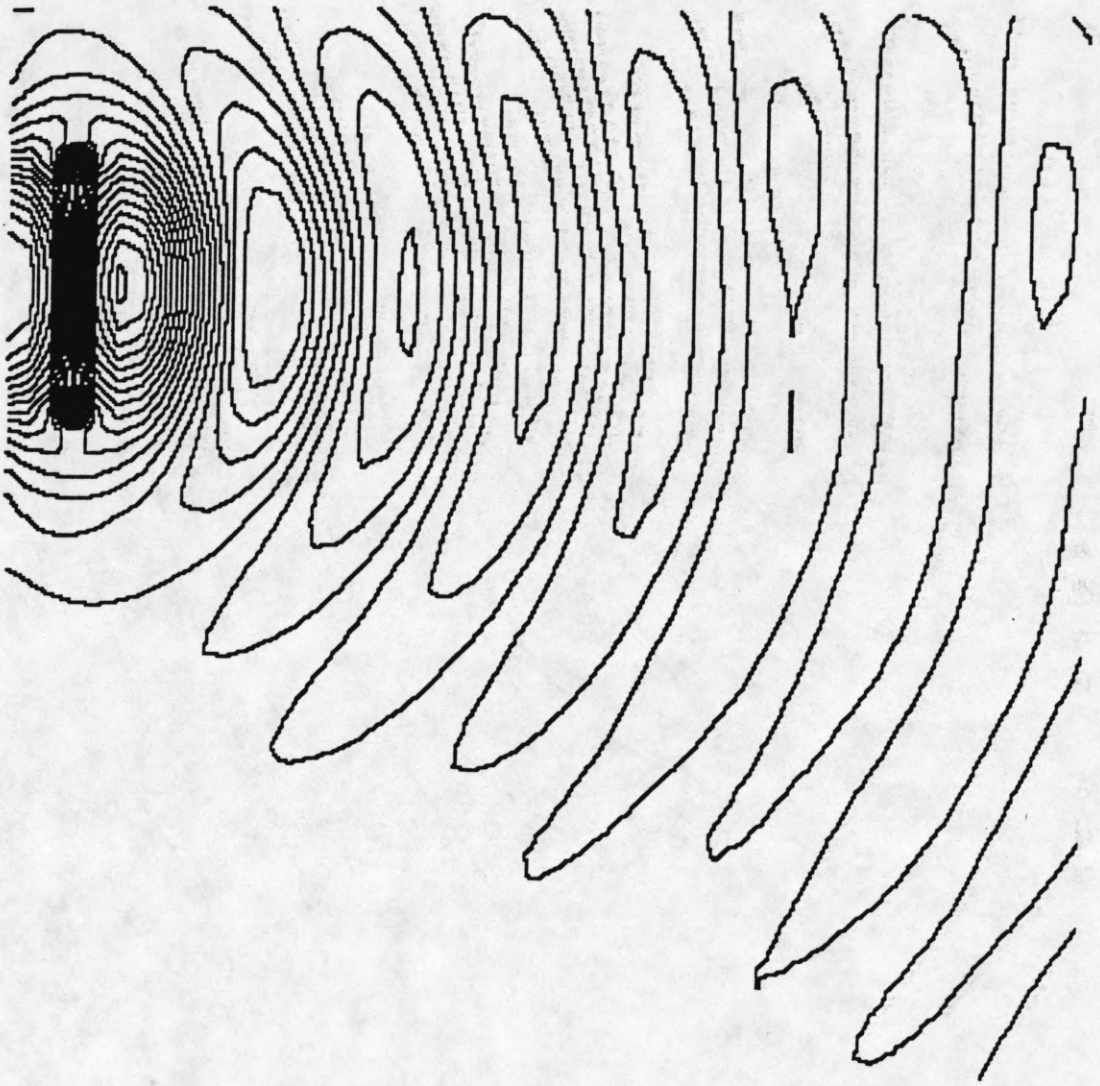

Fig. 6.3 Contour plot of the electric field distribution at x=18 of a ten cell electric field sinusoidal excitation located at (18,15,5) radiating in free space. The first-order Engquist-Majda ABC was applied to the normal component to the boundary in conjunction with a hybrid Yee algorithm/scalar-wave formulation. The problem domain was (50,50,50) and the number of iterations was 3000.

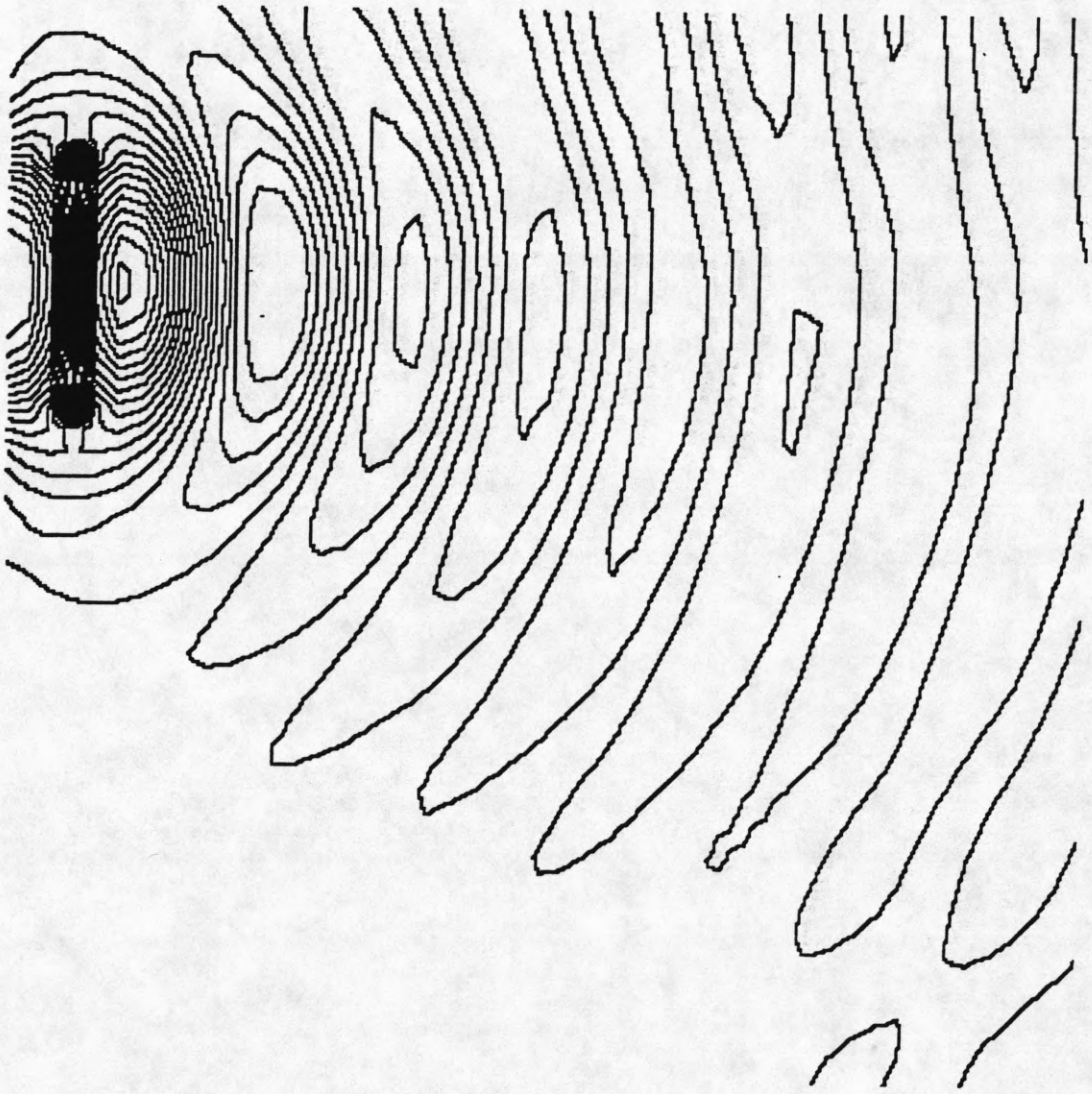

Fig. 6.4 Contour plot of the electric field distribution at x=18 of a ten cell electric field sinusoidal excitation located at (18,15,5) radiating in free space. The first-order Engquist-Majda ABC was applied to the tangential components to the boundary in conjunction with a full Yee algorithm formulation. The problem domain was (50,50,50) and the number of iterations was 3000.

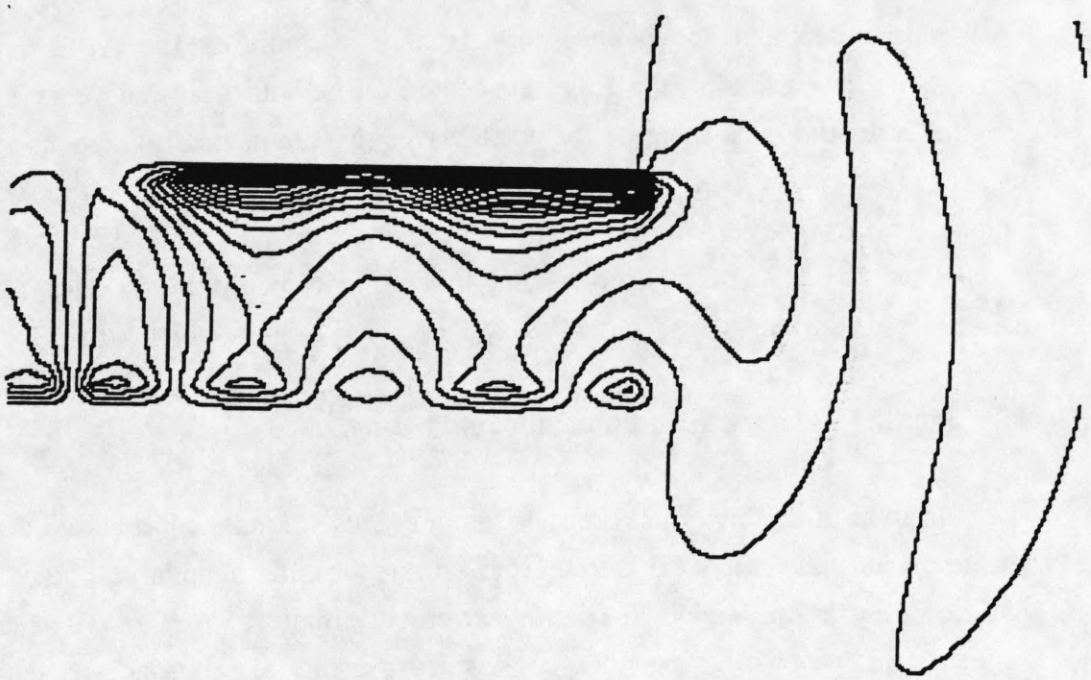

Fig. 6.5 Contour plot of the electric field distribution at x=18 of a ten cell electric field sinusoidal excitation located at (18,15,5) radiating inside an infinitely thin pec slot line 30 cells long in free space. The first-order Engquist-Majda ABC was applied to the normal component (relative to the boundary wall) in conjunction with a hybrid Yee algorithm/scalar-wave formulation. The problem domain was (50,50,50) and the number of iterations was 300.

free space with the slot placed asymmetrically in the 50x50x50 problem domain. In contrast to applying the ABC to the tangential components (Fig. 6.6), it can be seen that the fields are severely distorted by the absorbing boundaries. Furthermore, it is found that the system becomes unstable after a large number of iterations. A likely explanation for the poor performance is the inconsistency in applying the ABC to a normal component. In particular, the Engquist-Majda ABC, both first and second order, are designed to be the most accurate for plane waves that are normally incident to the outer boundary (this can be shown by substituting a plane wave function into the ABC). Such a plane wave, however, should have no normal component and, therefore, the very application of the ABC to the normal component would be in violation of the mathematical conditions for accuracy.

6.4.2 Setting the normal component equal to zero

In light of the previous discussion, an obvious alternate approach to applying an ABC to the normal component is to set it to zero on the outer boundary. Such a boundary condition has the advantage that it is extremely simple to implement and requires absolutely no computation or storage. Results of using this approach on the previous geometries are shown in Figs. 6.7 and 6.8. Figure 6.7 shows that setting the normal component equal to zero is noticeably less effective than applying the ABC to the normal component for the case of the source radiating in infinite free space. On the other hand, Fig. 6.8 shows that setting the normal component equal to zero results in a much more stable and accurate absorbing boundary than the previous approach. Comparing Figs. 6.7, 6.8 with Figs. 6.3 and 6.4, however, it is clear that applying the ABC to the tangential components is still more accurate.

6.4.3 Application of the ABC to the tangential components via the divergence relation

From the previous examples, we can conclude that applying directly the ABC to the normal components will provide varying degrees of absorption; however, the effectiveness is still not as good as that of the ABC applied to the tangential components. This leads us to consider other methods. In particular, we consider applying the ABC indirectly to the tangential fields through information about the normal components. The most obvious way to do this would be to assume that the fields at the outer boundary are

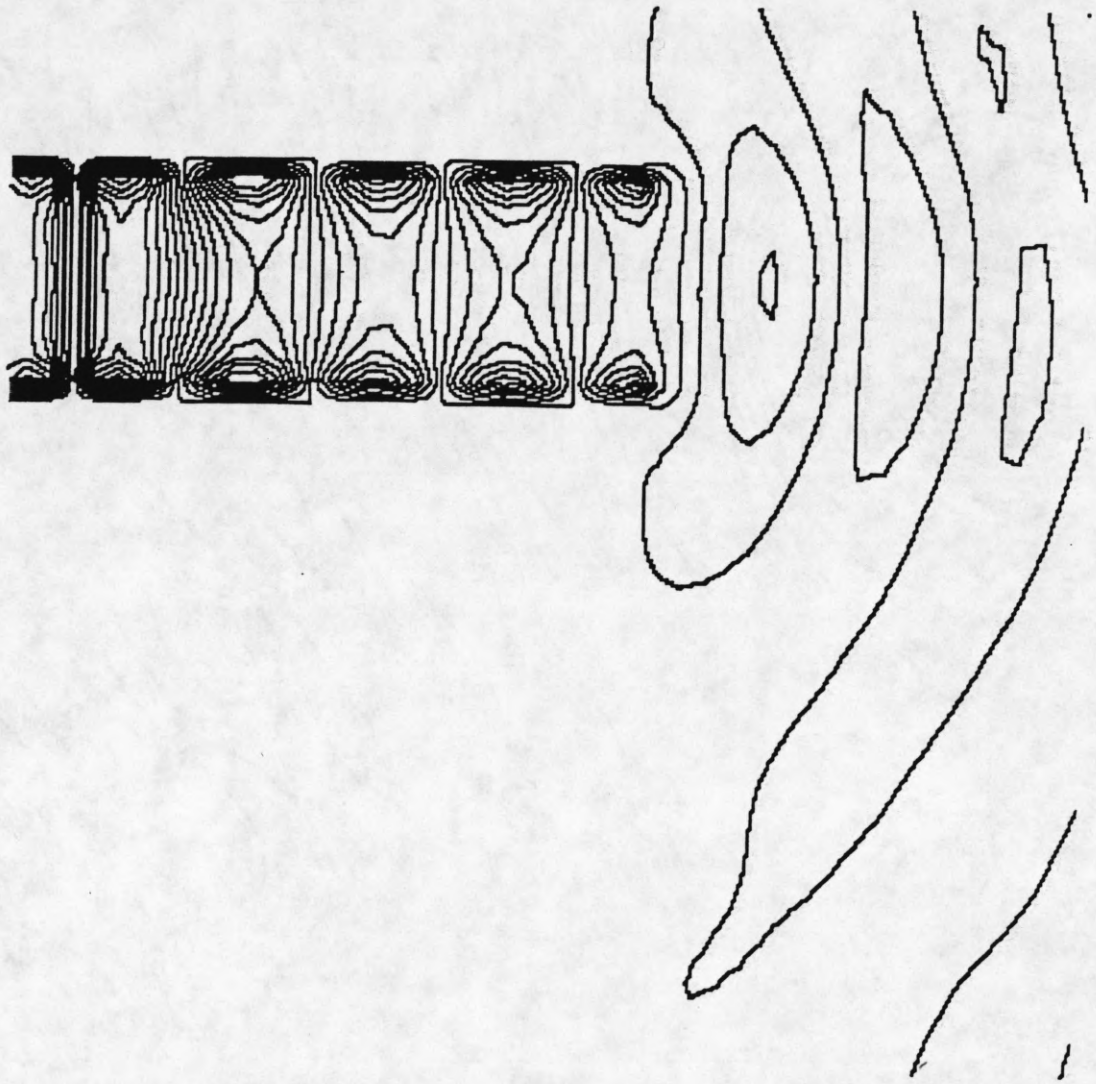

Fig. 6.6 Contour plot of the electric field distribution at x=18 of a ten cell electric field sinusoidal excitation located at (18,15,5) radiating inside an infinitely thin pec slot line 30 cells long in free space. The first-order Engquist-Majda ABC was applied to the tangential components to the boundary wall along with a full Yee algorithm formulation. The problem domain was (50,50,50) and the number of iterations was 3000.

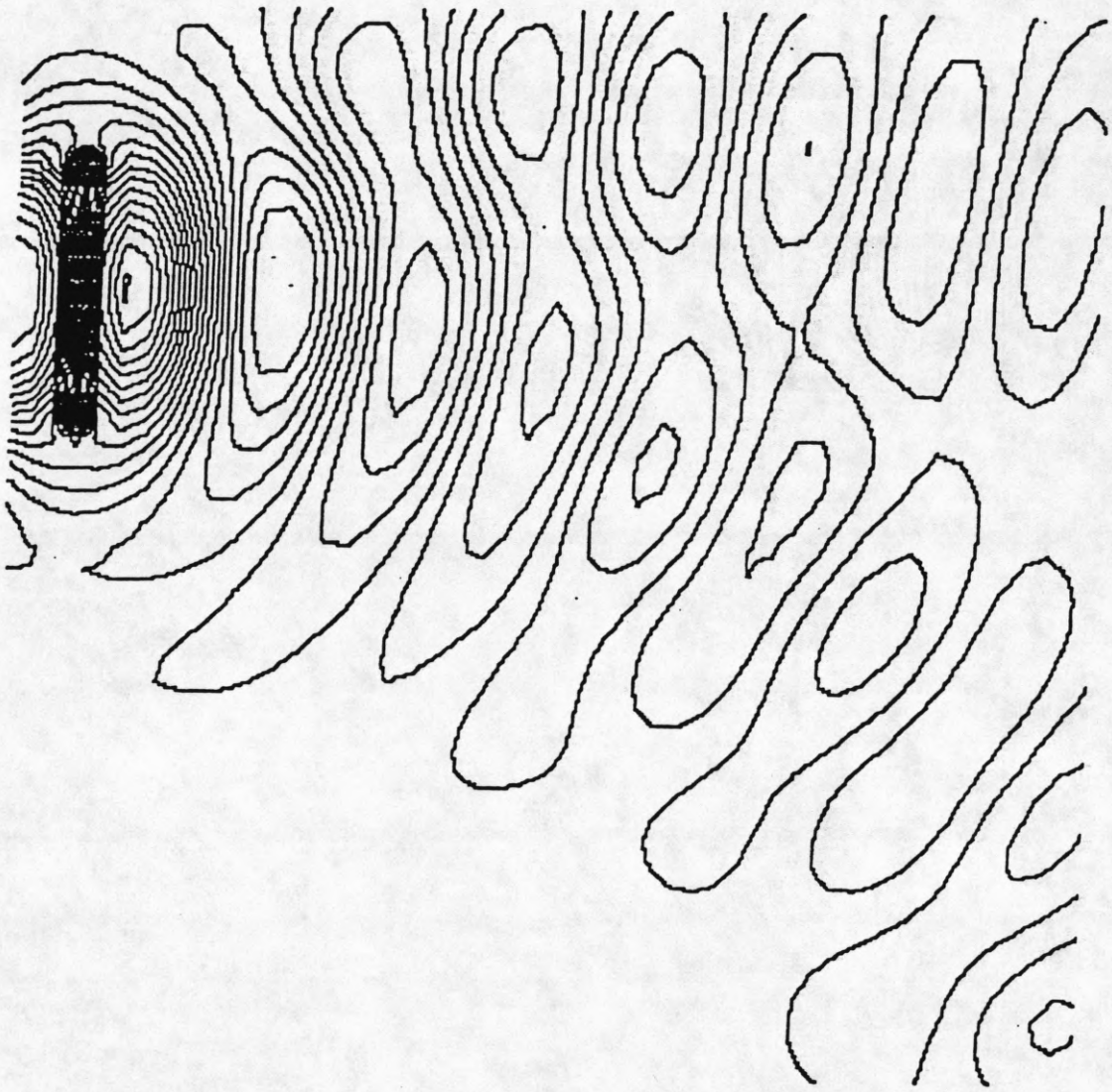

Fig. 6.7 Contour plot of the electric field distribution at x=18 of a ten cell electric field sinusoidal excitation located at (18,15,5) radiating in free space. The normal component to the boundary wall is set equal to zero and a hybrid Yee algorithm/scalar-wave formulation was used. The problem domain was (50,50,50) and the number of iterations was 3000.

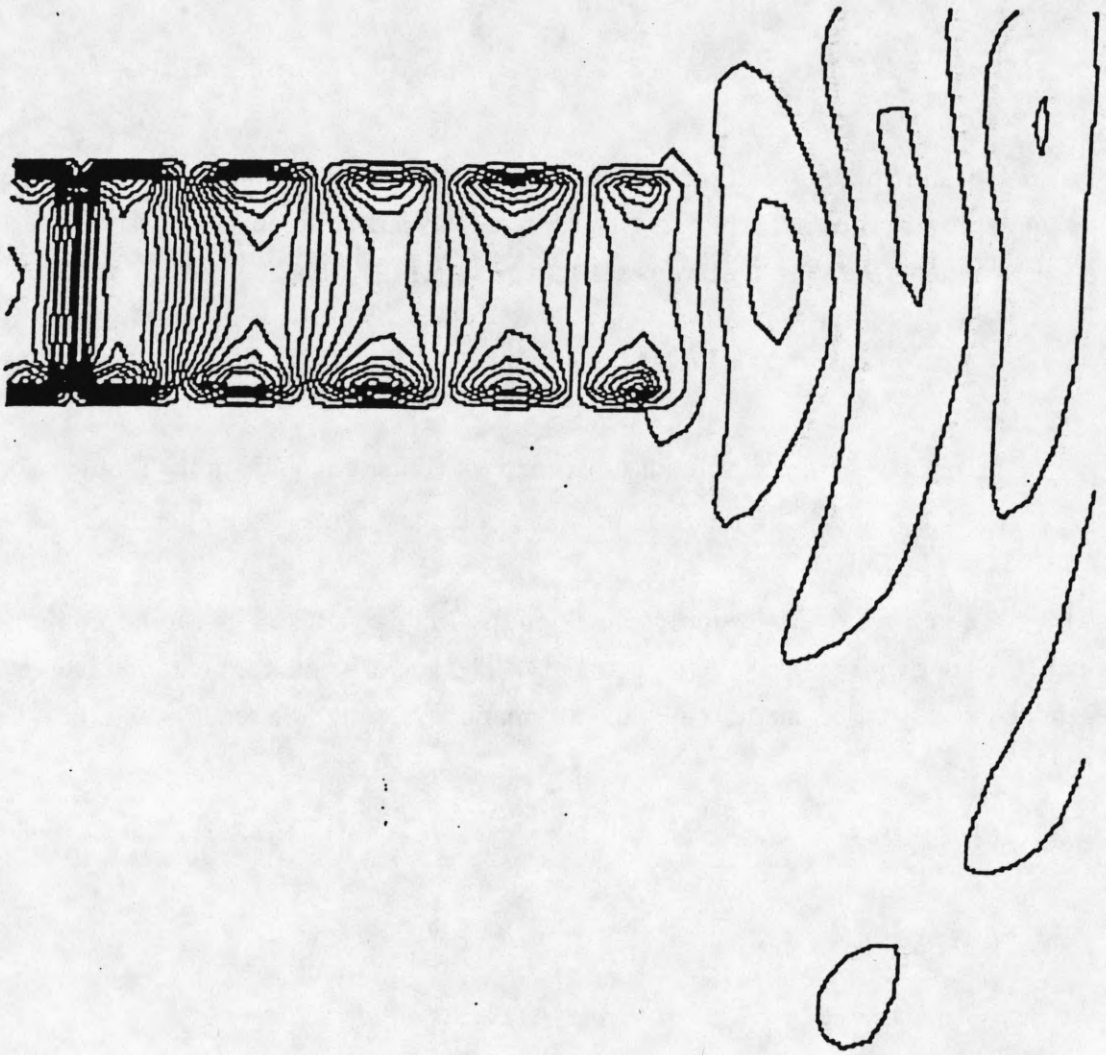

Fig. 6.8 Contour plot of the electric field distribution at x=18 of a ten cell electric field sinusoidal excitation located at (18,15,5) radiating inside an infinitely thin pec slot line 30 cells long in free space. The normal component to the boundary wall is set equal to zero and a hybrid Yee algorithm/scalar-wave formulation was used. The problem domain was (50,50,50) and the number of iterations was 3000.

divergence free. We can then use the central difference approximation of the divergence relation (5.5) to relate the normal derivative to the tangential derivatives, i.e.,

$$G_x = E_x^l(m+1/2,n,p) - E_x^l(m-1/2,n,p)$$
$$= -E_y^l(m,n+1/2,p) + E_y^l(m,n-1/2,p) - E_z^l(m,n,p+1/2) + E_z^l(m,n,p-1/2) \tag{6.8}$$

Having established a relation between the normal components with the tangential components, we now note that the first- and second-order Engquist-Majda ABC (as well as many other ABC's) are linear operators, i.e.,

$$\mathbf{L}(\phi_{1int}^l + \phi_{2int}^l) = \mathbf{L}(\phi_{1int}^l) + \mathbf{L}(\phi_{2int}^l) = \phi_{1bound}^{l+1} + \phi_{2bound}^{l+1}. \tag{6.9}$$

where $\mathbf{L}$ = Engquist-Majda ABC operator

$\phi_{1int}^l, \phi_{2int}^l$ = interior fields adjacent to the outer boundary at the l th iteration,

$\phi_{1bound}^{l+1}, \phi_{2bound}^{l+1}$ = fields on the outer boundary at the (l+1)th iteration

Therefore, one can apply the Engquist-Majda ABC to (5.8) and compute the tangential derivatives on the outer boundary. The vector-wave formulation given in (5.3) can then be used to re-incorporate this information back into the scalar-wave formulation, i.e.,

$$E_x^{l+1}(m+1/2,n,p) = (2 - 5\left(\frac{v(m+1/2,n,p)\Delta t}{\Delta s}\right)^2)E_x^l(m+1/2,n,p)$$
$$-E_x^{l-1}(m+1/2,n,p) + \left(\frac{v(m+1/2,n,p)\Delta t}{\Delta s}\right)^2 (E_x^l(m+1/2,n+1,p)$$
$$+E_x^l(m+1/2,n-1,p) + E_x^l(m+1/2,n,p+1) + E_x^l(m+1/2,n,p-1)$$
$$+E_x^l(m+3/2,n,p) - G_x)$$

(6.10)

where G_x, is computed by applying the ABC to the normal derivative with the outer boundary located at x=m. The results of using such an approach are shown in Fig. 6.9 for a source radiating in free space. It is found that they are virtually identical to that obtained using the standard Yee algorithm for approximately 500 iterations. However, as the iterations are increased the hybrid system becomes unstable and the two start to differ markedly from one another. The instability is believed to be linked to the fact that

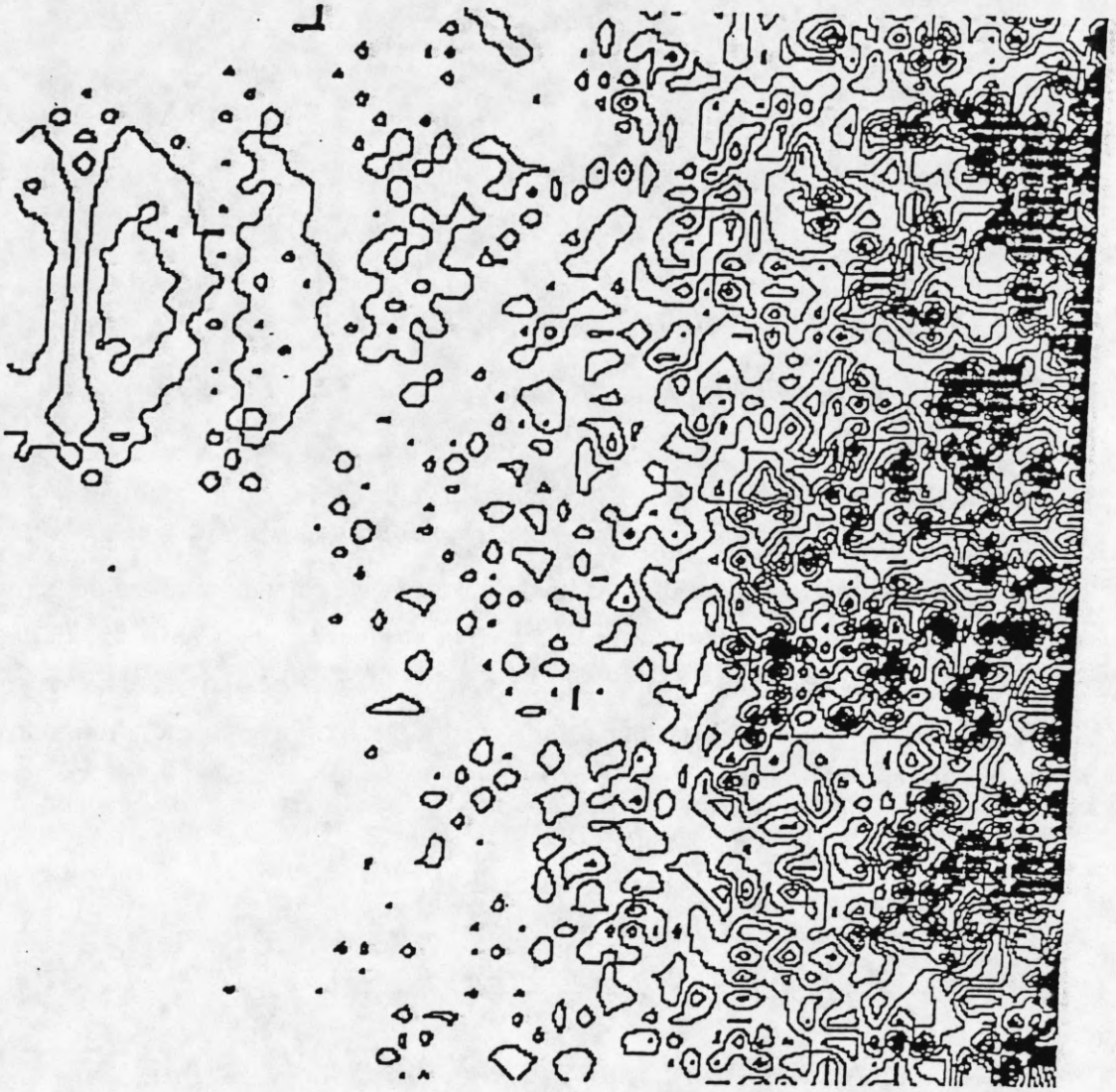

Fig. 6.9 Contour plot of the electric field distribution at x=18 of a ten cell electric field sinusoidal excitation located at (18,15,5) radiating in free space. The first-order Engquist-Majda ABC was applied to the normal derivative of the normal component to the boundary wall in conjunction with a hybrid Yee algorithm/scalar-wave formulation. The problem domain was (50,50,50) and the number of iterations was 3000.

1) the hybrid algorithm was being implemented near the upper limit of the stability criteria and 2) the application of the ABC did not explicitly preserve the divergence-free relation to sufficient accuracy. Further work needs to be done to determine the precise cause of this problem.

An alternate way of applying the divergence relation with the ABC is to use the known tangential component information in conjunction with the normal component information to compute the derivative of the unknown tangential component, i.e.,

$$G_y = E_y^l(m,n+1/2,p) - E_y^l(m,n-1/2,p)$$
$$= -E_x^l(m+1/2,n,p) + E_x^l(m-1/2,n,p) - E_z^l(m,n,p+1/2) + E_z^l(m,n,p-1/2) \quad (6.11)$$

where it is assumed that the E_x and E_z components are the known normal and tangential components, and E_y is the unknown tangential component to an x=m plane outer boundary. Recalling that the ABC is a linear operator, we can compute the derivative of the unknown tangential component, E_y, located at x=m+1/2 and solve for the derivative of E_y at x=m. This information can then be recombined with the derivative of the known tangential component and integrated back into the scalar-wave formulation using the following variation of the vector-wave equation

$$E_x^{l+1}(m+1/2,n,p) = (2 - 5\left(\frac{v(m+1/2,n,p)\Delta t}{\Delta s}\right)^2)E_x^l(m+1/2,n,p)$$
$$-E_x^{l-1}(m+1/2,n,p) + \left(\frac{v(m+1/2,n,p)\Delta t}{\Delta s}\right)^2 (E_x^l(m+1/2,n+1,p)$$
$$+E_x^l(m+1/2,n-1,p) + E_x^l(m+1/2,n,p+1) + E_x^l(m+1/2,n,p-1)$$
$$-E_x^l(m+3/2,n,p) + E_z^l(m,n,p+1/2) - E_z^l(m,n,p-1/2) + G_y) \quad (6.12)$$

where $E_z^l(m,n,p+1/2)$, $E_z^l(m,n,p-1/2)$, G_y are computed using the ABC.

Though there is a certain redundancy in this approach, it has the property of explicitly making the normal component and the tangential components satisfy the divergence-free condition in the presence of the ABC. In contrast, the previous approach assumed the divergence free relation would implicitly hold. To demonstrate the

the numerical values of this approach are virtually identical to that of the full Yee algorithm with the conventional ABC application. More importantly, there are no signs of the instability which had afflicted the previous formulation involving the divergence relation. Hence, we conclude tentatively that this formulation appears to be a more stable formulation.

6.5 Conclusions

A hybrid Yee algorithm/scalar-wave equation formulation has been proposed. Limitations on its application as well as the applicability of the absorbing boundary conditions were also discussed. It is found that this hybrid approach is a viable way to reduce the memory by 33% and the computation by at least 40% for many planar circuit structures. In addition, a method of applying the absorbing boundary condition on the normal components using the divergence relation in conjunction with the vector-wave equation is presented which yield results that are virtually identical with those obtained by applying the ABC on the tangential components. An advantage of this hybrid approach is that it may be adapted to help reduce the memory and computation in conjunction with many recent advances in the FDTD method such as nonuniform or curvilinear gridding schemes.

6.6 References

[1] S.S. Zivanovic, K.S. Yee, and K.K. Mei, "A subgridding method for the time-domain finite-difference method to solve Maxwell's equations," *IEEE Trans. Microwave Theory Tech.*, vol. MTT-39, no. 3, pp. 471-479, March 1991.

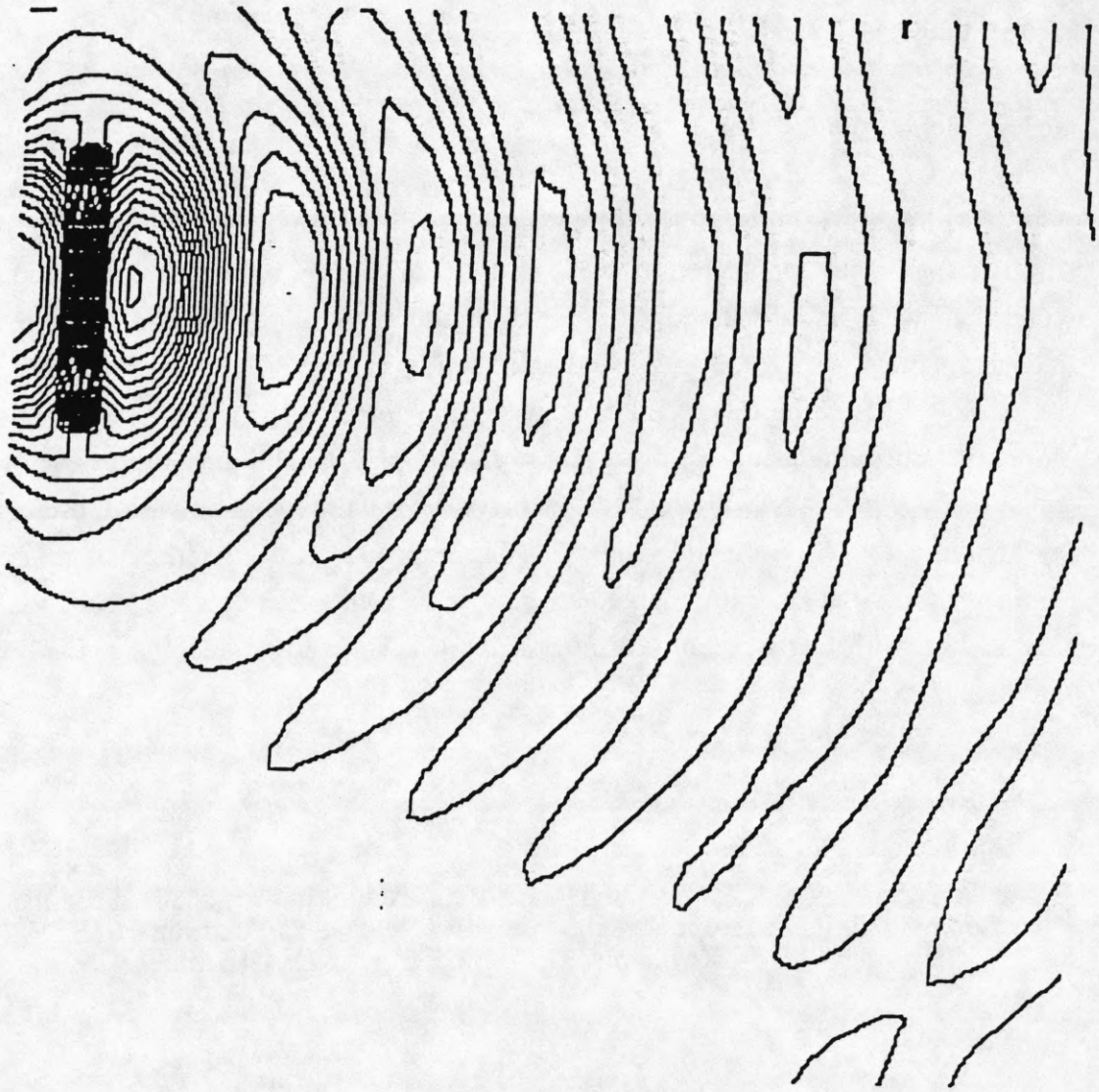

Fig. 6.10 Contour plot of the electric field distribution at x=18 of a ten cell electric field sinusoidal excitation located at (18,15,5) radiating in free space. The first-order Engquist-Majda ABC was applied by combining information about the known tangential and normal component in conjunction with a hybrid Yee algorithm/scalar-wave formulation. The problem domain was (50,50,50) and the number of iterations was 3000.

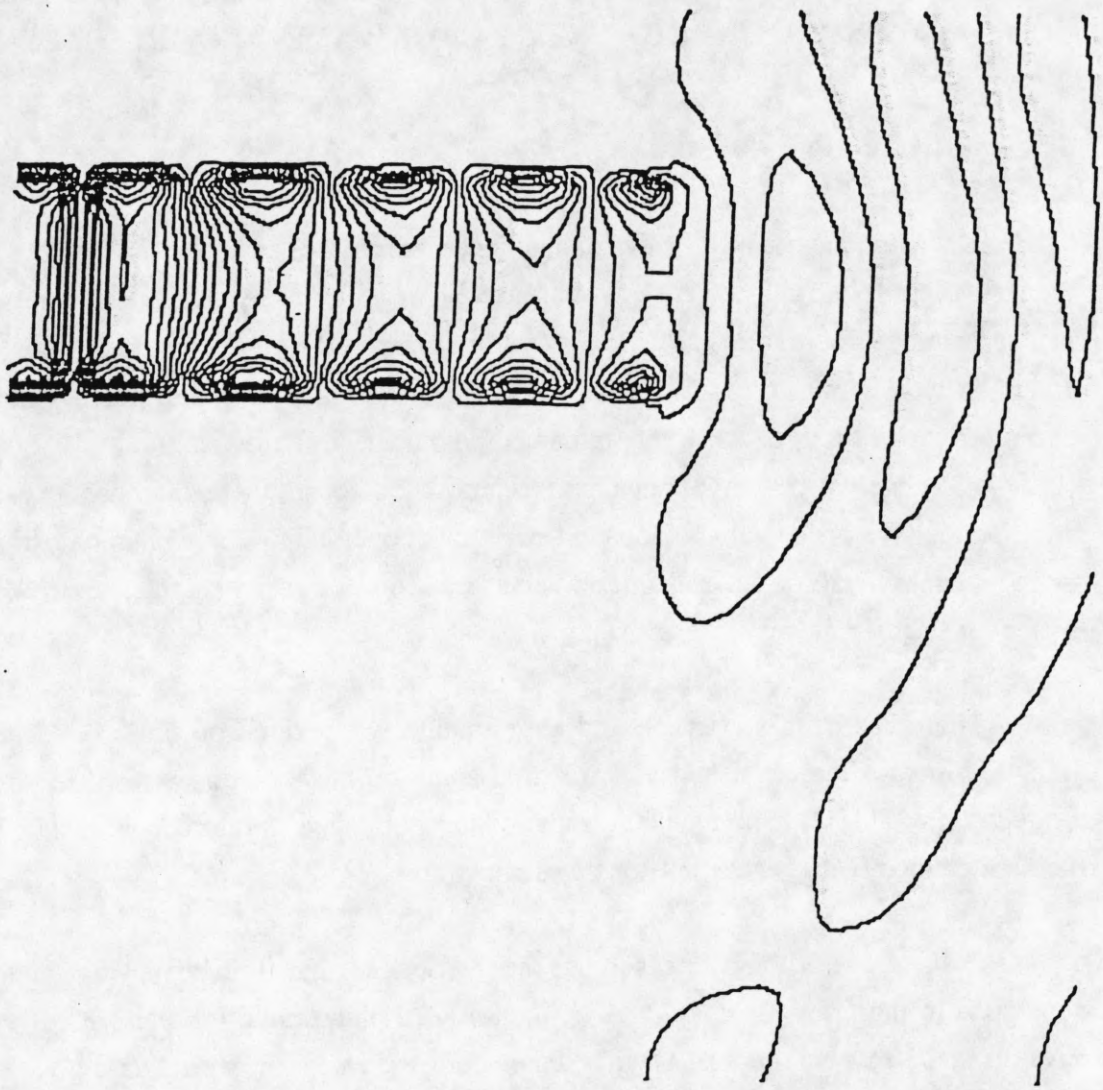

Fig. 6.11 Contour plot of the electric field distribution at x=18 of a ten cell electric field sinusoidal excitation located at (18,15,5) radiating inside an infinitely thin pec slot line 30 cells long in free space. The first-order Engquist-Majda ABC was applied by combining information about the known tangential and normal component in conjunction with a hybrid Yee algorithm/scalar-wave formulation. The problem domain was (50,50,50) and the number of iterations was 3000.

CHAPTER 7

ANALYSIS OF VIVALDI AND LINEAR TAPERED SLOT ANTENNAS USING A HYBRID YEE/SCALAR-WAVE ALGORITHM

7.1 Introduction

Recently, the use of the Vivaldi and linear tapered slot antennas (LTSA) has been of interest (Figs. 7.1a,b). They are traveling wave antennas that belong to a general class of planar, printed circuit antennas called by some the tapered slot antenna (TSA) [1]. These antennas were first suggested in 1979 [2], [3], and have two particularly attractive characteristics. First, because the antennas are planar structures, they can be fabricated easily and cheaply using standard etching techniques. Second, these antennas, in particular the Vivaldi, have a relatively broadband frequency of operation. These characteristics make these antennas ideal for the transmission and reception of transient signals as well as for a variety of steady-state applications [1], [4].

There has been numerical and experimental work done on the Vivaldi and the LTSA. Much of the published experimental study on these antennas has been done by Yngvesson et al. [1], [5], [6], while most of the published numerical work has been a moment method (MoM) analysis done by Jamaswamy [7], [8].

The purpose of this work is to use the hybrid Yee algorithm/scalar-wave approach developed in the previous chapter to compute the E-plane radiation patterns of various Vivaldis and LTSAs. The results will then be compared with measured data given in [5]-[7]. In general, it is found that the FDTD method yields better agreement with experimental results in the E-plane than the MoM approach given in [7], [8]. In the H-plane, however, it is found that the lack of information about the feed geometry coupled with modeling resolution errors results in poor agreement between the FDTD and measured radiation patterns. In addition, the accuracy of the far-field time domain transformation proposed in [9] and [10] is investigated. It is found that the smallest equivalent surface will produce the most accurate far-field results. It is also found that the far-field computations are expensive requiring a large percentage of overall FDTD simulation time.

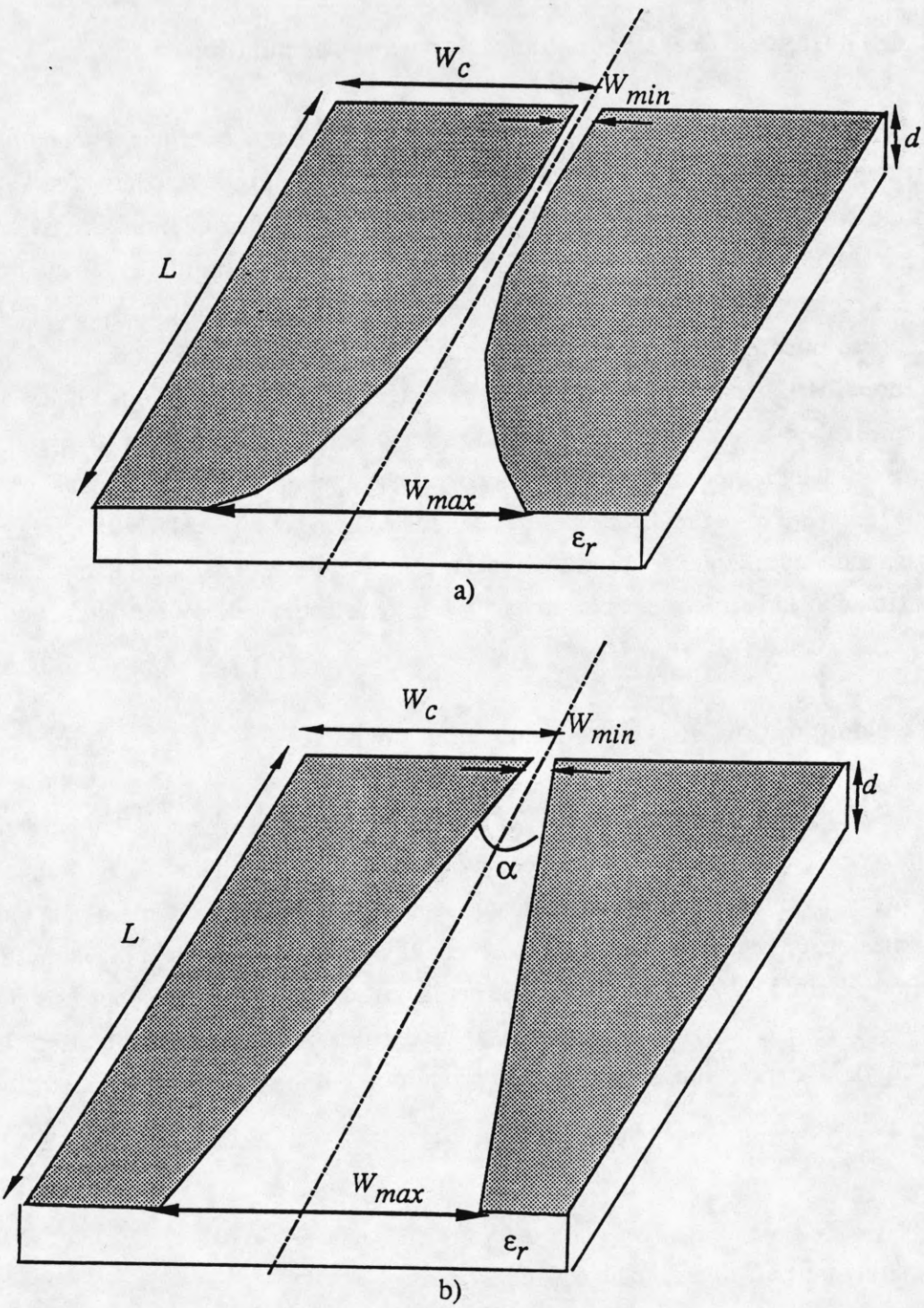

Fig. 7.1 a) The Vivaldi and b) the LTSA.

7.2 Numerical Analysis

7.2.1 The hybrid Yee algorithm/scalar-wave formulation

The antenna radiation patterns will be solved using a more efficient yet numerically equivalent formulation of the Yee algorithm which combines the standard Yee algorithm with the scalar-wave equation. The details of this hybrid formulation are given in the previous chapter. The simulations will be performed by placing the antenna structures inside a rectangular volume which has been discretized uniformly in space (Fig. 7.2). Since these antennas are open structures, a first-order Engquist-Majda absorbing boundary condition (ABC) is placed along the entire outer surface (see previous chapter). The problem is then broken into three regions: Regions 1 and 3 consist of divergence-free volumes in which the scalar-wave equation will be applied; Region 2 is made up of the nondivergence-free regions which must be modeled using the Yee algorithm, i.e., the pec edges and dielectric interfaces. All nonrectangular features are modeled using a staircase approximation and each antenna is fed by a y-directed electric field source placed across the slotline.

7.2.2 Computation of the far-field radiation patterns

Before comparing the results for the FDTD and experiment, it is instructive to known how much error can be introduced by the far-field computation. This computation is facilitated by an efficient algorithm that translates near-field time domain data into far-field time domain data [9], [10], and represents a significant improvement in what had been done in the past [11], [12]. The method is based on a central difference approximation of the time-dependent far-field expressions that are derived from the commonly used steady-state far-field expressions [12]. This derivation is done by making the following substitution

$$j\omega \rightarrow \frac{\partial}{\partial t} \tag{7.1}$$

The resulting far-field time domain equations become

$$E_\theta \cong -\frac{1}{4\pi rc}\frac{\partial}{\partial t}(L_\phi + \eta N_\theta) \tag{7.2a}$$

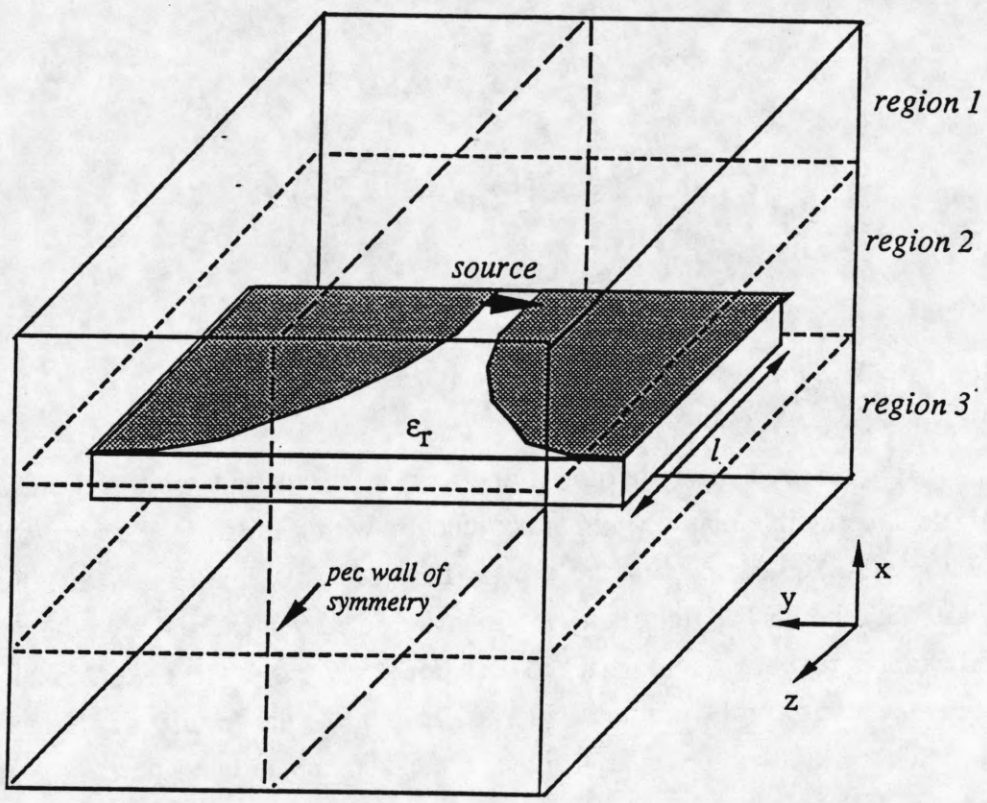

Fig. 7.2 Diagram of how the hybrid FDTD problem domain was partitioned. The six outer walls surrounding the antennas are absorbing boundary walls. The antenna is finite in width and length and is not in contact with the absorbing walls.

$$E_\phi \cong \frac{1}{4\pi rc}\frac{\partial}{\partial t}(L_\theta - \eta N_\phi) \tag{7.2b}$$

$$H_\theta \cong \frac{1}{4\pi rc}\frac{\partial}{\partial t}(N_\phi + \frac{L_\theta}{\eta}) \tag{7.3a}$$

$$H_\phi \cong -\frac{1}{4\pi rc}\frac{\partial}{\partial t}(N_\theta + \frac{L_\phi}{\eta}) \tag{7.3b}$$

$$E_r \cong H_r \cong 0 \tag{7.4}$$

where

$$\overline{N} = \iint_S \overline{J}_s(t + \frac{(\hat{r}\cdot\overline{r}' - r)}{c})ds' \tag{7.5a}$$

$$\overline{L} = \iint_S \overline{M}_s(t + \frac{(\hat{r}\cdot\overline{r}' - r)}{c})ds' \tag{7.5b}$$

$\overline{M}_s$, $\overline{J}_s$ are the equivalent magnetic and electric surface currents.

By enclosing the radiating structure in a closed (but arbitrary) surface, S, the equivalence principle may be used in conjunction with finite difference approximations of Equations (7.2)-(7.5) to compute the far-field radiation patterns using the time data generated by the FDTD algorithm. It should be noted that even though the approach is a significant improvement over what had been done previously, these extra computations can be time-consuming if the scatterer is large. In fact, for the simulations being considered later in this work, it will be found that the far-field computations require more computation than the FDTD simulation itself. Consequently, a more efficient scheme of implementing the far-field algorithm would be of some value.

7.2.3 Validation of the far-field calculations

To validate the accuracy as well as to determine the limitations of the time domain far-field computation the far-field patterns of a small z-directed dipole are computed using the hybrid Yee/scalar-wave algorithm to generate its transient response. Figures 7.3-7.5 show the E_θ and E_ϕ radiation patterns of a small dipole ($< 0.1\lambda_0$) computed using (7.2)-(7.5). It can be seen that the far-field computations are in good agreement with the analytical solution (to within 2 dB). Moreover, Fig. 7.5 shows that the patterns are relatively insensitive to the geometry of the equivalent surface and the position of the dipole used to compute the pattern as required by the equivalence theorem. Interestingly, Figs. 7.3-7.5 demonstrate

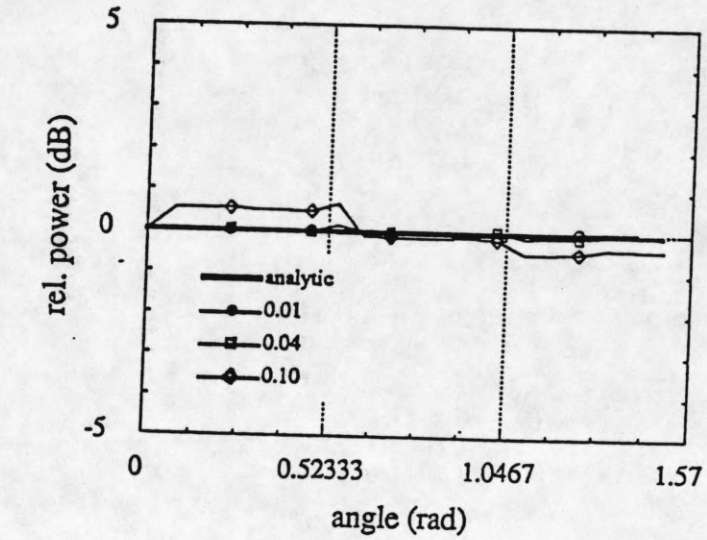

a) ϕ plane

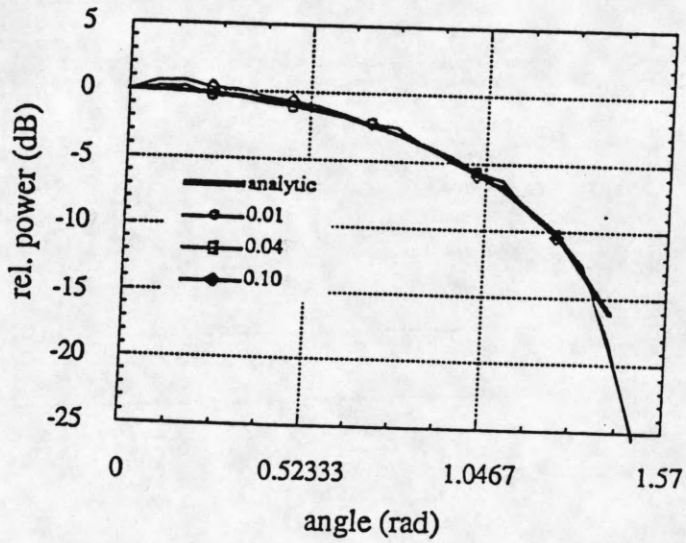

b) θ plane

Fig. 7.3 Comparison of the hybrid FDTD radiation patterns of a small z-directed dipole with the analytic solution at different frequencies. The equivalent surface is a rectangle of dimensions $2\Delta s \times 6\Delta s \times 3\Delta s$ with a dipole located at $(2\Delta s, 3\Delta s, 2\Delta s)$. Symmetry was used to create an overall problem domain of $(40\Delta s, 120\Delta s, 40\Delta s)$. The number of iterations was 500.

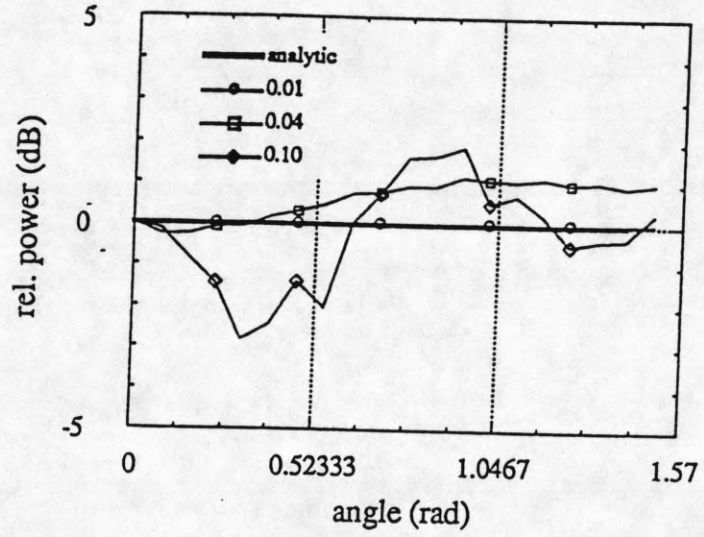

a) ϕ plane

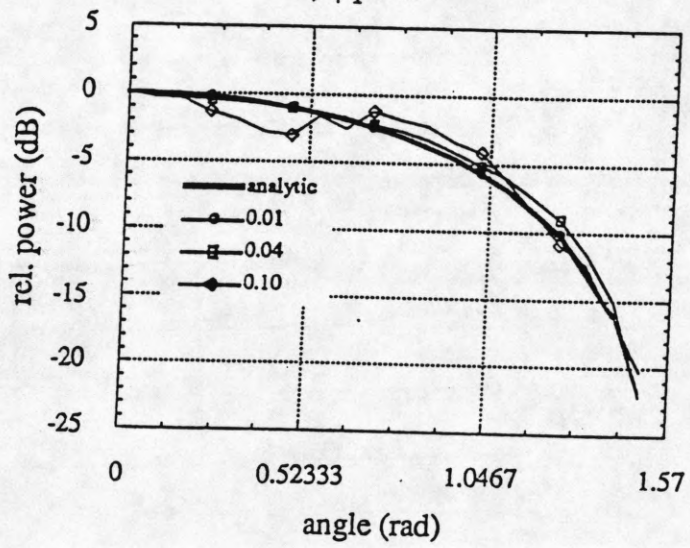

b) θ plane

Fig. 7.4 Comparison of the hybrid FDTD radiation patterns of a small z-directed dipole with the analytic solution at different frequencies, i.e., $\Delta s/\lambda$. The equivalent surface is a rectangle of dimensions $20\Delta s \times 40\Delta s \times 20\Delta s$ with a dipole located at $(10\Delta s, 20\Delta s, 10\Delta s)$. Symmetry was used to create an overall problem domain of $(40\Delta s, 120\Delta s, 40\Delta s)$. The number of iterations was 500.

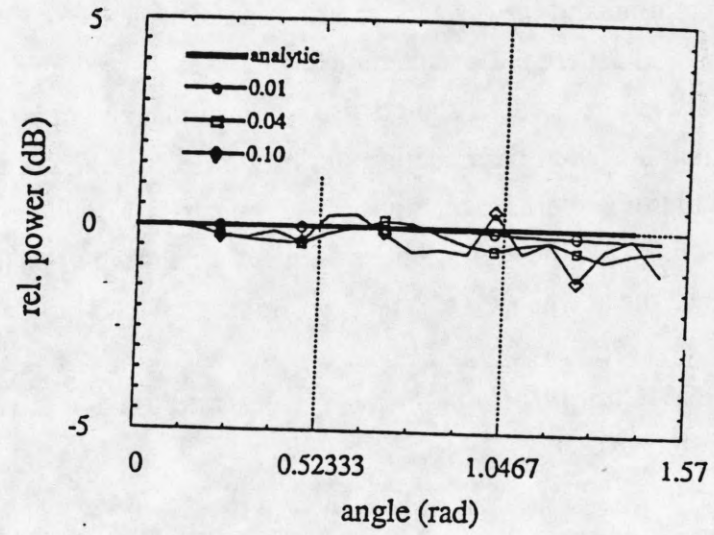

a) ϕ plane

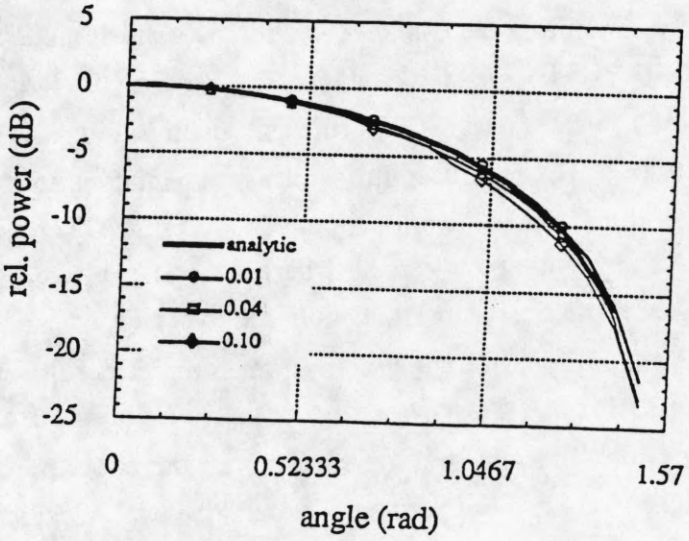

b) θ plane

Fig. 7.5 Comparison of the hybrid FDTD radiation patterns of a small z-directed dipole with the analytic solution at different frequencies, i.e., $\Delta s/\lambda$. The equivalent surface is a rectangle of dimensions $2\Delta s \times 60\Delta s \times 77\Delta s$ with a dipole located at $(1\Delta s, 30\Delta s, 3\Delta s)$. Symmetry was used to create an overall problem domain of $(40\Delta s, 120\Delta s, 40\Delta s)$. The number of iterations was 500.

that using smaller equivalent surfaces will result in better agreement with the analytical solution than using the larger equivalent surfaces. This can be attributed to the fact that the phase error introduced by the finite difference approximation is proportional to the frequency of operation and the distance traveled (see Chapters 3, 4). Hence, to accurately compute the far-field patterns of a scatterer using the Yee algorithm, the smallest equivalent surface should always be used. It should also be noted that an important benefit of using a smaller equivalent surface is a reduction in the somewhat high computational overhead associated with these far-field calculations. In all numerical simulations of the Vivaldi and LTSA given in this work, the equivalent surface will be chosen to be the minimum surface required to enclose the antenna.

7.3 Numerical Computation of the Vivaldi and LTSA E-plane Radiation Patterns

7.3.1 The LTSA results

We begin by computing the E-plane radiation patterns of an LTSA antenna with no dielectric substrate ($L = 5.08\ \lambda_0$, $\alpha = 11.4^o$, $W_c \cong W_{max} = 1.014\ \lambda_0$ $W_{min} \cong 0.025\ \lambda_0$, operating frequency, $f_o = 8.5$ GHz.) The results are given in Fig. 7.6a and compared with measured data from [5]. The feed used in the measurement consisted of a diode detector soldered across a slotline of unknown location. The hybrid FDTD model of the antenna was constructed assuming that $\lambda_0 = 20\Delta s$ where Δs = mesh size. For computational efficiency and accuracy, the time step, Δt, was chosen to correspond to the maximum value allowed by the CFL stability condition. To minimize the effect of reflections, the ABC walls were placed at least $0.5\ \lambda_0$ away from the antenna. After running several simulations, it was found that the best agreement with the experiment occurred when a dipole source was placed at the mouth of the LTSA and the equivalent surface extended just enough to include the source. It can be seen that the agreement between the E-plane patterns of theory and experiment is good. In particular, we can see very good agreement in the main beam and first side lobe. Discrepancies in the remaining side lobes are probably due to a combination of FDTD numerical error, i.e., anisotropy, stair casing, and experimental error.

The second example considered was an LTSA on a low dielectric substrate ($\varepsilon_r = 2.22$, $d = 0.06$ mm, $L = 6.1\ \lambda_0$, $\alpha = 14.25^o$, $W_{max} = 1.525\ \lambda_0$, $W_c = 2.55\ \lambda_0$, W_{min} approximately $0.02\ \lambda_0$, with $f_0 = 12$ GHz). The comparison between results for theory

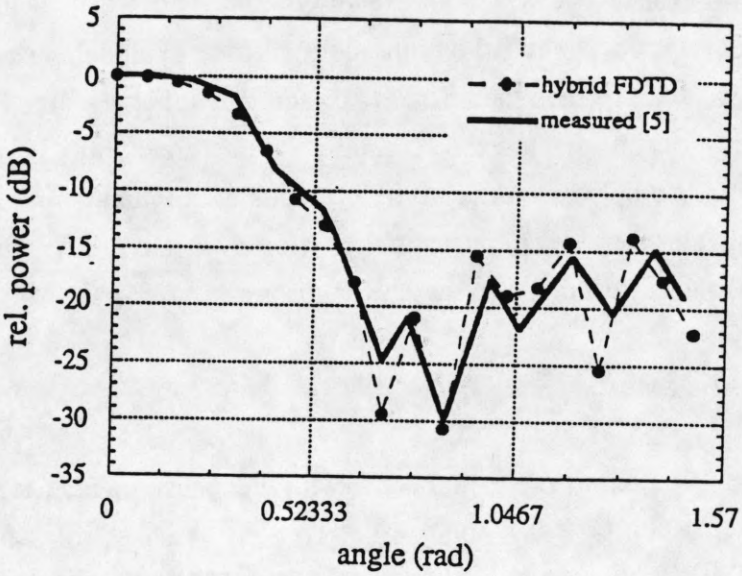

a)

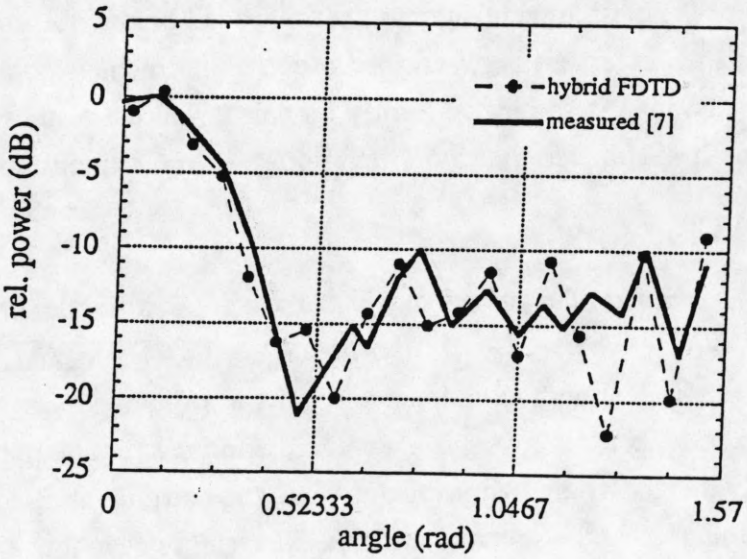

b)

Fig. 7.6 Comparison of the hybrid FDTD with measured E-plane radiation patterns for an LTSA antenna, a) without dielectric substrate, b) with dielectric substrate.

and experiment is shown in Fig. 7.6b. As before, the feed consisted of a diode soldered across a slotline. The mesh was chosen so that the dielectric thickness could be modeled by a single cell, i.e., $\Delta s = 0.059$ mm or $\lambda_0 = 17\Delta s$. This, in turn, resulted in approximating W_{min} to be $0.118\ \lambda_0$. As before, the ABC was placed at least $0.5\ \lambda_0$ away from the LTSA structure and the equivalent surface extended just enough to include a dipole source. It can be seen that there is fair agreement between the FDTD simulation and experiment in both the E- and the H-planes. The agreement, however, in the sidelobe regions is found to be worse than in the previous case which suggests that the dielectric may be having some effect on the accuracy. Moreover, the mesh resolution is not as good as in the previous case which also may be contributing to error.

7.3.2 Vivaldi results

Figure 7.7a compares the numerical with the measured results for a Vivaldi without a dielectric substrate ($L = 6.3\ \lambda_0$, $W_{max} = 1.77\ \lambda_0$, $W_{min} = 0.02\ \lambda_0$, $W_c = 2.55\ \lambda_0$ with $f_0 = 10$ GHz, dipole/diode feed). The FDTD mesh was chosen such that $\lambda_0 = 20\Delta s$. This resulted in modeling W_{min} to be much larger than the experimental W_{min}, i.e., $0.10\ \lambda_0$. It was found that this structure was more sensitive to the FDTD mesh than the LTSA. Due to the arbitrariness of the mesh, several attempts were needed before obtaining this result. It can be seen that the agreement between theory and experiment is good. In particular, though the first side lobe is somewhat poorly modeled, the rest of the side lobes are in good agreement. It is believed that more iterations will most likely result in improved agreement.

Figure 7.7b compares the numerical E-plane pattern for a Vivaldi on a low dielectric substrate ($\varepsilon_r = 2.22$, $d = 0.5$ mm, $L = 0.677\ \lambda_0$, $W_{max} = 0.315\ \lambda_0$, $W_{min} = 0.023\ \lambda_0$, $W_c = W_{max}$ with $f_0 = 35$ GHz) with experimental results in [6]. In contrast to the previous cases, the antenna was fed by a rectangular waveguide/finline structure rather than a diode. Though an FDTD method could handle such a feed, the extra memory and computation would have made simulating the structure difficult. Since it has been found that the E-plane is relatively insensitive to the feed [13], a dipole source was used instead. It can be seen that despite the use of a different feed the agreement between the numerical and measured radiation patterns is good. As before, however, different meshing schemes were needed to determine the scheme which would yield the best results.

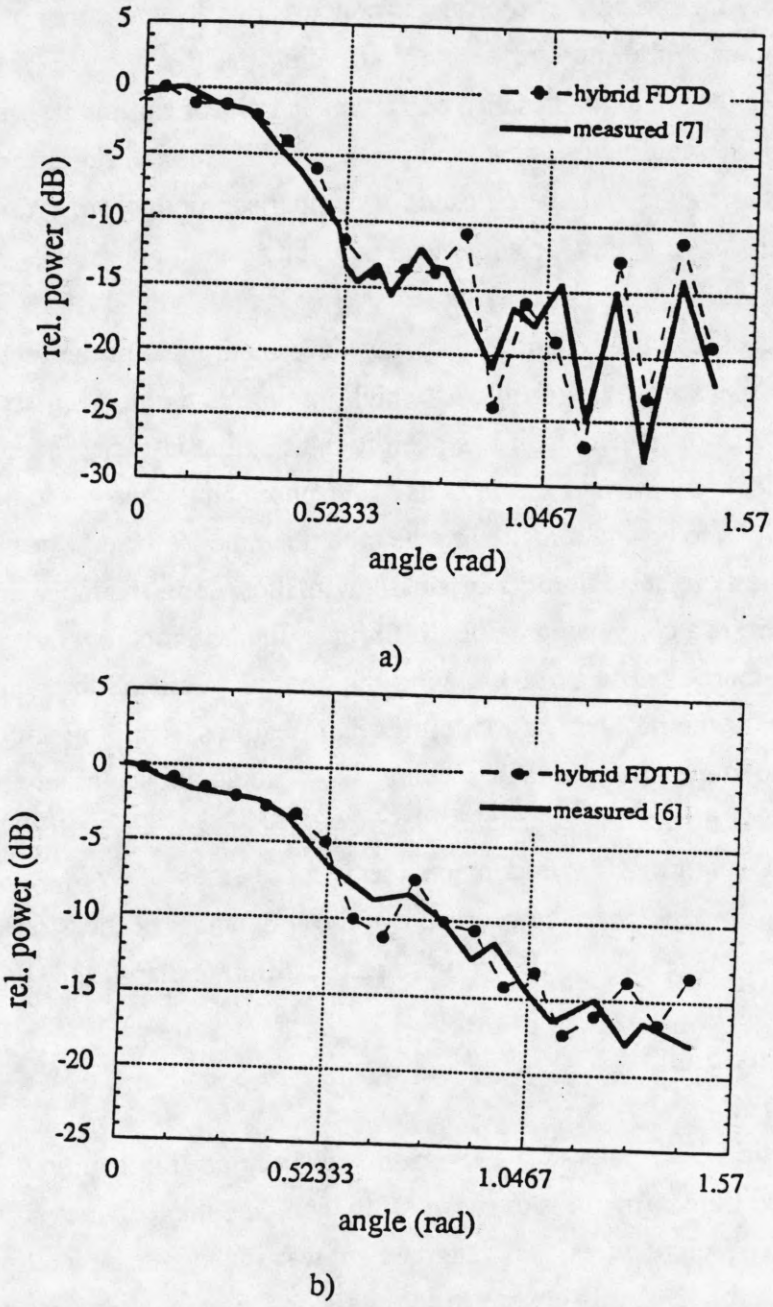

Fig. 7.7 Comparison of the hybrid FDTD with measured E-plane radiation patterns for a Vivaldi, a) without dielectric substrate, b) with dielectric substrate.

7.4 Comments about the Computation of the H-plane

In this work we have compared the FDTD results only with measured E-plane radiation patterns. The H-plane radiation patterns have been, as alluded to in the Introduction, omitted due to difficulties in modeling the feed. It has been shown experimentally that the feed will often introduce a significant amount of spurious radiation into the H-plane while only moderately affecting the E-plane [13]. Consequently, the position of the feed and the presence of varying lengths of slotline transmission line which precede the TSA can have a profound effect on the H-plane radiation pattern. For the published experimental data being used for comparison in this work, this information was not given and, consequently, accurate feed modeling was not possible.

However, even if all of the necessary information about the feed is provided, it is believed that there are other problems which might make obtaining an accurate H-plane pattern difficult. In particular, it has been found that the H-plane is very sensitive to the broadside field distribution of the antenna [6]. Consequently, we can expect the H-plane to be more sensitive to errors in modeling the taper than the E-plane. Because we are using a uniform mesh, there are a number of small anomalies along the taper due to stair casing. Moreover, there is a certain degree of arbitrariness in choosing how the stair casing should be done, and there is no way of knowing the optimum scheme that should be used. In addition, there is the problem of modeling small features. Due to the computer memory limitations, the minimum conductor spacing, W_{min}, could not accurately be modeled. This seemingly small error, however, can have a profound affect on the H-plane since the geometry of the taper is dependent on the relative sizes of W_{min} and W_{max}. If, for example, W_{min} is large, then the geometry of the conductors needed to flare out to Wmax over a fixed antenna length, L, can be significantly different than if the W_{min} were small.

7.5 Conclusions

The hybrid Yee/scalar-wave algorithm has been used in conjunction with the time domain far-field transformations to successfully compute the E-plane radiation patterns of four different LTSA structures. Good agreement was found with several published works, i.e., < 0.5 dB and < 2 dB difference in the main and first sidelobes, respectively. Poor agreement, however, was found in the H-plane due to lack of information regarding the geometry of the feeds used in the experiment and errors created by the mesh due to the use of a uniform, rectangular grid. It is believed that extensions to a curvilinear, nonuniform

grid may result in better agreement in the H-plane. Moreover, use of higher-order differencing schemes such as the 2-4 scheme may also improve the results.

7.6 References

[1] K. S. Yngvesson, T.L. Korzeniowski, Y.S. Kim, E.L Kollberg, and J.F. Johansson, "The tapered slot antenna-new integrated element for millimeter-wave applications," *IEEE Trans. Microwave Theory Tech.*, vol. MTT-37, no. 2, pp. 365-373, February 1989.

[2] P.J. Gibson, "The Vivaldi aerial, " Presented at the Ninth European Microwave Conference, Brighton, UK, 1979.

[3] S.N. Prasad and S. Mahaptra, "A Novel MIC slotline antenna," Presented at the Ninth European Microwave Conference, Brighton, UK, 1979.

[4] G. Arjavalingam, Y. Pastol, J.,-M. Halbout, and G.V. Kopcsay, "Broadband dielectric measurements with picosecond transient radiation," Presented at the Infrared and Millimeter Waves Conference, Hawaii, USA, 1988.

[5] K. S. Yngvesson, D.H. Schaubert, T.L. Korzeniowski, E.L. Kollberg, T. Thungren, and J.F. Johansson, "Endfire tapered slot antennas on dielectric substrates," *IEEE Trans. Antennas Propagat.*, vol. AP-33, no. 12, pp. 1392-1400, December 1985.

[6] T. Thungren, E.L. Kollberg, and K.S. Yngvesson, "Vivaldi antennas for single beam integrated receivers," Presented at the Twelfth European Microwave Conference, Helsinki, Finland, 1982.

[7] R. Jamaswamy and D.H. Schaubert, "Analysis of the tapered slot antenna," *IEEE Trans. Antennas Propagat.*, vol. AP-35, no. 9, pp. 1058-1065, September 1987.

[8] R. Jamaswamy, "An accurate moment method model for the tapered slot antenna," *IEEE Trans. Antennas Propagat.*, vol. AP-37, no. 12, pp. 1523-1528, December 1989.

[9] K.S. Yee, D. Ingham, and K. Shlager, "Time domain extrapolation to the far-field based on FDTD calculations," *IEEE Trans. Antennas Propagat.*, vol. AP-39, no. 3, pp. 410-413, March 1991.

[10] R.J. Luebbers, K.S. Kunz, M. Schneider, and F. Hunsberger, "A finite-difference time-domain near zone to far zone transformation," *IEEE Trans. Antennas Propagat.*, vol. AP-39, no. 4, pp. 429-433, April 1991.

[11] A. Taflove, K. Umashankar, and T. Jurgens, "Validation of FDTD modeling of the radar cross section of three-dimensional structures spanning up to nine wavelengths," *IEEE Trans. Antennas Propagat.*, vol. AP-33, no. 12, pp. 662-666, June 1985.

[12] C.A. Balanis, *Antenna Theory: Analysis and Theory*. New York, Harper and Row, 1982, pp. 454-457.

[13] K.M. Frantz, "An investigation of the Vivaldi flared radiator," M.S. thesis, University of Ilinois at Urbana-Champaign, 1992.

CHAPTER 8

CONCLUSIONS AND FUTURE WORK

With the growing interest in the FDTD method within the electrical engineering community , there has been an ever-increasing number of publications on the subject. It has been the author's observation that many of these works are focused almost exclusively on applications. Where applications are an extremely important aspect of understanding the limitation and accuracy of the FDTD method, this thesis was based on the premise that mathematical analysis could also be used to assist in understanding the method. Inspired by research done decades ago, this work has been a very modest attempt to mathematically examine the FDTD method in the hopes of not only improving the understanding of the technique but to suggest fundamental ways to improve its accuracy and efficiency. The mathematical analysis used in this work is by no means intended to match the rigor of many comparable papers on the subject published in standard mathematical journals. In fact, much of the analysis in this work, particularly, those involving Fourier analysis, should be considered heuristic in nature since the effect of possible boundary conditions, i.e., absorbing boundaries conditions, dielectric interfaces, was not taken into account. Nonetheless, this presentation is believed to provide the nonmathematician an easy to understand and familiar framework by which to understand the various forms of the FDTD method.

The purpose of Chapter 2 was to demonstrate an anomaly in the symmetric condensed node TLM algorithm. In particular, it is found that the transient electromagnetic fields modeled near the source region can exhibit spurious high-frequency oscillation which disappears suddenly when the observation point is moved only a few cells away. The accuracy of the low frequency response of this system, however, appears to be relatively unaffected by these oscillations. It is shown that using a different field/voltage relationship will eliminate these spurious oscillations while retaining the accuracy of the method. We conclude that a likely source of the spurious oscillations is the fact that the original field/voltage relation was not derived in accordance with the mathematical requirements required to insure convergence between the TLM solution and the exact solution to Maxwell's equations. It is suggested that further work on a rigorous mathematical proof be done to demonstrate the equivalence between the symmetric node TLM and Maxwell's equations. This will not only help define the proper field/voltage relationship but also allow a quantitative comparison with

the more commonly used Yee algorithm to be made to determine the relative advantages and disadvantages of each.

Chapter 3 provided a simple mathematical explanation for the presence of a fictitious dc offset field. It was shown mathematically and verified numerically that any transient charges present in the system will be artificially maintained by the Yee algorithm even after the charges have been removed from the system. Consequently, using field distributions as a transient source will generally result in a static charge buildup and an associated dc field. Several methods of removing this dc offset are presented. Though other approaches exist, including using divergence-free sources and filtering techniques, it is believed that the most efficient way to eliminate this offset field is to use a source with no dc component, because this approach requires no additional computations and offers a great deal of flexibility in choosing the distribution or the source.

Chapter 4 provided mathematical evidence verifying an empirical observation made several years earlier. In particular, it was found that the Yee algorithm has the highest accuracy when run at the largest time step. The eigenfunctions of the finite difference solution were derived using Fourier analysis and the bandlimited nature of the system demonstrated. Expressions for the truncation and the discretization error demonstrated that the leading-order error term of the Yee algorithm is generated by second-order error contributions from both the time and space discretizations. It is found that by choosing the maximum time step allowed by stability, maximum cancellation between the two errors will occur resulting in a smaller global error. It was concluded that the Yee algorithm should be run at the maximum allowable time step for not only maximum computational efficiency but accuracy as well.

Chapter 5 discussed the use of higher-order explicit differencing schemes to solve Maxwell's equations. In particular, a Fourier analysis of a higher order 2-4 differencing scheme was performed. A comparison with the Yee algorithm (2-2 scheme) was then made and the relative advantages of each discussed in detail. It is found that the 2-4 scheme has a better accuracy in the high-frequency response of a system and will have less from grid anisotropy than the 2-2 scheme. In addition, the accuracy of the 2-4 scheme can be increased from second-order to fourth-order accuracy by using 1) smaller time steps or 2) an effective dielectric constant concept. Potential drawbacks of a 2-4 scheme include an increase in computational requirements and a decrease in spectral

bandwidth compared to the 2-2 scheme. The decrease in spectral bandwidth can be of particular consequence resulting in errors due to aliasing or decreased spatial resolution requiring higher discretization than the 2-2 scheme. Further work needs to be done to evaluate the possible effects of these errors.

Chapter 6 introduced a new and efficient formulation of the Yee algorithm. In particular, the Yee algorithm was combined with the finite difference scalar-wave equation to reduce the number of computations and computer memory needed per iteration. It was found that the hybrid approach is optimal for planar structures and geometries, i.e., planar circuit boards, microstrip structures and TSA antennas, resulting in identical numerical results with the Yee algorithm but at approximately twice the speed and one-third less memory. The accuracy and applicability of the Engquist-Majda absorbing boundary condition (ABC) were also demonstrated.

Chapter 7 demonstrated the applicability of the hybrid Yee/scalar-wave algorithm by solving the E-plane radiation patterns of the Vivaldi and the linear tapered slot antennas. The far-field patterns were computed using recently introduced far-field time domain transformations and the results compared with the published measured data. Though the overall agreement was found to be good, the results were found to be sensitive to the discretization scheme. It is suggested that future work should be concentrated on using curvilinear discretization in conjunction with the hybrid scheme in an effort to improve the accuracy.

APPENDIX A

PROOF THAT THE DIVERGENCE RELATION WILL BE PRESERVED BY THE INITIAL CONDITIONS OF THE SCALAR-WAVE EQUATION

We wish to show that a solution to the initial value problem of the wave equation, i.e,

$$\nabla^2\overline{E}(x,y,z,t)-\frac{1}{c^2}\frac{\partial^2}{\partial t^2}\overline{E}(x,y,z,t)=0 \qquad \text{(A.1)}$$

where $\overline{E}=E_x\hat{x}+E_y\hat{y}+E_z\hat{z}$; c = const, will preserve the divergence relation, $\nabla\cdot\overline{E}(x,y,z,t)=0$ for $t\geq t_0$, if $\nabla\cdot\overline{E}(x,y,z,t=t_0)=0$.

Proof:

Taking the divergence of (A.1), we obtain

$$\nabla^2(\nabla\cdot\overline{E}(x,y,z,t))-\frac{1}{c^2}\frac{\partial^2}{\partial t^2}(\nabla\cdot\overline{E}(x,y,z,t))=0 \qquad \text{(A.2)}$$

This can be rewritten as

$$\nabla^2\phi(x,y,z,t)-\frac{1}{c^2}\frac{\partial^2}{\partial t^2}\phi(x,y,z,t)=0 \qquad \text{(A.3)}$$

where $\nabla\cdot\overline{E}(x,y,z,t)=\phi(x,y,z,t)$.

If we assume the following

$$\nabla\cdot\overline{E}(x,y,z,t=t_0)=0 \qquad \text{(A.4)}$$

then we have the following initial value problem (IVP),

$$\nabla^2\phi(x,y,z,t)-\frac{1}{c^2}\frac{\partial^2}{\partial t^2}\phi(x,y,z,t)=0 \quad ; \quad \phi(x,y,z,t=t_0)=0 \qquad \text{(A.5)}$$

By inspection, the solution to this IVP is given by

$\phi(x,y,z,t)=\nabla\cdot\overline{E}(x,y,z,t)=0$ for $t\geq t_0$.

Q.E.D.